Design Study of a Tokamak Power Reactor with an Electron Cyclotron Resonance Heating System

R. J. Temkin, K. E. Kreischer, J. Schultz
and D. R. Cohn

October 1979

MIT Plasma Fusion Center Report PFC/RR-79-20

Design Study of a Tokamak Power Reactor with an Electron Cyclotron Resonance Heating System[†]

R. J. Temkin[*], K. E. Kreischer[**], J. Schultz[††] and D. R. Cohn[*]

Massachusetts Institute of Technology
Plasma Fusion Center
Report PFC/RR-79-20

October, 1979

† Work supported by U.S. Department of Energy, Contract No. EG-77-5-02-4183.A002

* M.I.T. Plasma Fusion Center[a] and Francis Bitter National Magnet Laboratory[b]

** M.I.T. Plasma Fusion Center and Nuclear Engineering Department

†† Westinghouse Electric Corporation and Visiting Scientist, M.I.T.

a Supported by U.S. Dept. of Energy

b Supported by National Science Foundation

Abstract

A detailed design is presented of a tokamak power reactor with an electron cyclotron resonance heating system. Major research topics include: physics constraints imposed on the design of a reactor by the ECR wave absorption conditions; design of the high frequency (200 GHz) gyrotrons needed for plasma heating; the gyrotron power and magnet systems; a microwave transmission system in oversize waveguide for the ECR radiation and evaluation of its losses; absorption of the ECR radiation in the plasma; and techniques for improved reactor modularization. A 100 MW gyrotron system was designed for heating a previously derived tokamak power reactor, the High Field Compact Tokamak Reactor (HFCTR). Our major conclusion is that ECR heating appears to be feasible and potentially attractive for bulk heating of a moderate size, high density tokamak power reactor. However, if ECR heating is to be a reliable method for bulk heating of plasmas, it will be necessary to have an intensive development program for both high frequency gyrotrons and for transmission systems for high power, high frequency radiation.

Table of Contents

Executive Summary

1. Introduction

This report is a design study of a tokamak power reactor with an electron cyclotron resonance heating (ECRH) system. Both the physics and engineering characteristics of an ECRH system have been considered. The study addresses important physics questions relating to absorption of ECR radiation in the plasma and its impact on tokamak reactor design. It also identifies the areas of technology in which new research is needed to implement ECR heating on a reactor scale and those areas in which present technology can adequately solve future system requirements.

The major areas of research undertaken in the course of this study are: the physics constraints imposed on the design of a tokamak power reactor by the ECR wave absorption conditions; the selection of key parameters for an ECR heated tokamak power reactor; the design of the high frequency gyrotrons needed for heating the tokamak plasma; the design of the gyrotron power and magnet systems; the design of the microwave transmission system and evaluation of its losses; and the absorption of the ECR radiation in the plasma. In addition, some new results on modularization of the reactor have been obtained.

In most previous reactor designs, the tokamak plasma heating has been accomplished with neutral beam injection. However, neutral beam injection may be difficult to achieve with high efficiency and availability and low system cost when heating reactor-size tokamak plasmas. RF or microwave heating has been suggested as an alternative form of tokamak plasma heating. Major RF heating experiments have been carried out on tokamak plasmas primarily at one of the following three (resonant) frequencies: ion cyclotron resonance heating (ICRH), lower hybrid heating (LHH) and electron cyclotron resonance heating (ECRH). The relative frequencies required for heating in these three modes is roughly ratio as 1:30:1000, respectively.

In the present study, we have selected ECR heating for the following reasons. First, ECR heating has come to be more attractive in recent years because of advances in the development of high power gyrotrons operating for long pulses (see Fig. 1.B.2); because of the development of weakly relativistic theories of ECR heating of warm tokamak plasmas which predict successful heating of reactor-size tokamaks; and because of the continuing success of ECR heating experiments on tokamaks (see Fig. 1.B.1). Secondly, the physics of the ECR heating process appears to be fairly well understood, while the technology is relatively poorly understood. However, there is sufficient information about high frequency gyrotrons and the transmission of high frequency radiation

that is possible to make a fairly complete technological evaluation of this problem, as is done in this report. Thirdly, the heating of reactor-size plasmas with neutral beams, ICRH or LHH has been previously considered, while, to our knowledge, this is the first study to consider ECR heating.

2. Physics Constraints on an ECR Heated Tokamak Power Reactor

We have derived a set of constraints for the operating characteristics of tokamak power reactors which are bulk heated by electron cyclotron resonance heating (ECRH). Four heating modes have been considered: ordinary wave heating at the electron cyclotron frequency, Ω, and at the second harmonic frequency, 2Ω, and extraordinary wave heating at Ω and at 2Ω. For ordinary wave heating at Ω, which appears to be the most promising method, the wave frequency $\omega \approx \Omega$ must exceed the plasma frequency, ω_p, for wave penetration into the plasma. Our main conclusion is that the need for high density operation ($n_o > 4 \times 10^{20} m^{-3}$) in moderate size tokamak reactors, coupled with the wave accessibility condition $\Omega > \omega_p$, leads to the requirement of frequencies in the 200 GHz range for ECRH of reactor plasmas. A further condition on the heating frequency may be derived by consideration of the ignition condition using empirical scaling laws for the energy confinement time. This latter condition does not increase the heating

frequency requirement unless impurities are present or the energy confinement degrades with increasing temperature. We also find that for ordinary wave heating at Ω, the average plasma β is limited to less than 0.039 for a central temperature below 15 keV, assuming parabolic density and temperature profiles. The use of extraordinary heating at Ω might lower the frequency requirement for ECRH of a reactor. However, it appears to be unattractive for reactor operation because, in order for the wave to penetrate to the center of the plasma, the heating ports must be located on the inside (or the top side) of the torus. High beta, lower field reactors can be heated from the outboard side of the torus with second harmonic radiation. However, these devices will have to be heated at frequencies which are generally higher than those needed for devices which are heated with the ordinary wave at the fundamental frequency.

3. Description of Reactor and Plant

The major topic of research in the present report is the design study of an ECR heating system for a tokamak power reactor. In order to avoid the obvious additional effort related to developing a new reactor design just for this report, we have selected an existing tokamak power reactor design and modified the design from neutral beam to ECR heating. The selection of a reactor design was limited by the physics constraints for penetration of the ECR radiation to the plasma center, as previously mentioned.

The tokamak power reactor which was selected was the High Field Compact Tokamak Reactor, HFCTR [C079]. The major prarmeters of this device are:

Major radius, R_o (m)	6.0
Plasma halfwidth, a (m)	1.2
Plasma shape factor, S	1.5
Field at plasma, B_T (T)	7.4
Average toroidal beta, $<\beta_T>$	0.04
Plasma current, (MA)	6.7
Electron density, n (m^3)	$5 \times 10^{20}(1 - r^3/a^3)$
Electron-ion temp, T(keV)	$12.4\ (1 - r^2/a^2)$
Heating Power, P(MW)	100
Av. thermal power, P_{th} (85% duty,MW)	2470
Net electric power, P_n(MW)	775

The adaptation of the reactor design to ECR heating requires elimination of the neutral beam lines and ripple field coils and the substitution of a port structure for ECR heating, as described in detail in the report. In addition, we have taken the opportunity to include in the report some additional changes to the tokamak reactor design, particularly in the area of improved modularization.

The HFCTR reactor is shown in Figs. (II.B.1) and II.B.2). The plasma heating sequence is the same for neutral injection or ECR heating. After a plasma initiation and expansion phase, the plasma is bulk heated to ignition, with the major heating done between 3.9 sec <t< 8.4 sec (see Fig. II.B.3). After ignition, the plasma

burn is sustained by alpha heating. A plant layout of the tokamak power reactor with ECR heating was derived and is shown in Fig. II.B.4. This layout was needed to define the distance between the gyrotron tubes and the tokamak power reactor (about 30 m), so that a microwave transmission system could be designed.

4. Design Study of High Power, High Frequency Gyrotrons

The ECR heating of the tokamak plasma to ignition will require over 100 MW of RF radiation at 200 GHz. The most promising source at the present time for providing the required radiation is the gyrotron. Based on present day gyrotron technology, we project a power level of about 100 kW at 200 GHz for a 5 sec. pulse. We have carried out a detailed design analysis of such a gyrotron. More than 1000 gyrotrons would then be needed for heating the tokamak plasma. This approach requires a very large number of sources, but the cost of such an RF heating system can be shown to be less than that of a comparable neutral beam system. The gyrotrons should also prove to be reliable at a power level of 100 kW, with easy replacement of failed tubes. In the future, megawatt power level tubes, based on variations of the gyrotron or on free electron lasers, may be available. Such devices, however, will not necessarily lead to reduced system costs, in part because of the difficulty of transmitting megawatt beams through windows or of operating without windows.

The 100 kW, 200 GHz gyrotron was designed by a parametric analysis using design principles previously applied to a 10 kW, 200 GHz gyrotron [TE 78]. The analysis included the electron beam and gun parameters and their correlation to the operating characteristics of the gyrotron cavity. The goal of this analysis was to maximize the overall efficiency of the gyrotron, in order to reduce power supply requirements and enhance cavity and collector lifetime, while maintaining the operating parameters at realistic values. The design included optimization of a wide range of parameters, including the electron beam voltage, U, and current, I, the working mode of the cavity, TE_{mpq}, the beam radius, R_c, the cavity radius, R_o, the cavity length, L, the ratio of transverse to parallel velocity $\beta_\perp/\beta_\parallel$, the system (total) quality factor, Q_t, and the overall efficiency, η. Space charge effects were included in the analysis using an approximate, analytic theory. The results of the analysis are listed below. The overall efficiency, η, is estimated to be 33%.

200 GHz Gyrotron Parameters

ν = 200 GHz

λ = 1.5mm

U = 70kV

I = 4.4A

TE_{051} mode

R_o = 3.94mm

R_c = 2.82mm

L = 12.5mm

$\beta_\perp/\beta_\parallel$ = 1.8

B_o = 7.5T

$Q_t = 2.3 \times 10^3$

η = 0.33

P_{rf} = 100 kW

This design represents a significant extension of present day gyrotron technology. The use of a TE_{051} mode, which is a relatively high order mode, indicates that mode competition may be a serious problem and that techniques for suppressing parasitic modes will have to be developed. The ohmic heating of the cavity walls will amount to 5 kW/cm^2. This value is very high, although it is consistent with modern microwave tube manufacturing capabilities. A detailed design of the cavity cooling system is presented, indicating that the required power dissipation should be feasible. For cavity wall heating of 2.5kw/cm^2, a TE_{081} mode will be required.

5. Gyrotron Power and Magnet Systems

A basic design of the gyrotron power and magnet systems was carried out. The gyrotron power supply design is similar to that of the state-of-the-art klystron and neutral beam power supplies. The gyrotron cathodes and first anodes require high voltage, moderate current power supplies. A voltage ripple of 0.6% was calculated to be adequate for maintaining full gyrotron efficiency and was incorporated into the design. A standard series regulator configuration was selected, with protection of gyrotron and regulator tubes provided by crowbars, as shown in Fig. II. D. 1. Six cathodes are supplied by a single switch/regulator tube.

The solenoid magnets used to create the ECR magnetic field of 7.5 T, for 200 GHz emission in the gyrotron cavity, are long, superconducting NbTi solenoids with graded current density to enhance field homogeneity. Field uniformity of better than 1% can be achieved in the cavity region.

6. Microwave Transmission and Wave Launching

A system was designed for transmission of the 200 GHz radiation from the gyrotrons to the plasma of the tokamak power reactor. A variety of techniques are available for millimeter wave propagation, including both microwave and quasi-optical techniques. Many of these techniques have been extensively tested in high frequency microwave communications systems. The various techniques were first compared and several methods were found to be too lossy for transmission over the estimated 30 m path length from the gyrotron buildings to the tokamak port. However, specific configurations using quasi-optial or microwave techniques were found to yield satisfactory low loss propagation. A transmission system consisting of propagating the TE_{01} mode in oversize copper pipe was selected for the present design for several reasons, the foremost reason being that accurate data are available concerning this technique from field tests of communications systems. A single transmission line for each gyrotron was specified, yielding a total of about 1,250 lines, each carrying 100 kW of power. Although such a system has a large number of components, it avoids the problem of attempting to combine radiation from several sources. It also avoids problems associated with transmitting extremely high (megawatt) power levels through windows.

The main transmission system component is a 30 m length of 14 mm diameter circular copper waveguide at atmospheric pressure.

This is an oversize guide used to transmit 1.5 mm radiation in the TE_{01} mode. The gyrotron output is transormed from the working mode of the cavity into a TE_{01} mode by a quasi-optical mode transformer. Radiation is inserted into the 30 mm waveguide run through a mitred, right angle bend. There are a mode filter and isolator in the system. The waveguide run traverses the reactor cell at a height greater than that of the reactor modules, then makes two right angle bends to feed the ECR radiation into the plasma. The radiation is transformed into a linearly polarized mode and launched as a free space wave towards the plasma center. The waveguide system may be easily unbolted from the reactor module for module replacement. The estimated transmission of the microwave system is 80%. However, several components of the system will require further research. In particular, new techniques, possibly quasi-optical methods, must be developed for transformation of the gyrotron output mode to the TE_{01} mode in oversize waveguide. Furthermore, although there have been extensive tests of high frequency microwave transmission, these tests have not been carried out in the high power regime.

7. Wave Absorption in the Plasma

Recently, there have been a number of extensive theoretical analyses of ECR heating of tokamak plasmas, including reactor-size plasmas. Some of these studies have included relativistic effects

to first order, which are needed for treating plasmas with temperatures of up to 15-20 keV. These studies have concluded that ECR heating should lead to bulk plasma heating. In this study, we have briefly reviewed the major results of the studies. We have also obtained some results for ECR heating of the HFCTR reactor in the quasi-transverse limit, neglecting refraction. A wave trajectory analysis of plasma heating, which would be valuable, was beyond the scope of this report.

For reactor-size plasmas, the absorption of ECR radiation is so strong that the wave cannot penetrate to the resonance point. Hence, in order to heat the plasma center, the heating frequency must match a point located toward the inside of the torus. The ECR frequency should be increased roughly by an amount $3\Omega_o (1-q)^{1/2} \beta_T \cos\theta$, where Ω_o is the central ECR frequency, q is ω_p^2/ω^2, β_T is $\sqrt{2T_e/Mc^2}$ and θ is the launch angle with respect to the magnetic field. This effect is rather small, of order 10% or less, and it goes to zero for transverse propagation ($\theta = 90°$). The absorption point in the plasma is found to depend on angle of launch (θ), density (n) and temperature (T). Assuming that θ and n are constant, then as T increases to ignition, the location of the absorption point shifts significantly, the shift in major radius being of order $0.3R_o (1-q)^{1/2} \cos\theta$. The heating point, however, stays in the plasma center.

8. Improved Modularization of the Reactor

HFCTR presented an advanced, fully automated, modularized reactor design which permitted rapid replacement of modules for either scheduled or unscheduled maintenance [CO 79]. The potential advantage of the HFCTR design relative to unautomated designs, using manipulators, was that the down-time due to mechanical operations in a module replacement could be reduced from several months to two days. All of the magnet systems were also modularized so that a magnet module suffering unexpected damage could be rapidly replaced. However, the HFCTR modularized approach was limited by time delays due to nonmechanical operations such as detritiation of the vacuum vessel prior to disassembly and reestablishment of high vacuum after reassembly. In this report, we suggest that the down-time due to scheduled replacement of reactor modules may be minimized by removing all of the modules at once. It is possible for all old modules and replacement modules to simultaneously move to their desired positions. This technique has the advantage of reducing the total time required in scheduled module replacements for detritiation of the vacuum vessel and for reestablishment of high vacuum after reassembly. It also increases the projected service life of the first generation modules and reduces the activation of the reactor cell, permitting the possibility of human entry (with shielding) into the reactor cell, if needed, during reassembly. A detailed discussion of detritiation and a comparison with previous maintainability studies are presented.

9. Summary of Advantages and Disadvantages of ECR Heating

The major advantages of ECR heating may be summarized as follows:

- ECR radiation is predicted to penetrate to the center of a reactor-size tokamak plasma, to be nearly 100% absorbed and to result in bulk heating.
- ECR heating has several advantages over neutral beam heating. Gyrotrons are sealed and do not share the reactor vacuum system. Failure of a single gyrotron unit will not effect reactor operation. The projected cost of an ECR heating system is less than that of a neutral beam injector system. The microwave transmission system requires no routine maintainance.
- ECR heating is highly localized, allowing control of the temperature profile and improving confinement. Such improved confinement can lead to a very significantly reduced requirement on the power level and time duration needed for heating to ignition. [CA79] The gyrotrons can be applied to gas breakdown and plasma preheating, possibly reducing the size and cost of the ohmic drive system.

The major disadvantages of ECR heating include:

- The efficient, high power, high frequency gyrotrons (or other sources) required for ECR heating of reactor-size plasmas have not yet been demonstrated and will require a lengthy development

program. Some components, such as the gyrotron output windows, may be particularly difficult to fabricate. The microwave transmission system will also require a major development program.

- The efficiency, cost and reliability of microwave systems developed for ECR heating will, at least for the next decade or two, be inferior to that of lower frequency microwave systems used for lower hybrid or ion cyclotron resonance heating.
- ECR heating provides direct heating of electrons, with collisional energy transfer required to heat ions. ECR heating does not appear to be usable for an RF-driven, steady-state tokamak.
- If an average β exceeding 4% at central temperatures ~ 15 keV or 8% at central temperatures ~ 30 keV is desired, ECR heating will have to be at the second harmonic, and the required heating frequency will be increased.

10. Conclusions and Recommendations

- A detailed design has been carried out of an ECR heating system for a specific tokamak power reactor, the High Field Compact Tokamak Reactor (HFCTR). The present results, when combined with those of the HFCTR report, represent the first detailed study of an ECR heated tokamak power reactor.

- Our major conclusion is that ECR heating appears to be both feasible and potentially attractive for bulk heating of a moderate size, high density tokamak power reactor.
- Ordinary wave heating at the fundamental cyclotron frequency appears to be the most advantageous option for heating. The wave cutoff condition for this mode limits the average plasma β to less than about 4% for central temperatures ~ 15 keV and 8% for central temperatures ~ 30 keV.
- For bulk heating of the tokamak plasma to ignition, a power level of about 75 MW, at a frequency of 200 GHz, for about 5 seconds is required. We have designed for a power level of 100 MW in this report in order to prove a safety margin. However, power levels significantly less than 75-100 MW could be required if profile control is effective. Present-day gyrotron technology indicates that a power level for a single 200 GHz gyrotron of 100 kW should be practical, with 33% overall efficiency.
- A microwave system has been designed for transmission of the radiation from the gyrotrons to the tokamak plasma. Estimated overall transmission efficiency using the TE_{01} mode in oversize waveguide is about 80%. The number of individual gyrotrons required would then be about 1,250. Although the quantity of tubes used is large, this design will reduce the importance of individual tube failures and allow the use of windows at the gyrotron output end and at the reactor.

- If ECR heating is to be a viable alternative for bulk heating of tokamak plasmas, it will be necessary to have an intensive development program for high-frequency gyrotrons, as well as for transmission systems for high-frequency, high-power radiation. Key gyrotron problems include electron guns for producing cold beams with large $v_\perp/v_\parallel$; mode competition in the cavity; and output coupling and window construction. The microwave transmission system will require development of mode converters and, possibly, isolators and mode filters.
- The ECR radiation is predicted to be absorbed in the central region of the plasma and to lead to bulk heating. However, a more detailed investigation should be carried out of the effect of the rising plasma temperature on the location of the absorbing point, including the effect of plasma pressure and poloidal field. The possibility of tail heating of the electron distribution also merits further analysis.
- The RF heating system leads to a considerably simpler technique for removal of individual reactor modules relative to a neutral beam injector heating system. The cost of an ECRH system is also projected at less than that of a neutral beam system. The simultaneous replacement of all reactor modules at scheduled intervals is found to minimize the total down-time for module replacement.

I. Introduction

I.A Background and Motivation

The primary purpose of this study is to evaluate the physics and engineering characteristics of an electron cyclotron resonance heating (ECRH) system for a tokamak power reactor. This study identifies the areas of technology in which new research is needed to implement ECR heating on a reactor scale; it also identifies those areas in which present technology can adequately solve future system requirements. This study also addresses important physics questions relating to wave absorption in the plasma and its impact on reactor design. The major areas of research undertaken in the course of this study are: the physics constraints imposed on the design of a tokamak power reactor by the ECR wave absorption conditions; the selection of key parameters for an ECR heated tokamak power reactor; the design of the high frequency gyrotrons needed for heating the tokamak plasma; the design of the gyrotron power and magnet systems; the design of the microwave transmission system and evaluation of its losses; and the absorption of the ECR radiation in the plasma. In addition, some new results on modularization of the reactor have been obtained.

The major areas of research of the present study thus focus on a detailed analysis of the ECR heating system. It is necessary to carry out the study in depth in order to provide a

detailed or microscopic view of the system components and to identify potential technological problems. Having accomplished such a microscopic system analysis, it is then possible to address the macroscopic viewpoint and to evaluate the ECR heating system as a whole. This latter viewpoint is needed to establish system feasibility, to analyze system costs, to evaluate recirculating power and to provide a comparison to other heating techniques.

In most previous reactor designs, the tokamak plasma heating has been accomplished with neutral beam injection. It is known, however, that neutral beam injection may be difficult to achieve with high system efficiency and low system cost when heating reactor-size tokamak plasmas. RF or microwave heating has been suggested as an alternative form of tokamak plasma heating. Major RF heating experiments have been carried out on tokamak plasmas primarily at one of the following three (resonant) frequencies: ion cyclotron heating (ICRH), lower hybrid heating (LHH) and electron cyclotron resonance heating (ECRH). The relative frequencies required for heating in these three modes is roughly 1:30:1000, respectively. The advantages and disadvantages of heating in these three modes may be briefly summarized as follows. The technology of RF heating is decidedly simpler at the lower frequencies (ICRH and LHH), where high power sources and microwave transmission and launching systems are presently available. For ECR heating, high frequency gyrotrons operating at high power and high efficiency are not presently available and will have to be developed for heating

reactor size plasmas. From the point of view of wave absorption in the plasma, however, ECR heating appears at present to be more attractive. The ECR heating radiation, according to well developed theoretical treatments, will be absorbed at the plasma center and will heat the bulk of the electron velocity distribution. For ICRH and LHH, wave launching is presently not very well understood; and penetration of the wave to the center of a reactor-size plasma may not be possible. We conclude that, at the present time, it is not possible to project with certainty which of these three RF heating techniques (if any) will eventually find application in the heating of a tokamak power reactor.

In the present study, we have selected ECR heating for the following reasons. First, the heating of reactor-size plasmas with neutral beams, ICRH or LHH has been previously considered, while, to our knowledge, this is the first study to consider ECR heating. Secondly, the physics of the ECR heating process appears to be fairly well understood, while the technology is relatively poorly understood. However, there is sufficient information about high frequency gyrotrons and the transmission of high frequency radiation that it is possible to make a fairly complete technological evaluation of this problem, as is done in this report. Thirdly, ECR heating has come to be more attractive in recent years because of advances in the development of high power gyrotrons operating for long pulses; the development of weakly relativistic theories of

ECR heating of warm tokamak plasmas which predict successful heating of reactor-size tokamaks; and the continuing success of ECR heating experiments on tokamaks.

It should also be recognized that the time scale for design and implementation of the first experimental and demonstration tokamak power reactors will allow a period of up to 10 to 20 years for development of the high frequency sources needed for ECR heating. One purpose of this report is to evaluate the feasibility of developing suitable gyrotron heating systems on that time scale. Future gyrotron research will benefit from the fact that the development of gyrotrons will be useful not only for heating tokamak plasmas, but also for heating other plasma devices such as the EBT machines and mirror devices, and for non-plasma applications such as high frequency radars. Also, the development of high frequency gyrotrons will have a large research and development base in the established microwave tube industry. Furthermore, in considering a development program which will span one or two decades, there will be ample opportunity for the development of alternative high frequency sources, such as relativistic gyrotrons, free electron lasers, or other systems.

I.B Current Status of ECRH Experiments and Gyrotron Development

Part of the motivation for undertaking a study of an ECR heated tokamak power reactor is the recent progress in both

gyrotron development and in the application of gyrotrons to ECR heating of tokamaks. This recent progress is summarized in this section.

I.B.1 ECRH Experiments

Early ECR heating experiments were carried out at low density and low initial electron temperature, resulting in heating of the electron tail distribution to high energies [DA64, AL68]. In 1972, the first successful ECR heating experiments were reported in two separate tokamak experiments in the Soviet Union. At the Kurchatov Institute in Moscow, V.V. Alikaev et al. reported heating results [AL72] on the TM-3 tokamak. A gyrotron with a wavelength of about 1 cm, a power of about 40 kW and a pulse length of about 0.5 msec was used. The electron temperature rise was 200 - 400 ev, with an initial temperature of about 250 ev. The heating efficiency was 20 - 30%. On the Tuman -2 tokamak at the Ioffe Institute in Leningrad, ECR heating experiments were reported by Golant et al. [GO72]. The microwave power at 34 GHz was up to 40 kW for 100 μsec. A heating efficiency of several tens of percent was obtained.

More recent experiments have been carried out at both Institutes with higher power levels, longer pulse lengths, larger tokamaks and, at Kurchatov, higher frequencies. In the time period from 1971 - 1976, experiments were performed at wavelengths of 10 and 5 cm on the TM-3 tokamak. Heating was carried out at magnetic

fields of up to 2.5 T and plasma density of up to 1×10^{13} cm^{-3}. The experiments at $\lambda \sim 5$ mm had a power of about 60 kW and those at 10 mm had a power of about 100 kW, for a pulse duration of 1 ms. [AL75, AL76, AL78]. At present, experiments are being carried out on the T-10 tokamak at Kurchatov Inst. with two, 200 kW gyrotrons of 3.5 mm wavelength and 20 - 100 msec pulse duration. Initial results from this experiment indicate successful heating of the plasma.

A major committment has been made to ECR heating for the T-15 tokamak which will be built at the Kurchatov Institute. Ordinary wave heating will be carried out at a field of 3.5 T and density of up to 7×10^{13} cm^{-3} using 5 MW of gyrotron power. The gyrotron system will consist of 24 units, each emitting 200 kW for a pulse length of 1.5 sec. The experiment should commence in 1983 - 1984. This ECR heating experiment should certainly be viewed as a major test of both ECR heating theory and gyrotron technology. If successful, it could pave the way for future application of gyrotrons to heating reactor-size tokamak plasmas.

In the U.S., the major recent application of ECR heating of plasmas has been to the ELMO bumpy torus (EBT) experiment at ORNL. This experiment is performed in a CW mode, unlike the pulsed mode of tokamaks. Consequently, gyrotrons developed for this experiment will have to fulfill the more difficult specifications of CW operation. A 28 GHz, 200 kW gyrotron is currently under development at

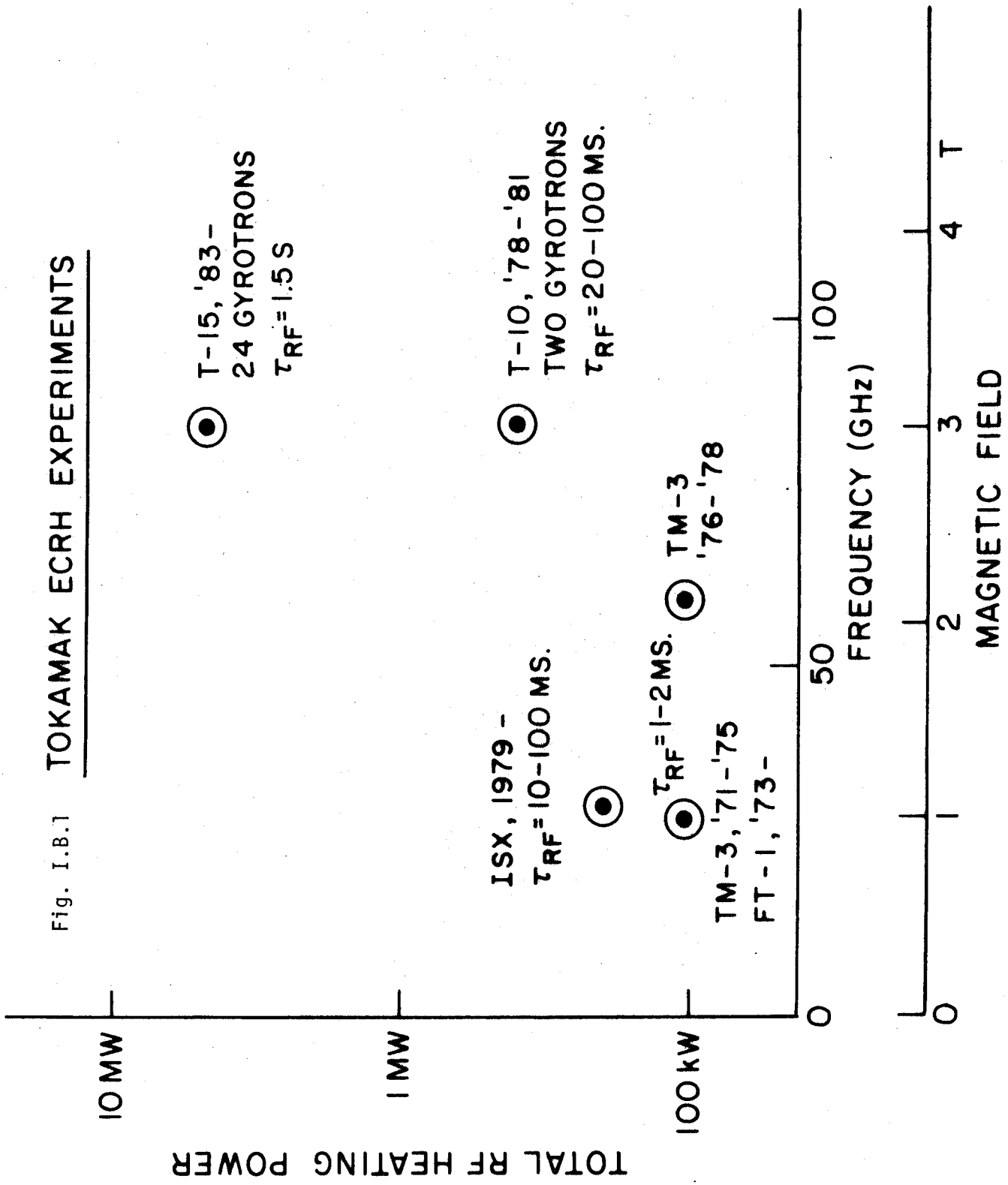
TOKAMAK ECRH EXPERIMENTS
T-15, '83-
24 GYROTRONS
τ_{RF}=1.5 S
T-10, '78-'81
TWO GYROTRONS
τ_{RF}=20-100 MS.
ISX, 1979 -
τ_{RF}=10-100 MS.
τ_{RF}=1-2MS.
TM-3
'76-'78
TM-3, '71-'75
FT-1, '73-
10 MW
1 MW
100 kW
TOTAL RF HEATING POWER
0
50
100
FREQUENCY (GHz)
0
1
2
3
4 T
MAGNETIC FIELD

Fig. I.B.1

Varian Co. for use on the EBT experiment [JO77]. For the EBT-II experiment, a 2 MW system of ten, 200 kW, CW gyrotrons, operating at 110 GHz, will be needed. These gyrotrons could be used in 1983, if they are available at that time. Pulsed gyrotrons are currently under development for tokamak heating applications, partly as a spinoff from the EBT development. A pulsed, 200 kW, 28 GHz gyrotron will be used in 1979 to heat the ISX tokamak at Oak Ridge [EN76]. A 100 - 200 kW, 35 GHz, 10 msec. pulsed gyrotron, developed at N.R.L., has been applied to heating the ISX tokamak and will also be used on experiments at the Versator tokamak at M.I.T. [GA79]. Numerous other ECR heating experiments are being planned for a variety of other tokamaks throughout the world. The level of effort represented by those experiments adds greatly to the credibility of ECR heating as an eventual option for bulk heating of a reactor-size tokamak plasma to ignition. A summary of current ECR heating experiments is shown in Fig. I.B.1

I.B.2 Gyrotron Experiments

The gyrotron is a form of electron cyclotron maser developed by A.V. Gaponov and coworkers [FL77, HI77]. An electron cyclotron maser (ECM) is a weakly relativistic electron beam device operating in a uniform magnetic field and emitting electron cyclotron radiation or its harmonics. Although a variety of ECM's have been constructed, the most successful results have been obtained with the

gyrotron. The gyrotron is characterized by an electron gun of the magnetron injection type and by a cavity operating near cutoff. Results for CW and pulsed gyrotrons, obtained at high frequency and high efficiency, were announced by Kisel' et al [KI74] and by Zaytsev et al. [ZA74] in 1974. Since then, new results at high pulsed powers have been presented by Flyagin et al [FL77] and by Andronov et al. [AN78]. All of these results were obtained at the Institute of Applied Physics in Gorky, U.S.S.R. Recently developed high power gyrotrons have found application in tokamak plasma heating experiments in the U.S.S.R.

In the U.S., development programs for high power gyrotrons are being carried out at Varian Co. [JO77] and at N.R.L. The Varian program has a goal of a CW, 200 kW, 28 GHz gyrotron. Although that goal has not yet been achieved, CW operation at lower power has been obtained as well as pulsed operation at full power. The N.R.L experiments have achieved pulsed operation in the 100 - 200 kW range in a 35 GHz gyrotron oscillator [GR79].

Fig. I.B.2 illustrates the recently announced gyrotron results. For the Soviet results, a line is drawn illustrating the $\nu^{-5/2}$ power law for extrapolating power vs. frequency. It may be seen that a 100 kW, 200 GHz, 4 sec pulsed gyrotron needed for heating a reactor-size tokamak plasma is well beyond present day gyrotron technology. However, it is possible to project to high frequency based on current results. For example, estimates of efficiency vs.

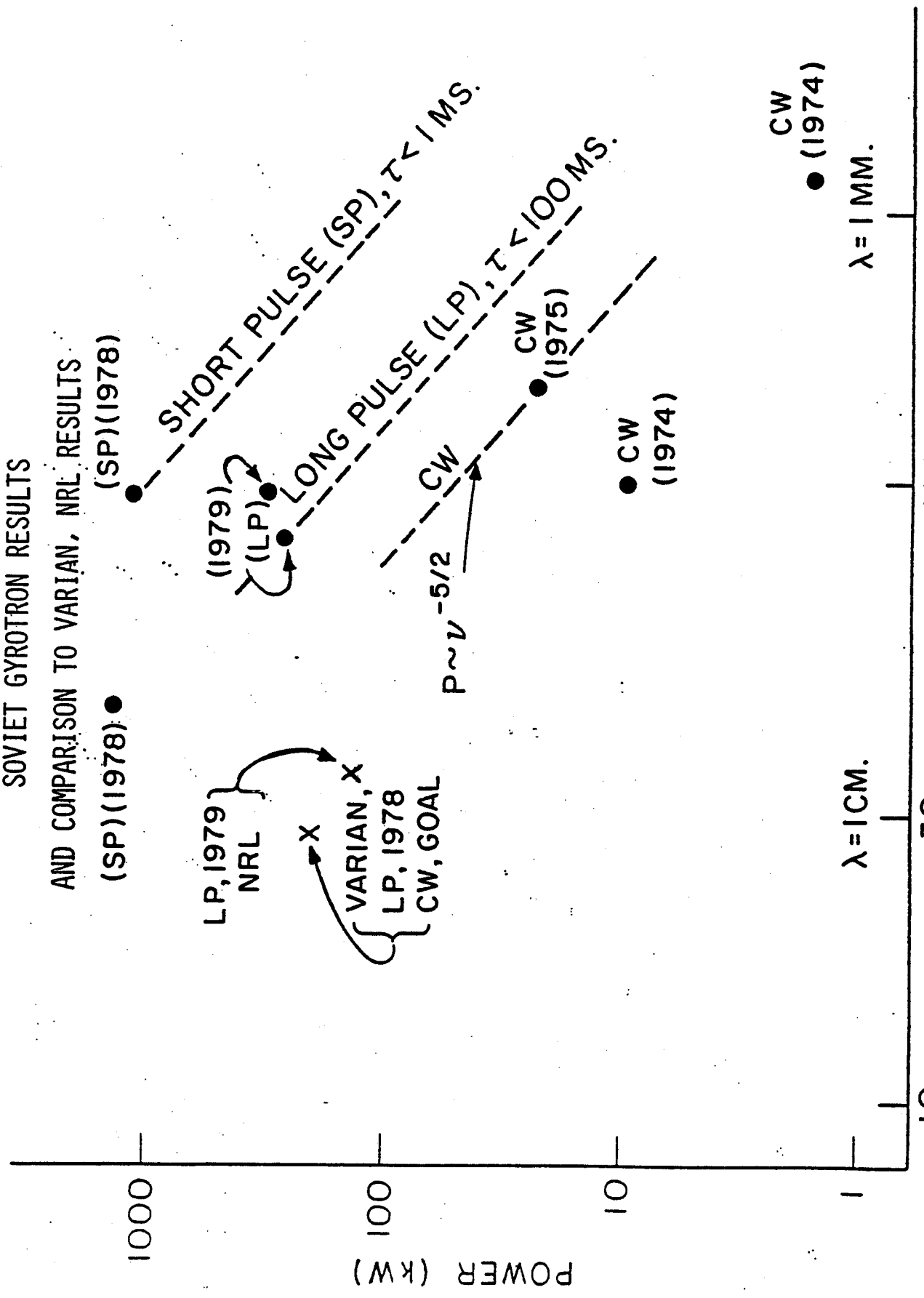
SOVIET GYROTRON RESULTS
AND COMPARISON TO VARIAN, NRL RESULTS
(SP)(1978)
(SP)(1978)
SHORT PULSE (SP), τ < 1 MS.
(1979)
(LP)
LONG PULSE (LP), τ < 100 MS.
CW
(1975)
CW
(1974)
CW
(1974)
P ~ ν^-5/2
LP, 1979
NRL
X
VARIAN, X
LP, 1978
CW, GOAL
POWER (KW)
1000
100
10
1
λ = 1 CM.
λ = 1 MM.
10
30
100
300
FREQUENCY (GHz)

Fig. 1.B.2

frequency [TE78a, b, AN78] indicate that an efficiency exceeding 30% should be possible in the 200 - 300 GHz range.

I.C Plan of Report

This report is organized into four sections, as suggested in the "Standard Fusion Reactor Design Study Contents" memorandum of March, 1979 (U.S. D.O.E., RS&A: CRH: #478). Section I is an introduction. Section II contains the major results of this study. The constraints on the design of an ECR heated tokamak reactor are evaluated using the conditions for absorption of ECR radiation. Using these constraints, a previous reactor design, the HFCTR [CO79], is selected for modification from neutral beam injection to ECR heating. Many reactor parameters remain unchanged for ECR heating. Section II includes an analysis of high frequency gyrotrons and their attendant magnet and power systems. The microwave transmission and wave launching systems are analyzed. Improved modularization of the reactor is described. Section III presents a summary and conclusions. Section IV is a table of fusion reactor design parameters.

II. Power Reactor and Gyrotron ECR Heating System

II.A. Physics Constraints on an ECR Heated Reactor

II.A.1. Introduction

The design of a tokamak power reactor heated at electron cyclotron resonance must take into account the conditions for the absorption of the RF radiation in the plasma. These conditions impose additional constraints on the reactor design, constraints which can ultimately correlate the plasma density and the magnetic field. The origin of the constraints may be briefly summarized as follows. Good absorption of the microwave radiation will only occur when the frequency of the radiation, ω, is close to the electron cyclotron frequency, Ω, or to a harmonic of that frequency, such as $2\,\Omega$. However, it is important to consider (and will be discussed in detail in this section, II.A) that the incident electromagnetic radiation at frequency ω can penetrate to the center of the plasma only if there is no cutoff region. The condition for cutoff depends on the heating mode and plasma parameters and will be analyzed in detail below. For the mode of greatest interest, however, namely heating with the ordinary mode at $\omega \approx \Omega$, the condition for avoiding cutoff is $\omega > \omega_p$, where ω_p is the plasma frequency which depends on plasma density. It is this condition which provides the correlation of magnetic field and plasma density.

In this section, the implications of the physics constraints on an ECR heated tokamak power reactor are investigated in detail.

The approach is intended to be general, so that the conclusions are general and are not specifically tied to any single reactor design or concept. Four heating modes are considered: ordinary wave heating at the electron cyclotron frequency, Ω, and at the second harmonic frequency, 2 Ω, and extraordinary wave heating at Ω and at 2 Ω. For each heating mode, the wave propagation and absorption are described. This section is therefore also useful as background for a later, more detailed discussion of wave absorption in Section II.G. The implications of the wave absorption for reactor parameters are then discussed. Limits are derived for the plasma $<\beta>$. The average fusion power density and ignition conditions are discussed. On the basis of those results, a set of bounds on the allowed regime of reactor operation is derived. A rather conservative set of technological and economic assumptions is made, but results can be extended to other evaluations of these fundamental assumptions. The total heating power for the reactor is estimated. Finally, some conclusions based on the results are presented.

II.A.2. Wave Propagation and Absorption

We will consider the requirements for propagation and absorption of electromagnetic radiation at the fundamental and second harmonic of the electron cyclotron frequency. The frequencies of interest are the cyclotron frequency, Ω,

$$\Omega = eB/m \qquad \text{(II.A.1)}$$

where B is the magnetic field; the plasma frequency, ω_p,

$$\omega_p = (ne^2/\varepsilon_o m)^{1/2} \qquad \text{(II.A.2)}$$

where n is the electron density; the upper hybrid resonance frequency, ω_{UH},

$$\omega_{UH} = \left(\omega_p^2 + \Omega^2\right)^{1/2} \quad ; \qquad \text{(II.A.3)}$$

and the right-hand and left-hand cut-off frequencies

$$\omega_{\pm} = \pm \left(\frac{\Omega}{2}\right) + \left[\left(\frac{\Omega}{2}\right)^2 + \omega_p^2\right]^{1/2} \quad . \qquad \text{(II.A.4)}$$

We define the dimensionless parameter α as

$$\alpha \equiv \frac{\omega_{po}^2}{\Omega_o^2} = \frac{m}{\varepsilon_o} \frac{n_o}{B_o^2} \qquad \text{(II.A.5)}$$

where ω_{po}, Ω_o, n_o and B_o are the values of these parameters evaluated on the plasma axis. Four possible heating modes will be considered, namely ordinary wave heating with frequency $\omega = \Omega_o$, where the wave is launched from the outside (low-field region); extra-ordinary wave heating with $\omega = \Omega_o$, where the wave is launched from the inside of the torus (high field region); extra-ordinary wave heating with $\omega = 2\Omega_o$, with the wave launched from the outside of the torus (low field region); and ordinary wave with $\omega = 2\Omega_o$.

The wave accessability for each case is illustrated in Fig. II.A.1. Note that an extra-ordinary wave launched from the outside with a frequency corresponding to the central cyclotron frequency will always encounter the cut-off at ω_+ (right-hand cut-off) and be reflected before reaching the resonant layer. This mode is therefore unsuitable for central heating; the same restriction exists for heating at the upper hybrid resonance if the wave is to be launched toward the center from the low field side.

Absorption of the ordinary wave at the fundamental cyclotron resonance derives from the theory of propagation in a warm plasma with non-vanishing density and may be considered as a finite Larmor radius effect. The wave damping increases with temperature and density and is at maximum for quasi-perpendicular propagation. The optical depth is approximately given by [LI77, FI78]:

$$\tau_{10} \approx \frac{\pi}{2} \frac{T_o}{mc^2} \alpha \, |k| R_o \qquad \text{(II.A.6)}$$

where the total absorption integrated along the wave trajectory is given by:

$$A_{10} = 1 - \exp(-\tau_{10}) \qquad \text{(II.A.7)}$$

and T_o is the central temperature, $|k|$ is the wave number at the resonance and R_o is the major radius. Numerical evaluation of (II.A.6) shows that any reasonable reactor grade plasma will be optically thick to the ordinary mode, insuring good absorption.

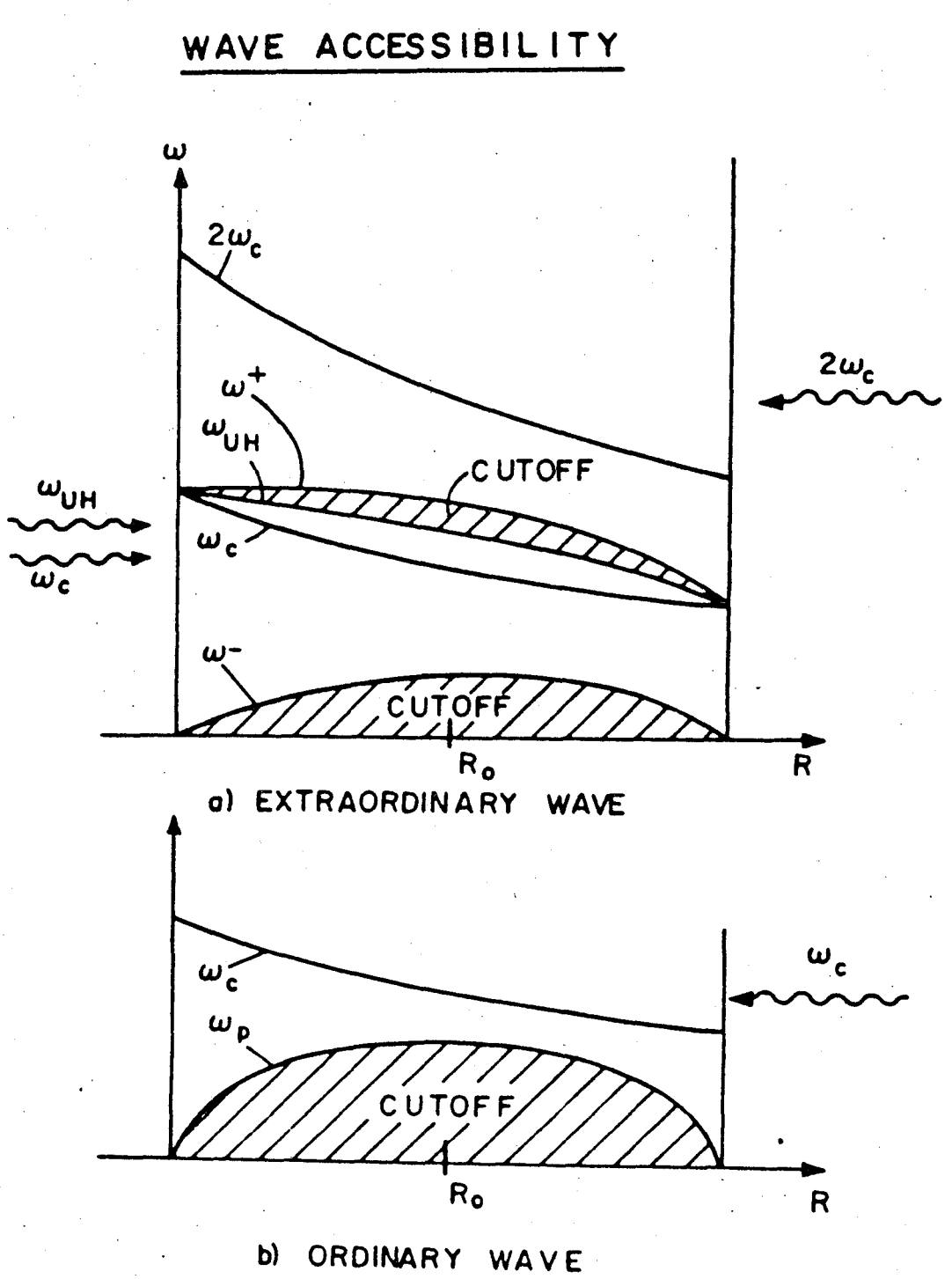

Fig. II.A.1 Wave accessibility diagram. A parabolic density profile is assumed with $\omega_{po}^2/\Omega_o^2 = 0.5$.

The ordinary wave will propagate to the central resonance providing the plasma frequency does not exceed the wave frequency, i.e.

$$\alpha < 1 \qquad \text{(II.A.8)}$$

Note that as $\alpha \to 1$ the wave number $k \to 0$ by definition of cut-off, and by (II.A.6) the optical depth $\Gamma \to 0$; hence operation exactly at the cut-off is not possible. For a given Ω, the value $\alpha \simeq 2/3$ optimizes the optical depth when $\theta \simeq \pi/2$; however, for reactor grade plasmas the numerical value of Γ_{10} is very large and optimization of this quantity is not required. Values of $\alpha > 2/3$ are therefore permissable; we note that near $\theta = \pi/2$ operation at $\alpha = 0.95$ reduces Γ_{10} by less than a factor or two below its optimum.

Propagation of the extra-ordinary wave to the resonant layer requires launching from the high field side as noted earlier. Then the wave propagates as long as the wave frequency everywhere exceeds that of the left-hand cut-off. For $\omega = \Omega_o$ this leads to the propagation condition

$$\alpha < 2 \quad . \qquad \text{(II.A.9)}$$

The absorption of the extra-ordinary wave arises from resonant energy transfer to the gyrating electron from the right circularly polarized component of the wave. However, as the density is increased the extra-ordinary wave becomes predominatly lef-circularly polarized, leading to a decrease in absorption [AL77]. The optical depth is approximately given by [LI77]

$$\Gamma_{1x} \approx \frac{\pi}{2} \frac{T_o}{mc^2} \cos^2\theta \, \frac{1}{\alpha} \, [2 + \alpha(1 - \alpha)^2 \, |k|R_o \qquad \text{(II.A.10)}$$

where θ is the angle of propagation with respect to the magnetic field and (II.A.10) is valid for $(2T_o/mc^2)^{1/2} << \frac{\pi}{2} - \theta << 1$. Thus, depending on the angle θ, the resonant layer may become partially transparent to the extraordinary wave for values of α somewhat less than the cut-off value. In this case it is conceivable that the radiation would propagate through to the upper hybrid layer (see figure 1) where either nonlinear absorption or linear mode conversion to the Bernstein wave [GO72] may take place. In the latter case subsquent cyclotron damping of the backward Bernstein mode could deposit the wave energy near the resonant layer.

Finally we consider radiation at the second harmonic of the central cyclotron freuqency. The propagation of the extraordinary mode is limited by the requirement $\omega > \omega_+$ everywhere. In terms of the parameter α this is equivalent to

$$\alpha < 2 \qquad \text{(II.A.11)}$$

which is the same as equation (II.A.9). We here consider a wave launched from the low field side. Propagation from the high field side will have a smaller limiting α, since the maximum value of ω_+ will be located at $R < R_o$. The optical depth [TA78, EN73] has a simple form for values of α well below the cutoff and for $\theta = \pi/2$,

$$\Gamma_{2x} \approx \frac{\pi}{2} \alpha \frac{T_o}{mc^2} |k| R_o \qquad \left(\Theta = \frac{\pi}{2}\right) \tag{II.A.12}$$

The ordinary mode at the second harmonic will also be absorbed, with an optical depth smaller than the above by a factor of (T/mc^2) for perpendicular propagation [TA78]

$$\Gamma_{2O} \approx \frac{\pi}{2} \alpha \left(\frac{T_o}{mc^2}\right)^2 |k| R_o \qquad \left(\theta = \frac{\pi}{2}\right) \tag{II.A.13}$$

For a reactor grade plasma $\Gamma_{2O} >> 1$ so heating at this mode is also possible. Ordinary mode propagation requires only that $\omega = 2\Omega_o > \omega_{po}$ so we find

$$\alpha < 4 \quad . \tag{II.A.14}$$

Inequalities (II.A.8), II.A.9), II.A.11), and (II.A.14) represent cut-offs for electron cyclotron and second harmonic resonance heating for both modes of polarization. Heating will typically take place with α slightly below the cut-off value, in order to maintain strong absorption while optimizing the plasma parameters. An exception may be the X-mode at the fundamental, for which absorption decreases strongly as α approaches 2. In the following treatment we use the various cut-off values for similicity; it should be understood that actual operation would in any case require α to be at least a few percent lower than this.

The X-mode at the fundamental propagates only from the high-field side, which will lead to considerable access problems in a

tokamak reactor. The other three modes considered are accessible from the outside (low-field side). All the modes considered can be shown to be optically thick for a reactor grade plasma. To be suitable for auxilliary heating, the radiation must also satisfy a start-up condition, namely that the plasma be optically thick at a relatively low temperature of 1 or 2 keV. This condition is easily satisfied by all the modes considered with the possible exception of the O-wave at $\omega = 2\Omega_o$, for which the optical depth scales with $(T/mc^2)^2$; for this mode the start-up capability is marginal, depending sensitively on the initial plasma parameters.

For each of the modes considered, the absorption will take place over a relatively narrow region of space near the resonant surface. The extent of the absorbing region and the deposition profile within that region depend on the absorption line shape and on the angle of which the propagation vector approaches the resonance, as well as the magnitude of the local absorption coefficient. The spatial width of the resonant region may be obtained from the linewidth in frequency space. For a Doppler broadened absorption profile the width of the region is approximately equal to $n_{\parallel}(T/mc^2)^{1/2}R_o$, where $n_{\parallel} \equiv ck_{\parallel}/\omega$ is the parallel index of refraction. For propagation nearly perpendicular to the magnetic field, such that $n_{\parallel} \lesssim (T/mc^2)^{1/2}$, the absorption line shape is determined by the relativistic transverse Doppler effect; this effect may be considered as arising from the relativistic variation of the electron mass. The resulting line shape is asymmetric about the non-relativistic

resonance, with the absorbing region having a width of approximately $(|k|c/\omega)(T/mc^2)R_0$ shifted toward lower field (low frequency). It should be noted that the direction of the propagation vector approaching the resonance depends not only on the launch angle but also on refraction of the wave inside the plasma, which in turn will depend on the density and density gradients. If the absorption coefficients are large, most of the power will be deposited in the wings of the resonance on the side from which the wave is launched, before reaching the nominal resonant surface. Since the absorption increases with temperature, this effect may result in a shift in the location of the absorption as the plasma is heated. In any case it is important to note that the energy deposited near a resonant layer is rapidly diffused over a flux surface. Therefore, the effective volume in which heating takes place is a toroidal shell defined by the flux surfaces passing through the energy deposition layer. For stable bulk heating and especially for control of the temperature profile it will be desireable to employ radiation sources operating over a range of frequencies, corresponding to different resonant layers in the plasma, so that the energy deposition profile can be varied in a controlled manner.

II.A.3. Implication for Reactor Parameters

As we have seen, the propagation limits for each possible

heating mode can be expressed in terms of the parameter α. By casting the reactor quantities of interest in terms of this parameter we can derive the applicable operating regime for each case. In order to determine illustrative reactor parameters, we will consider a circular cross-section tokamak reactor with parabolic density and temperature profiles, i.e.

$$n = n_o(1 - r^2/a^2)$$

$$T = T_o(1 - r^2/a^2) = T_e = T_i \qquad \text{(II.A.15)}$$

Where necessary we will further specialize to an aspect ratio $A = R_o/a = 5$ and a limiter safety factor $q(a) = aB_o/RB_p = 3.0$, where B_p is the poloidal field. The generalization to other values and profile shapes is straight-forward.

Let us first consider the scaling of average beta, $\langle\beta\rangle$, with the parameter α. Here $\langle\beta\rangle$ is defined as

$$\langle\beta\rangle = \frac{\langle n(T_e + T_i)\rangle}{B_o^2/2\mu_o} \qquad \text{(II.A.16)}$$

where the brackets signify an average over the plasma volume. Combining (II.A.15) and (II.A.16) gives

$$\langle\beta\rangle = \frac{2}{3}\frac{n_o T_o}{B_o^2/2\mu_o} = \frac{4}{3}\alpha\frac{T_o}{mc^2} \qquad \text{(II.A.17)}$$

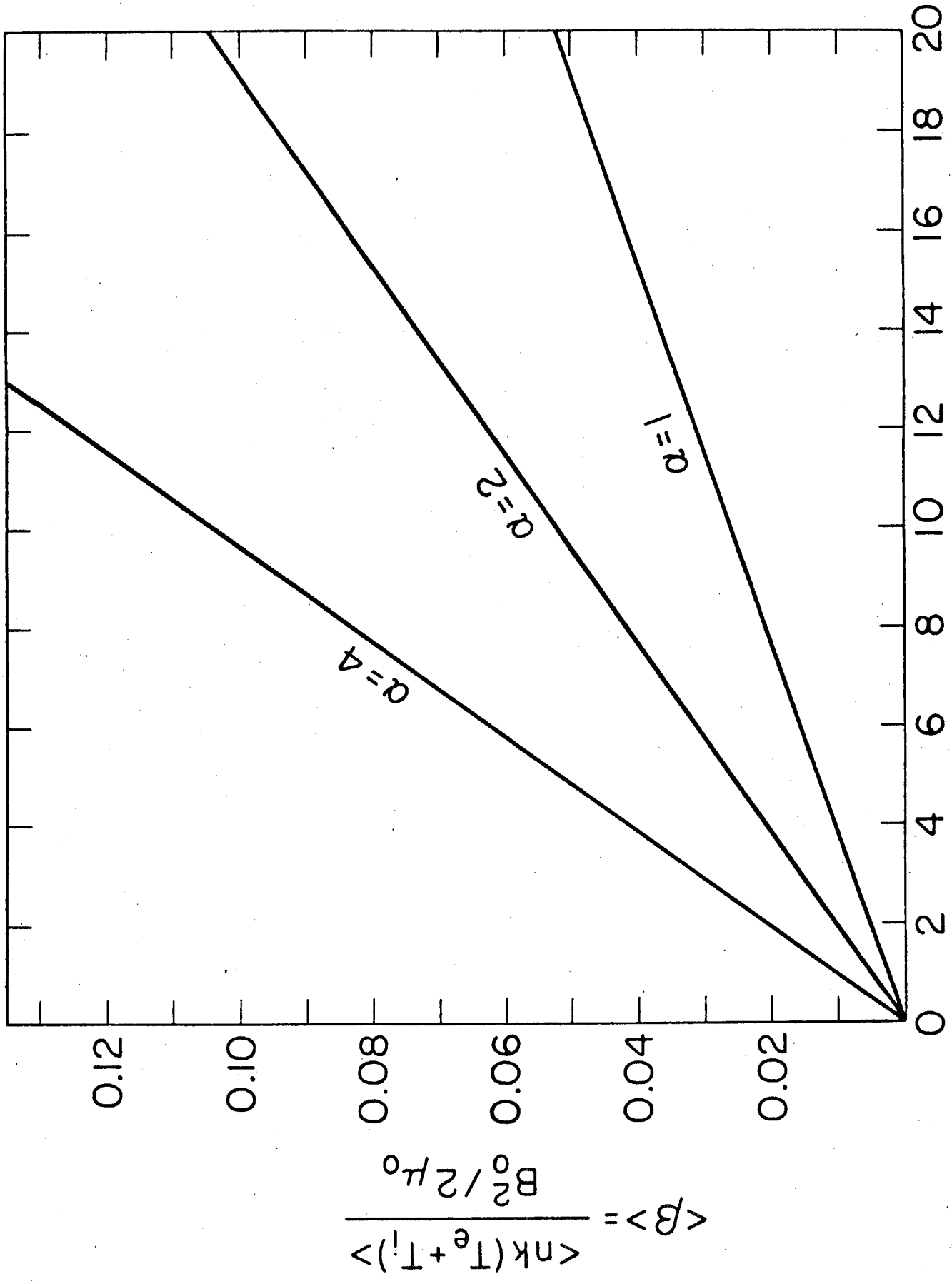

Fig. II.A.2 $\langle\beta\rangle$ vs. T_o

where we have made use of the definition $\alpha = mn_o/\varepsilon_o B_o^2$. The $<\beta>$ limits corresponding to the various cut-offs are shown in Fig. (II.A.2); note that for $\alpha = 1$, which is the limiting value for propagation of the ordinary mode at the fundamental, and a typical central reactor temperature of 15 keV, $<\beta>$ is 3.9%.

The average fusion power density $<P_f>$ is given by

$$<P_f> = 7.04 \times 10^{-7} <n^2(\overline{\sigma v})_{DT}> \text{ MW/m}^3$$
$$= n_o^2 f(T_o) \qquad \text{(II.A.18)}$$

where f is a function only of T_o and profile shape. By introducing the parameter α we can rewrite (12) in terms of the toroidal field and obtain the relation

$$B_o = \left(\frac{m}{\varepsilon_o \alpha}\right)^{1/2} \left(\frac{<P_f>}{f(T_o)}\right)^{1/4} \qquad \text{(II.A.19)}$$

Thus we see that the operating field scales with $(<P_f>^{1/4} \alpha^{-1/2})$. Curves corresponding to typical values of $<P_f>$ as a function of B_o and T_o are shown in Figs. II.A.3, II.A.4 and II.A.5. The frequency appropriate to each field is shown on the right hand axis. Note that for ECRH heating to be utilized when the reactor is run at a moderate value of $<P_f> = 5$ MW/m^3 the technically attractive O-wave fundamental technique requires a central field greater than 6 Tesla for a central temperature of 15 keV. X-wave heating at Ω_o permits the lowest combination of field and frequency, but is unfavorable from an engineering standpoint because of the difficulty of inside

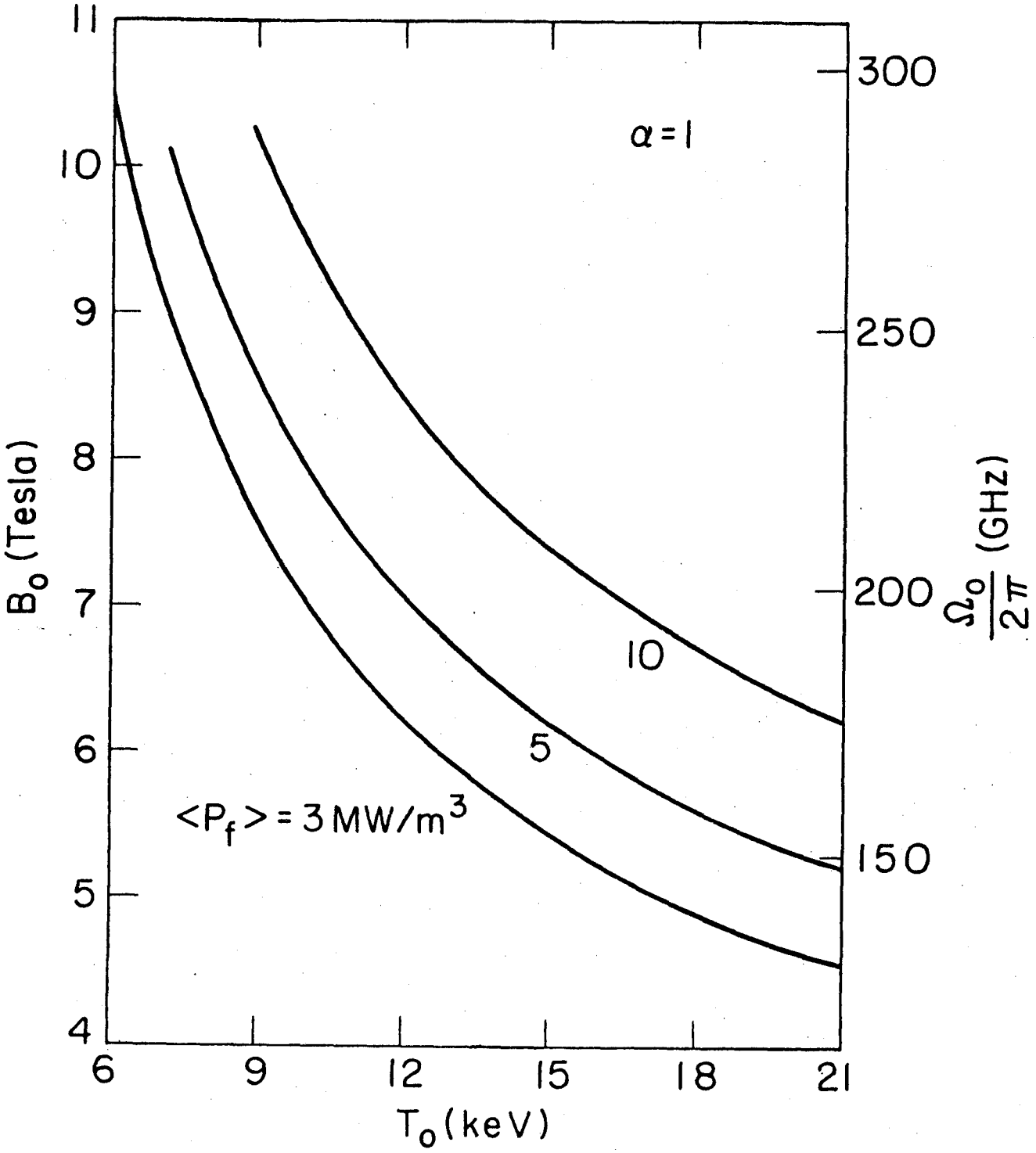

Fig. II.A.3 Fusion power density vs. B_o and T_o for O-wave heating at $\omega = \Omega_o$.

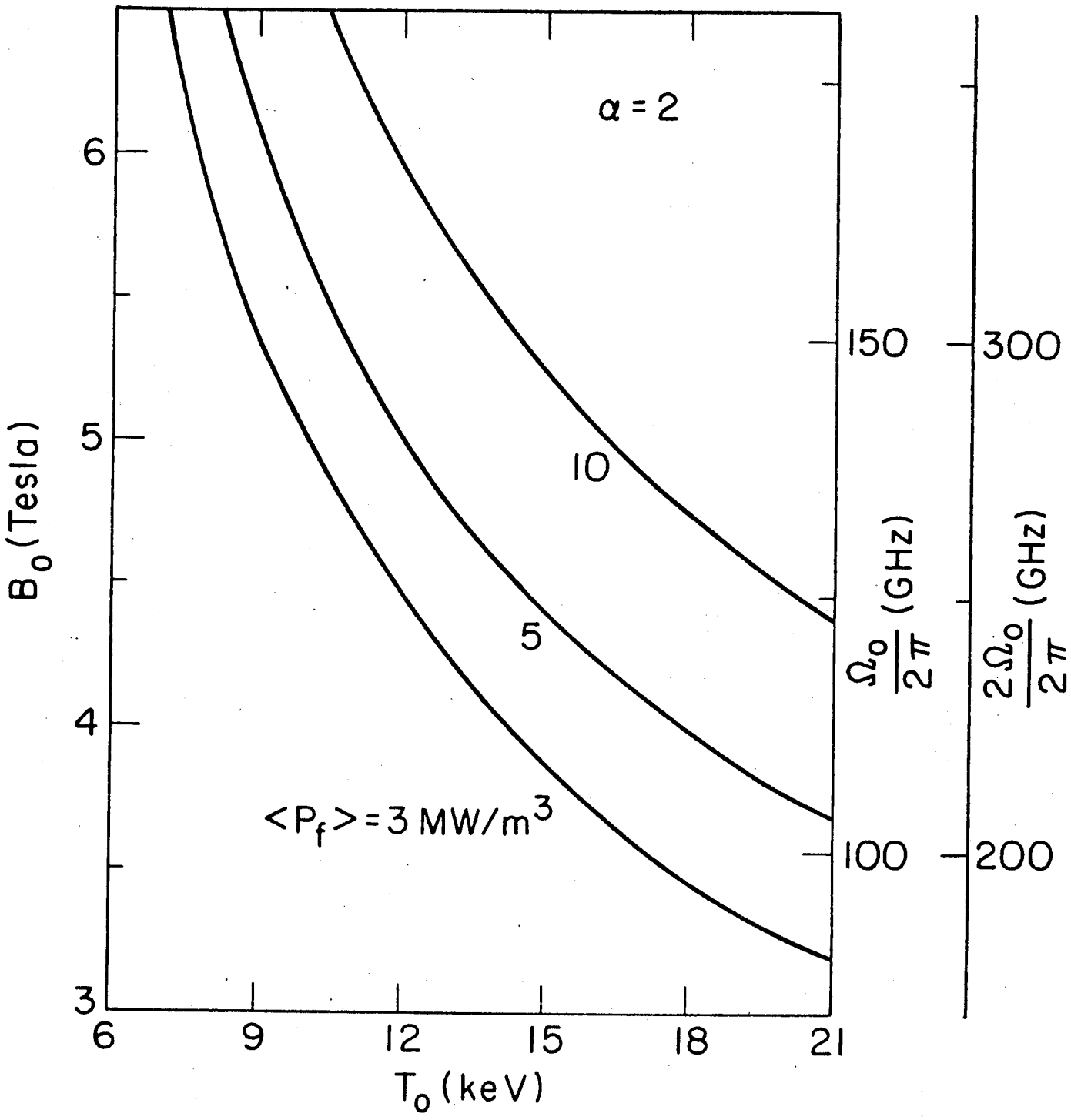

Fig. II.A.4 Fusion power density vs. B_0 and T_0 for x-wave heating at $\omega = \Omega_0$ or $2\ \Omega_0$.

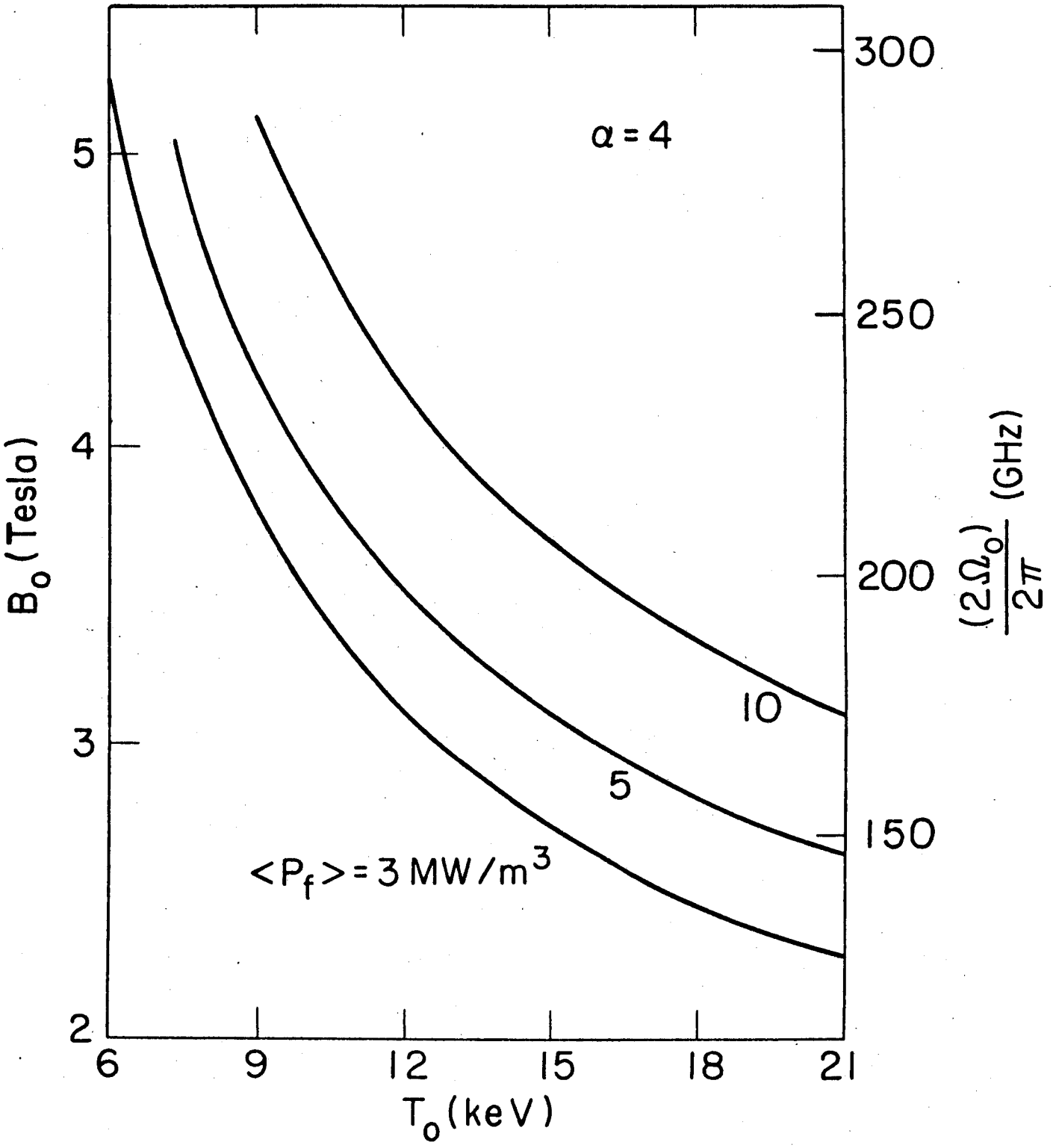

Fig. II.A.5 Fusion power density vs. B_0 and T_0 for O-wave heating at $\omega = 2\,\Omega_0$.

access. Second harmonic heating with the O-wave is consistent with a low field (3.5 T), high beta device, providing the target plasma is sufficiently hot to provide adequate absorption at start-up. The required field for a given $\langle P_f \rangle$ is reduced somewhat by operation at elevated temperature. However, there are disadvantages to operating at increased temperature which will be discussed below.

Ignition in a reactor plasma is achieved when the power deposited directly by charged fusion products exceeds losses due to thermal conduction and radiation. The ignition condition can be expressed in terms of the quantity $[n_o\tau_E]_{ign}$ as a function of temperature, where τ_E is the global energy confinement time. We introduce the empirical scaling law for τ_E [JA76],

$$[n_o\tau_E]_{emp} = 3.8 \times 10^{-21}(n_o a)^2 \ m^{-3}s \qquad \text{(II.A.20)}$$

which may be applied provided $(n_o\tau_E)_{emp}$ does not exceed the neoclassical value. We can define the margin of ignition M_I as the ratio

$$M_I \equiv \frac{[n_o\tau_E]_{emp}}{[n_o\tau_E]_{ign}} \qquad \text{(II.A.21)}$$

and the donominator can be written

$$[n_o\tau_E]_{ign} = \frac{n_o^2 T_o}{P_f^* - P_b} \qquad \text{(II.A.22)}$$

where P_f^* is the fusion power density emitted in charged particles, equal to 20% of $<P_f>$, and P_b is the radiation power due to bremmsstrahlung. Equation (II.A.22) is appropriate for plasmas with $Z_{eff} = 1.0$, i.e. where impurity radiation is insignificant. Since P_f^* is directly proportional to $<P_f>$ and the scaling of P_b with temperature is well-known, we can evaluate the ratio M_I in terms of the propagation parameter α. The result is shown as a family of curves in the B_o - T_o plane in Figs. II.A.6, II.A.7 and II.A.8, where we have taken the minor radius a = 1.2 meters, which is typical of recent tokamak reactor designs; we have also included the increased radiation loss due to the presence of alpha particles. From equations II.A.20 - II.A.22, we note that M_I scales as $B_o^4\ a^2\ \alpha^2$ for any given temperature. For $\alpha = 1$(O-mode, $\omega = \Omega_o$) ignition at a central temperature of 15 keV requires an axial field of 5.3 T, corresponding to a frequency of 150 GHz.

The empirical scaling law II.A.20 is derived from results in present experimental devices, which typically operate in the collisional or plateau regimes. Extrapolation of II.A.20 to higher temperature and reduced collisionality is uncertain, and values of M_I greater than unity may be required to achieve ignition. Significant impurity radiation will also necessitate an increased M_I. If a margin of ignition of 3 is required, a field of 7 T and frequency of 200 GHz will be needed for $\alpha = 1$ and $\omega = \Omega_o$. Heating at the second harmonic reduces the magnetic field requirement, since α can be increased, Fig. II.A.7 and II.A.8, but does not permit a reduction

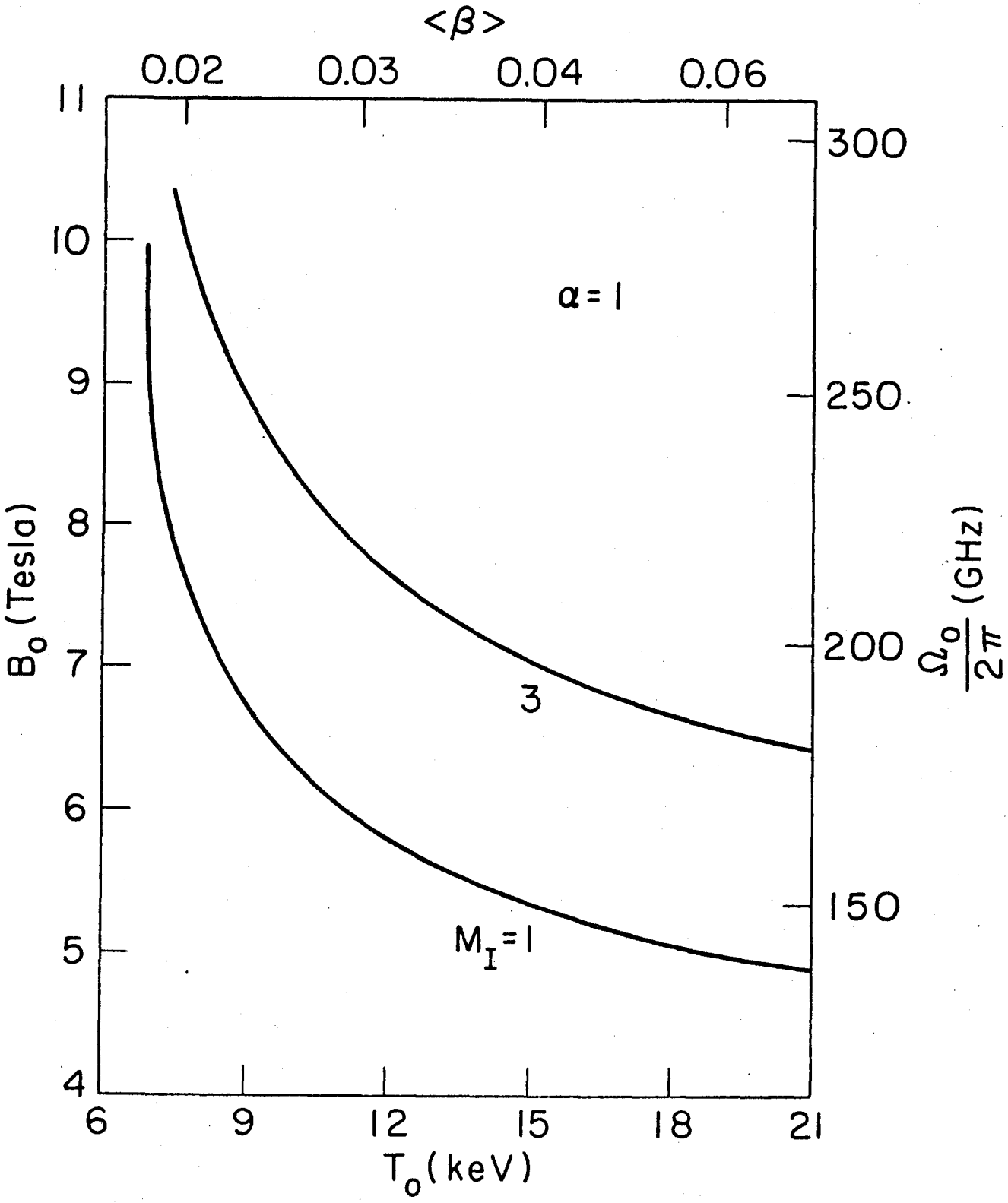

Fig. II.A.6 The margin of ignition, M_I, is plotted vs. B_o and T_o (or Ω_o and $\langle\beta\rangle$) for $\alpha = 1$.

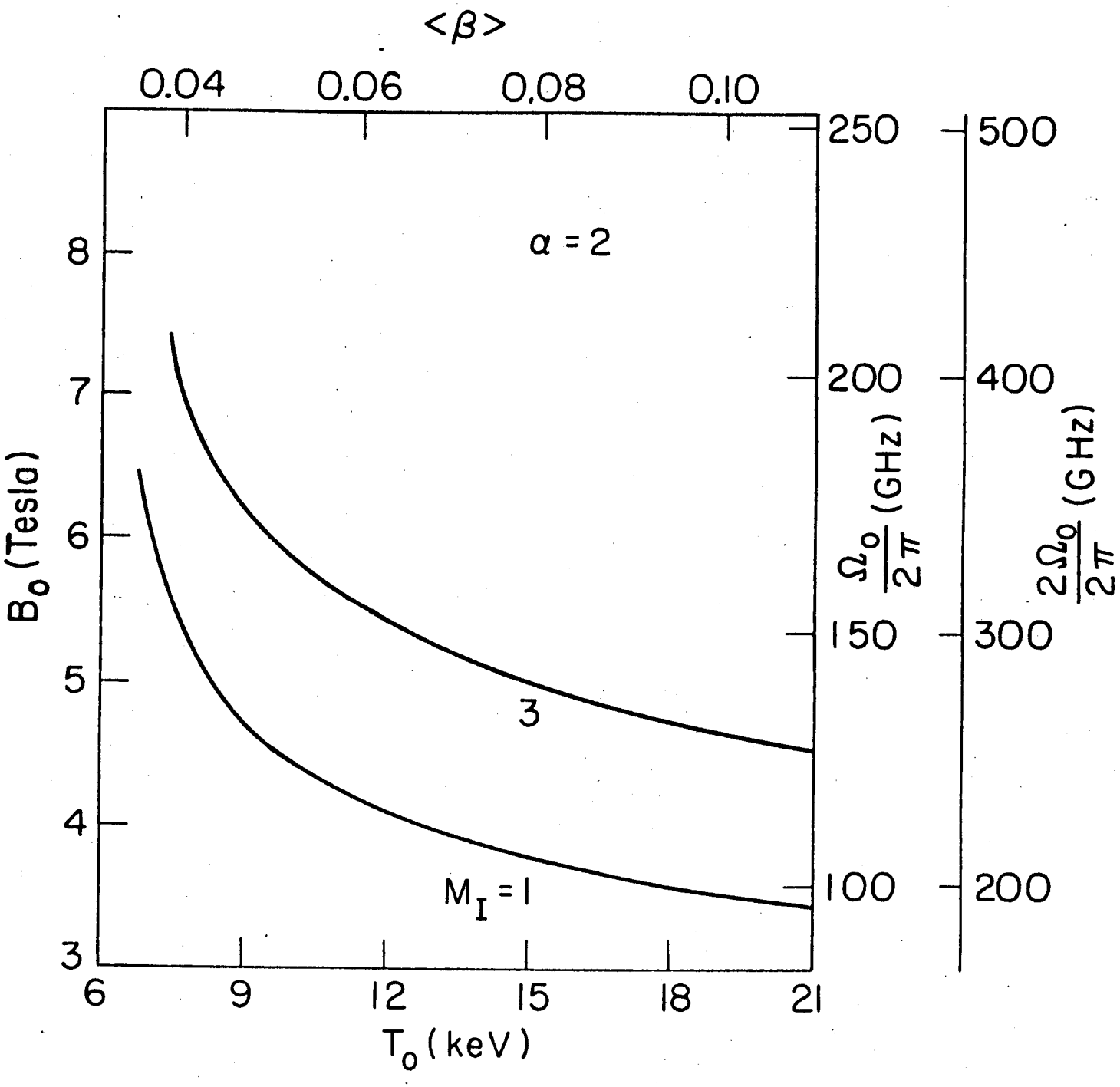

Fig. II.A.7 Same as II.A.6 but $\alpha = 2$.

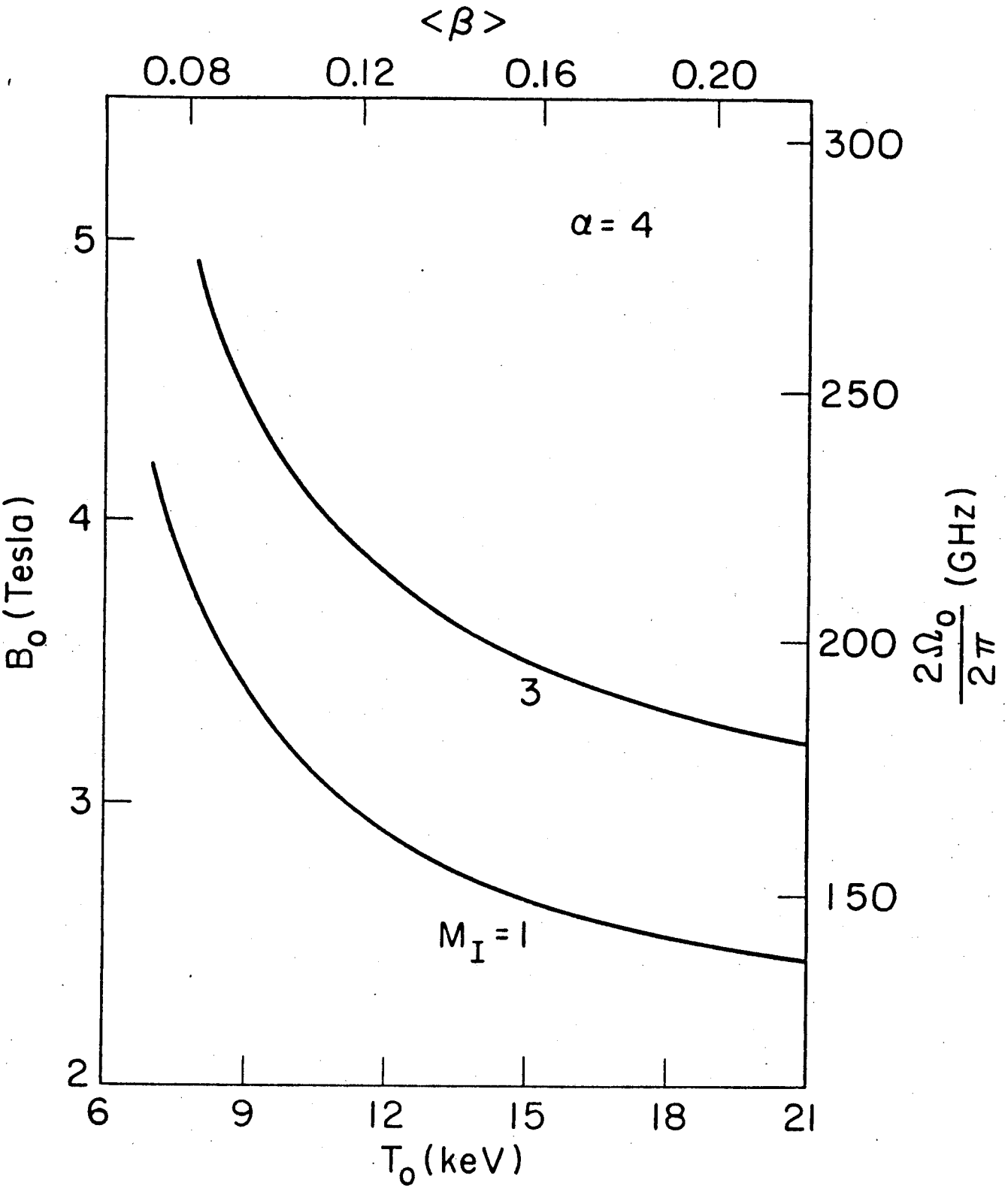

Fig. II.A.8 Same as II.A.6 but $\alpha = 4$.

in frequency. As shown in Fig. II.A.7 the frequency is reduced for the case of the X-mode at $\omega = \Omega_o$ and $\alpha \approx 2$. However, the necessity of providing access on the inboard side of the tokamak for this mode may be very difficult to meet, and efficient absorption might not be realized for values of α much above 1, in which case the higher fields and frequencies of Fig. II.A.6 will apply to this mode as well. We note that while increasing the temperature somewhat reduces the requirements to obtain a given M_I, the resulting lowered collisionality may degrade confinement such that a higher margin is needed to achieve ignition. Moreover, as will be discussed below, the attendant increase in plasma beta can adversely affect the MHD stability of the system.

II.A.4 Characteristics of an ECR Heated Tokamak Reactor

By combining the previously derived relationships with possible technological and economic boundaries we can now characterize a tokamak power reactor which is heated with ECRH. We will consider a thermal power rating of 1500 MW_{th}, including exothermal tritium breeding interactions in the blanket such that Q_{fus} = 22.4 MeV. The thermal power output for a circular plasma is then written as

$$W_{th} = 2\pi^2 A a^3 \langle P_f \rangle \left(\frac{22.4}{17.6}\right) = 1500 \quad MW_{th} \qquad \text{(II.A.23)}$$

Since we have taken A = 5, Eq.(II.A.23) provides a relationship

between the minor radius a and $\langle P_f \rangle$, which in turn can be written as a function of B_o, T_o, and the propagation parameter α. We now introduce an engineering limit due to the neutron wall loading and assume that the neutron power flux through the first wall should not exceed 4 MW/m^2. Taking the first wall radius to be $r_W = (1.15\ a)$ and making use of (II.A.23) gives the inequality

$$a \geq 1.02 \text{ m} \tag{II.A.24}$$

An upper limit on the size of a reactor may be imposed by cost considerations. For illustrative purposes we will require that the minor radius satisfy

$$a \leq 1.5 \text{ m} \tag{II.A.25}$$

which is consistent with current tokamak power reactor designs. [ST98]. It should be observed that since we have fixed the reactor thermal power, the size limitations of (II.A.24) and (II.A.25) may be alternately expressed as bounds on the permissible fusion power density. In this form we may rewrite the wall loading restriction as

$$\langle P_f \rangle \leq 11.25 \text{ MW/m}^3 \tag{II.A.26}$$

while the maximum size implies that

$$\langle P_f \rangle \geq 3.54 \text{ MW/m}^3 \tag{II.A.27}$$

The technology of the radiation source, assumed to be a gyrotron-type cyclotron resonance maser, imposes a limit on the

frequency utilized. The power generated by a single tube can be expected to decrease strongly with increasing frequency. For this discussion, we assume $\nu_{RF} \leq 300$ GHz for adequate power capability. This corresponds to a maximum central field of

$$B_o \leq \begin{cases} 10.7 \text{ Tesla } (\omega = \Omega_o) \\ 5.36 \text{ Tesla } (\omega = 2\Omega_o) \end{cases} \qquad \text{(II.A.28)}$$

It should be pointed out that we are here considering only that class of reactors for which ECRH is used to heat the plasma to the operating point, where ignition or near-ignition driven operation is assumed to take place. One could conceive of a class of "alpha-boosted" reactors in which ignition occurs for parameters corresponding to values of $\langle P_f \rangle$ lower than (II.A.27). In this case excess power in the emitted alpha particles would be used to increase the temperature and density to "boost" the system to an acceptable operating point. Since ECRH would be used only for the first stage of the two-step heating process, the final operating point would not need to satisfy the propagation conditions (II.A.8), (II.A.9), (II.A.11) or (II.A.14). Since only ECR heating to ignition is required for an alpha boosted reactor, the curves of Figs. (II.A) alone define the relevant parameters. Another possible means of relaxing in ECRH requirement would be the use of adiabatic compression in major radius following initial heating at low magnetic field. [CO77]. Although the parameter α would not be changed by

compression, heating at low magnetic field would reduce the ECRH frequency requirement by C, where C is the ratio of the major radius of the initial plasma to the major radius of the final plasma. However, the use of large compression ratios in power reactors is unattractive.

For 1500 MW_{th} reactor heated to the operating point by ECRH, the boundaries of the operating regimes given by (II.A.26) - (II.A.28) are depicted in Fig. (II.A.9). Three nonintersecting regions corresponding to the propagation limits α = 1, 2, and 4 are shown. Additional constraints on the operating space arise from considerations of ignition and MHD stability. Within the bounds depicted in Fig. (II.A.9), the ignition condition is met or exceeded if the empirical scaling law for confinement applies. However, as noted earlier, the validity of this law at high temperature is uncertain. Dashed lines in Fig. (II.A.9) indicate the restrictions introduced by assuming that M_I = 3 is required to achieve ignition. Horizontal lines at B_o = 10.7 and 5.36 T define the probable high frequency limit of 300 GHz, for fundamental and second harmonic interaction respectively, as indicated in Eq. (II.A.28). For ordinary wave heating (α = 1,4) these lines intersect the operating space at the high-field, low temperature extreme; the region appropriate for α = 2, corresponding to extraordinary wave heating at either the fundamental or harmonic, however, lies partially above the high frequency limit for the harmonic. Heating with the X-wave at $2\Omega_o$ and $\alpha \approx 2$ will be restricted unless CRM technology is extended

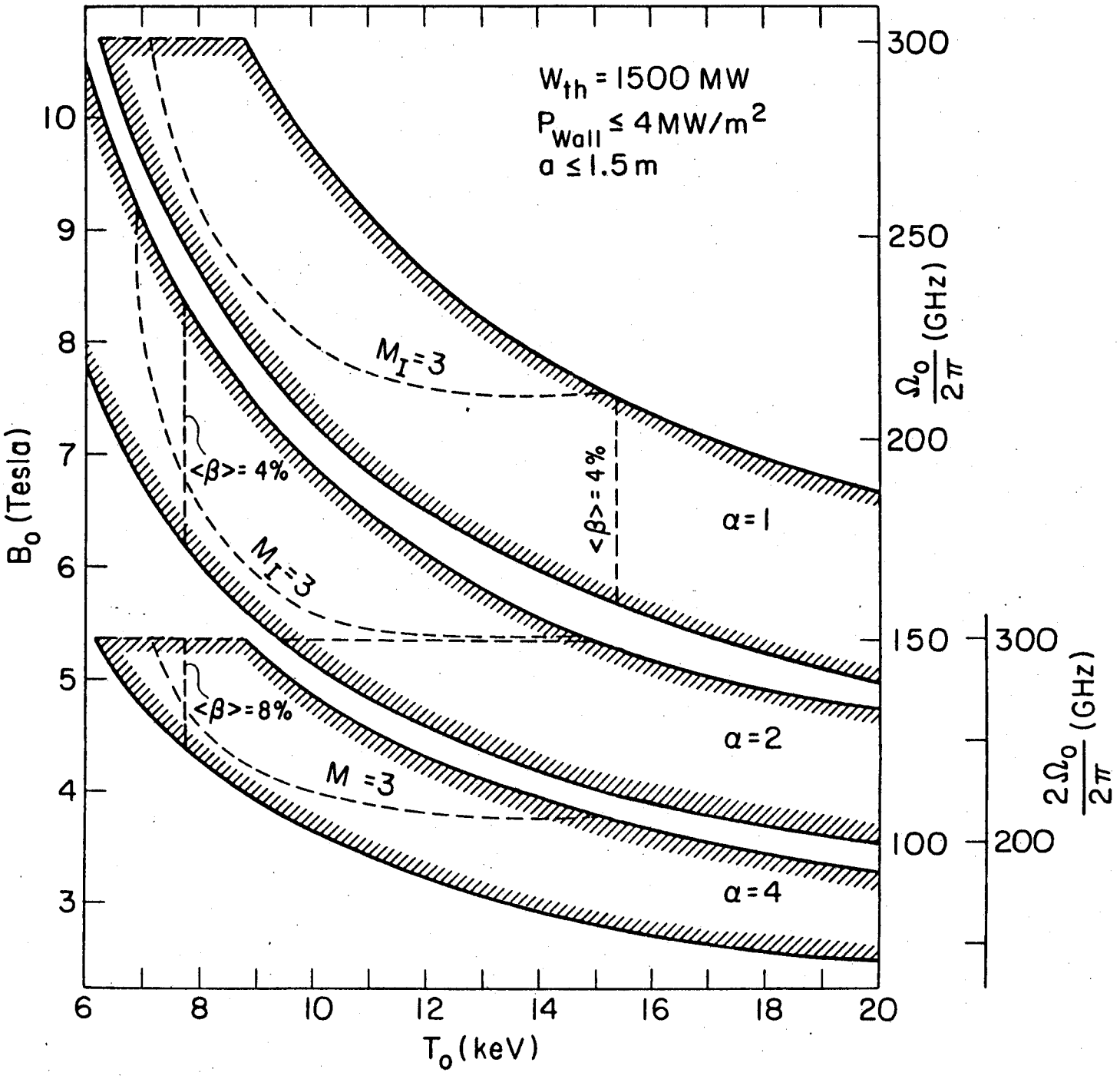

Fig. II.A.9 Allowed regimes of ECR Heated Tokamak Reactor Operation.

well into the submillimeter band.

Vertical bars of constant $\langle\beta\rangle$ are indicated for each region (see Eq. (II.A.17), Fig. (II.A.2)). We note that the $\alpha = 1$ island lies mostly to the left of the line representing $\langle\beta\rangle = 4\%$, which represents a possible limit imposed by the onset of the ballooning mode [TO77]. For the X-wave island, only the section below $T_o = 7.7$ keV satisfies this condition, while essentially the entire region for $\alpha = 4$ has $\langle\beta\rangle \geq 8\%$. Thus, the latter two cases will be viable only if stable high $\langle\beta\rangle$ equilibria can be produced, as for example, in a flux conserving tokamak configuration. [CL77, BA77].

II.A.5 Estimated Heating Power

The power, P, required to heat the tokamak plasma to ignition temperature can be calculated using the empirical scaling relation. The total energy of the plasma, W, is given by:

$$W = \frac{3}{2} \langle n(T_e + T_i) \rangle V \qquad \text{(II.A.28)}$$

where T_e and T_i are given in energy units, the brackets indicate a volume average, and V is the plasma volume. We assume that at time $t = 0$, the plasma has been heated to a temperature of 1 or 2 keV by the ohmic heating power, P_{OH}, and that the plasma energy is W_o. The gyrotrons are then turned on at a power level P. The equation governing the change in plasma energy, W, is:

$$\frac{dW}{dt} = P - \frac{W}{\tau_E} + P_{OH} \qquad \text{(II.A.29)}$$

In order to solve this equation, we assume that the energy confinement time, τ_E, is independent of plasma temperature, and, therefore of time. We fix P to be independent of time also. Although P_{OH} will vary with temperature and, therefore, time, we may neglect this variation if $P >> P_{OH}$. Then the solution of Eq. (II.A.29) is:

$$W = W_0 + P\tau_E \left[1 - \exp\left(- t/\tau_E\right)\right]$$

Let us assume that we wish to heat to a final temperature $T_f = T_e = T_i$, with the total plasma energy equal to W_P when $T = T_f$, and that we wish to accomplish this in a time τ. Then the ratio of plasma energy W_P at time τ to energy supplied by the gyrotrons, $W_G = P\tau$, is given by:

$$\frac{W_P}{W_G} = \frac{\tau_E}{\tau}\left[1 - \exp\left(-\tau/\tau_E\right)\right] \qquad \text{(II.A.30)}$$

This shows that if $\tau << \tau_E$, W_P will be nearly equal to W_G, which means that all of the power emitted by the gyrotrons will be expended in heating the plasma. However, the heating power, $P = W_G/\tau = W_P/\tau$ will be unacceptably high if $\tau << \tau_E$. On the other hand, if $\tau >> \tau_E$, the heating power will be small, but W_P/W_G will also be very small, indicating that most of the gyrotron power will be wasted. An optimum heating time, τ, is τ roughly equal to τ_E.

If $\tau = \tau_E$, then $W_P/W_G = 0.63$, so that most of the gyrotron energy is absorbed by the plasma. On the other hand, the gyrotron power $P = W_G/\tau = W_G/\tau_E = 1.6\ W_P/\tau_E$ will be close to the minimum possible value of heating power (which is W_P/τ_E and applies for $\tau >> \tau_E$).

A parametric study could be undertaken of the optimum heating time, τ. This optimum time would depend on the relative importance of minimizing the gyrotron power level by increasing τ vs. the importance of minimizing the energy expenditure in heating by decreasing τ. However, the total reactor operation must also be taken into account. A more complete analysis of plasma considerations during the gyrotron heating phase may be obtained by consulting the start-up description of the final report of the HFCTR reactor conceptual design study [CO79]. As a reasonable approximation, we proceed under the assumption that the heating time $\tau \approx \tau_E$.

The power, P, required to heat the tokamak plasma to ignition temperature can then be written approximately as:

$$P = \frac{3 \langle n(\Delta T_e + \Delta T_i) \rangle V}{2\tau_E} \qquad \text{(II.A.31)}$$

where ΔT_e and ΔT_i are the temperature rise of electrons and ions, respectively, and V is the total plasma volume, ignoring alpha particle heating and radiation loss. Using the empirical scaling relation for $n_o\tau_E$ vs. $n_o^2 a^2$, Eq. (II.A.31) leads to the simple result:

$$P \approx 0.8\ R\ \Delta T_o \quad MW \tag{II.A.32}$$

where R is the major radius in meters and ΔT_o is in keV. For a tokamak power reactor with a major radius of 6.0 m and a central temperature of 15 keV the required heating power is approximately 75 MW.

Eq. (II.A.31) is predicted on 100% coupling of the ECR radiation to the plasma, and any reduction in coupling will require an increase in P. Poor coupling and confinement will result, for example, if heating causes a tail of hot electrons [LI77]. Such tail heating was not observed in experiments at lower plasma densities [AL72] but may occur at higher heating intensities.

II.A.6 Summary of Physics Constraints

Based on this simple treatment we can make several statements about operating regimes, as well as about the probable microwave source requirements.

For ordinary wave heating ($\alpha \leq 1$) at $\omega = \Omega_o$, $\langle\beta\rangle$ is limited to less than 0.039 for $T_o < 15$ keV. We may derive two constraints on the characteristics of a reactor, one based on the fusion power density and the other based on the margin of ignition. To heat typical tokamak reactors operating at central temperatures of around 15 keV and fusion power densities of 5 MW/m^3 requires a magnetic field of order 6.25 T and an ECRH frequency of about 175 GHz.

Based upon the empirical scaling law for the energy confinement time a magnetic field of 5.4 T and an ECRH frequency of 150 GHz are needed to insure ignition for typical tokamak parameters of $a = 1.2$ m and $T_o = 15$ keV. Higher magnetic fields and ECRH frequencies will be necessary if impurities are present of if the energy confinement degrades with increasing temperature.

Heating with the extraordinary mode at $\omega = \Omega_o$ close to $\alpha = 2$ can be used to lower the magnetic field and ECRH frequency requirements if high $\langle\beta\rangle$ (> 4%) MHD stability is allowed. The frequency requirement would be around 125 GHz for typical reactor parameters. However, the necessity of launching this wave from the inboard side of the vacuum chamber may severely complicate the engineering of the reactor.

Based upon propagation requirements second harmonic absorption using the extraordinary mode permits heating at α close to 2 at relatively high $\langle\beta\rangle$ (0.05 - 0.10) and low field. However, ECRH frequencies greater than those required for ordinary mode fundamental heating will be needed to achieve the same fusion power densities and ignition margin. For example, for $T(0) = 15$ keV and $P_f = 5$ MW/m^3 a field of only 4.4 T is sufficient but a frequency of 250 GHz is necessary; beta for this case would be 0.078.

An extremely high $\langle\beta\rangle$ (10 - 15%), low field reactor is consistent with O-wave heating at $\omega = 2\Omega_o$, and propagation parameters $\omega_{po}^2/\Omega_o^2 \approx 4$. However, although this technique reduces magnetic field requirements relative to ordinary mode fundamental heating, the

gyrotron frequency requirement is not decreased. Furthermore, this technique depends on creating an initial target plasma of sufficiently high temperature to absorb the microwave radiation; central temperatures of the order of 2-3 keV would have to be achieved during the ohmic heating phase. Thus O-wave heating at $\omega = 2\Omega_0$ may have very limited applicability.

A two-stage reactor, heated by ECRH to ignition at low $\langle P_f \rangle$ and low $\langle \beta \rangle$ and subsequently driven to an operating point at higher plasma density by alpha particle heating alone can be envisioned. In this case the magnetic field and the ECRH frequency requirements would no longer be determined by the desired fusion power density. However, the inability to heat at the operating point can significantly restrict the options for controlling thermal equilibrium and stability. Furthermore, since $\langle \beta \rangle$ must be substantially increased by the alpha heating, its value at ignition should be relatively low to insure MHD stability at the operating point. Because $\langle \beta \rangle$ is proportional to (αT_0), and T_0 required for ignition must exceed 6 keV, α may well be restricted during the ECRH heating phase to values of order 1, regardless of the propagation limit for the specific mode used. From Fig. (II.A.6) we see that even for a two-stage reactor central fields of the order of 5 Tesla or greater will be required, even if ignition occurs at $M_I = 1$.

Each of the ECRH reactor models discussed requires the use of high RF frequencies, with the possible exception of X-mode heating at the fundamental. The most favorable approach, i.e.

the one satisfying the most conservative assumption, as well as the most straight-forward, is for a reactor heated by the ordinary mode at $\omega = \Omega_o$. High fields will probably be needed since $<\beta>$ will be limited to modest values by the propagation requirement. The required frequency will thus be of the order 150 - 200 GHz. Lower field, high beta reactors heated at the second harmonic would require as high or higher frequencies, (approaching 300 GHz). Hence, it is likely that the development of high frequency ($\geq$ 150 GHz) gyrotron sources will be necessary for the use of ECRH to heat tokamak power reactors.

II.B. Description of Reactor and Plant

II.B.1 Selection of Tokamak Power Reactor Design

The major topic of research in the present design study is the ECR heating system for a tokamak power reactor. In order to avoid the obvious additional effort related to developing a new reactor design just for this study, we have selected an existing tokamak reactor design. The selection of a reactor design was made consistent with the physics constraints for penetration of the ECR radiation as described in Section II.A. Previous tokamak power reactor designs have generally incorporated neutral beam heating of the plasma to ignition. The adaption of the reactor design to ECR heating thus requires the elimination of the neutral beam lines and associated equipment, such as ripple field coils. The elimination of ripple field coils can effect the procedure for control of the burn and this will be discussed below. The ECR system may be designed into the power reactor without changing any of the major systems, such as toroidal magnets, blanket, etc. The ports, however, must be redesigned for the launching of the high frequency RF radiation. In addition, we have taken the opportunity to include in this report some additional changes to the tokamak reactor design. These changes are in the area of improved modularization and will be discussed in a separate sub-section of Section II.

The conditions for wave penetration and absorption in ECR

heating impose constraints on the tokamak reactor characteristics, as was discussed in Section II.A. The selection of a reactor design that is compatible with ECR heating may be analyzed as follows. The preferred mode for ECR heating is ordinary wave heating at $\omega \approx \Omega$, as discussed in Section II.A. One advantage of this mode is that it minimizes the frequency requirement of the RF radiation. If we further impose the condition of a moderate size tokamak reactor, then high density operation, $n_o > 4 \times 10^{20}$ m^{-3} is required. The option space for reactor operation under these conditions is discussed in greater detail in Section II.A. and is shown in Fig. (II.A.9). We conclude, however, that, for good penetration of the ECR radiation, the tokamak toroidal field on axis will have to be in the range of about 5.5 to 7.5 T. This means that the required gyrotron frequency will be in the range of 150 - 200 GHz.

The major requirements for the selection of a tokamak reactor design are that the field on axis be about 5.5 to 7.5 T and that the reactor be relatively compact, with high density operation. The reactor design which fulfills these requirements, and was selected for this study, is the high field, compact tokamak reactor (HFCTR). The HFCTR reactor is compact (R_o = 6.0 m) and operates at high field (B_T = 7.4 T). The gyrotron frequency corresponding to B_T = 7.4 T is 207 GHz. For convenience, we will assume a gyrotron frequency of 200 GHz in later portions of this study. The design value of the central electron density in HFCTR is 5.2×10^{20} m^{-3}. This yields a value of $\alpha = \omega_{po}^2/\Omega_o^2$ of 0.98. Since α is less than unity, the ECR

radiation should penetrate to the center of the plasma. However, when α is very close to unity, refraction of the microwave radiation is a major problem. If α is about 0.9, which requires a central denstiy of 4.8×10^{20} m^{-3}, refraction is expected to be of small consequence. This difference in central density amounts to only 10% and has only a negligible effect on other machine parameters [see HFCTR study, C079]. Rather than modify the HFCTR design slightly to accommodate a small change in density, we will, for convenience, continue to utilize the original HFCTR parameters throughout most of this report. In the discussion on wave absorption, we will allow the design value of density to vary slightly to obtain $\alpha \approx 0.9$; this change will be explicitly stated.

II.B.2 Description of HFCTR (High Field Compact Tokamak Reactor)

II.B.2.1 General Description of HFCTR

In this section, we will give a brief description of the HFCTR reactor. This description should be useful as background information for the later sections on the ECR heating system. The drawings utilized will show the original HFCTR design with neutral beam lines. The redesign of the ports for microwave heating is shown in Section II.F of this study.

The HFCTR reactor is shown in Fig. (II.B.1) and, in elevation view, in Fig. (II.B.2). The major features of this reactor may be summarized as follows. The reactor is a compact (R_o = 6.0 m),

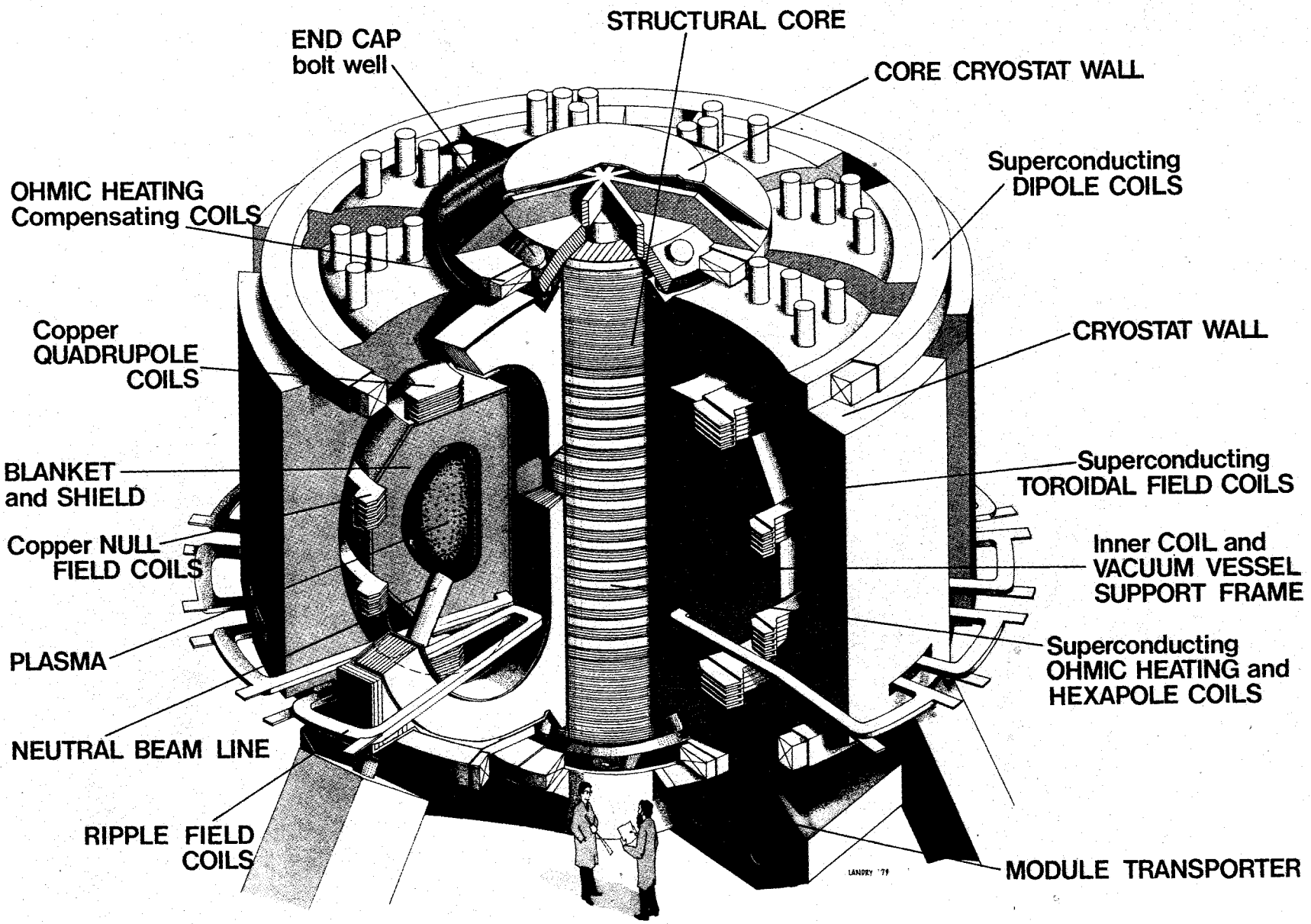

Fig. II.B.1 High Field Compact Tokamak Reactor (HFCTR)

TABLE 1 - II

HFCTR MAGNET SYSTEM PARAMETERS

TF Coils	
Number of coils	16
Current in each coil	13.9 MA
Field at R_o = 6 m	7.4 T
Maximum field in coil at R = 3.4 m	13.1 T
Inside aperture	6.5 m wide 10.5 m high
Ripple at outside plasma surface	1% max.
Maximum stress in winding structure	210 MPa (0.1% strain)
Stored energy	40 GJ
Weight of each coil assembly	425 tonnes
VF Coils	
Superconducting dipole coils	-21.2 MA
Copper quadrupole coils	6.4 MA
Copper null-field coils	6.4 MA pulsed
Copper null-field stored energy	500 MJ
Superconducting hexapole coils	-8.0 MA
VF Stored energy	2 GJ
OH Coils	38 MA total
OH Field	4.1 T max.
OH Stored energy (fast and slow pulsed)	1 GJ
Magnet System	
Peak power input (5 sec start-up)	565 MW
Average power input (500 sec burn)	80 MW
Startup flux requirement	120 Wb
Burn flux requirement	60 Wb

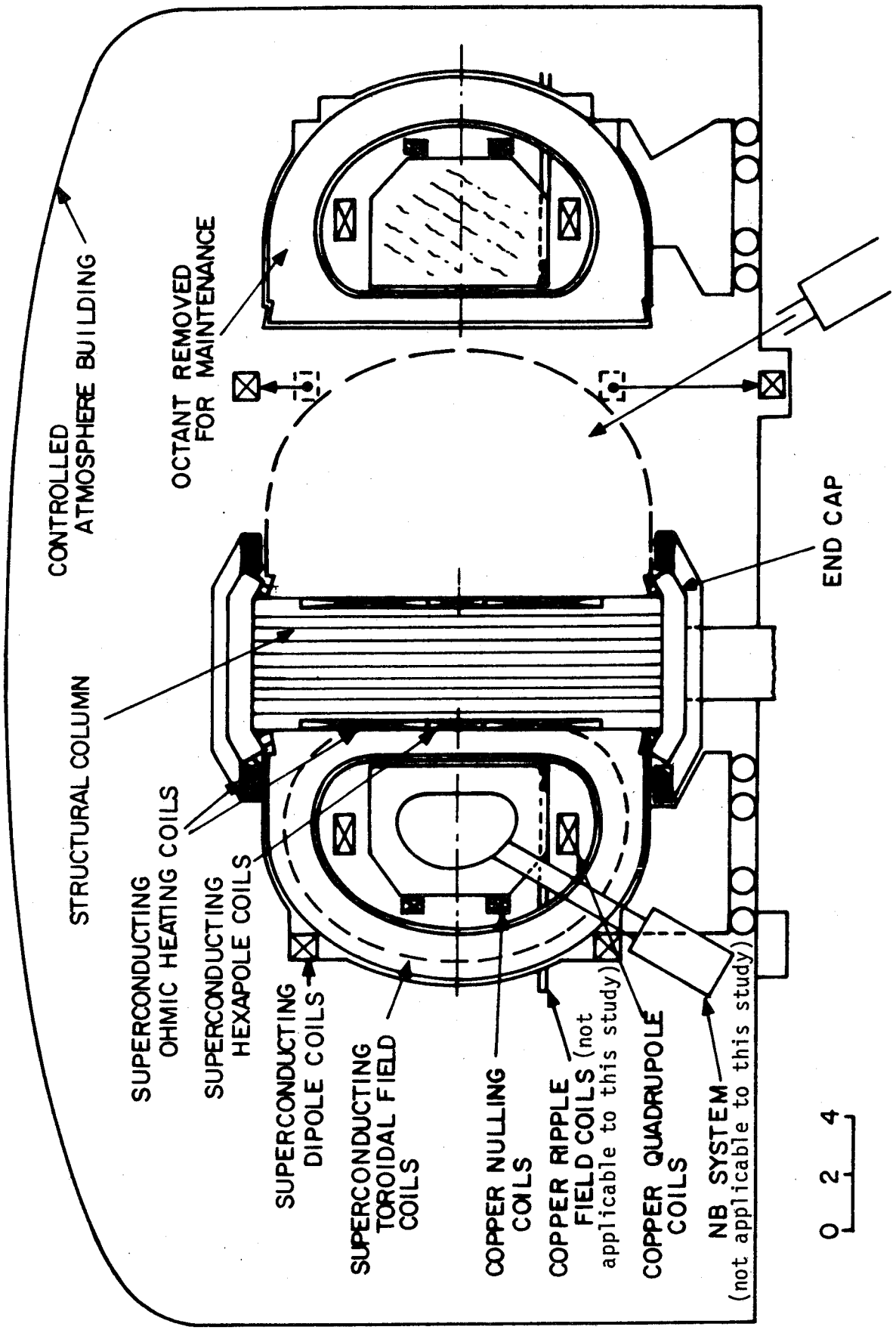

Fig. II.B.2 Elevation view of HFCTR showing all magnet systems.

high field (7.4 T) tokamak demonstration power reactor which can produce fusion power densities as high as 10 MW/m^3 with a spatially averaged value of toroidal beta of less than 5%. The HFCTR design is based upon minimal extrapolation from experimentally established plasma confinement and MHD stability in tokamak devices. A unique design for the NB_3Sn toroidal-field magnet system reduces the stress in the high-field trunk region and allows the achievement of high fields with a small radial build. An integrated system of automated actuators, vacuum and current-carrying mechanical joints and flexible cryostats allow total modularization of the reactor, including the coil systems. A detailed estimate of maintenance operation time indicates the possibility of very high plant availability. The modest value of toroidal beta permits a simple plasma-shaping coil system, located inside the TF coil trunk. In the original design, heating of the central plasma was achieved by the use of ripple-assisted injection of 120 keV D° beams. This will be replaced in the present study by ECR heating of the central plasma by 200 GHz gyrotrons. The plasma heating, in both cases, will be used for dynamic control of the plasma temperature during the burn period. A FLIBE-lithium blanket is designed especially for high-power-density operation in a high-field environment, and gives an overall tritium breeding ratio of 1.05. Thermal power levels as high as 3,300 MW can be obtained. Ignition can be obtained with a toroidal beta as low as 2.5% and the reactor can be operated at power levels as low as 1,000 MW. An advanced toroidal field coil design allows

all reactor subsystems other than the TF coil to have approximately the same size and specific power as those in higher beta (8 - 10%) designs operated at lower field with more conventional magnet systems.

II.B.2.2 Plasma Characteristics

The empirical scaling relation for the energy confinement time was used as a guideline for determining the plasma half-width needed to ensure ignition. The reference base case operating parameters for the HFCTR are listed in Table II.B.1

TABLE II.B.1

REFERENCE HFCTR PARAMETERS

Machine Parameters	
Major radius, R_o(m)	6.0
Plasma halfwidth, a(m)	1.2
Aspect ratio	5.0
Plasma shape factor, S	1.5
Field at plasma, B_T(T)	7.4
Maximum field at winding, B_{T_o} (T)	13.1
Plasma volume, $V_p(m^3)$	317
First wall area, $A_W(m^2)$	475
Plasma Parameters	
Safety factor at r = a, q(a)	3.0
Average toroidal beta, $\langle\beta_T\rangle$	0.04
Plasma current, (MA)	6.7
Electron density, $n(m^{-3})$	$5.2\ 10^{20}(1 - \frac{r^3}{a^3})$
Electron ion temp, T (keV)	$12.4\ (1 - \frac{r^2}{a^2})$
Z_{eff} (Helium + Mo)	1.2
$(\bar{n}\tau_E)_{emp}/(\bar{n}\tau_E)_{ign}$	2.4
Heating Power, P(MW)	100
Power Production	
Av. fusion power density, $\bar{P}_f(MS/m^3)$	7.7
14-Mev neutron wall loading, P_W(85% duty, MW/m^2)	3.4
Total fusion power, $\bar{P}_f V_p$	2440
Av. thermal power, P_{th}(85% duty, MW)	2470
Machine Parameters	
Gross electric power, P_g(35% efficiency, MW)	870
Net electric power, P_n(MW)	775
Plant efficiency, n_p(%)	31

II.B.2.3 Plasma Heating Sequence

In the reference HFCTR design, plasma heating is carried out by injection of 120 keV D° beams using the ripple-trapping injection method. In the present study, as previously stated, the gyrotron ECR system replaces the neutral injectors. The general characteristics of the plasma heating and temperature control are not greatly affected by this change.

The gyrotron system will be in operation at full power only during the final stages of the plasma start-up sequence. Plasma start-up occurs in three phases: (1) the plasma initiation phase; (2) the plasma expansion phase; and (3) the bulk heating phase. In the plasma initiation phase (0 sec. $< t \lesssim 0.03$ sec.) the plasma is broken down at an ion density of $n = 10^{19}\ m^{-3}$ with a loop voltage of $V_{loop} = 250$ volts. Preionization may be required to assist in the breakdown. The minor radius is 0.25 meter, set by forcing the plasma center 0.25 meter from the limiter. An initial oxygen concentration of 0.8%, giving $Z_{eff} = 1.5$, is assumed. When oxygen line radiation becomes small, the density increases to $n = 3 \times 10^{19}\ m^{-3}$ and the current density rises to $J = 410\ \frac{kA}{m^2}$. It may be possible to utilize the gyrotron system, designed for bulk heating to ignition, in the plasma initiation phase for preionization and in the early stages of plasma heating. The use of gyrotrons for tokamak start-up has been discussed in detail by Peng et al. [PE78]. Rosenfeld has considered the use of a 1 MW gyroklystron

system for preionization in a TNS sized machine [RO79].

In general, the power requirements for bulk heating are much greater than for start-up and therefore represent a much greater challenge to gyrotron tube and microwave transmission technology. The possibility of tokamak start-up with gyrotrons is currently under investigation at the ISX-B experiment at O.R.N.L. If this technique should prove feasible on ISX-B and other tokamaks, it could be incorporated into tokamak reactor design. The advantage of the technique is that it reduces the loop voltage required during start-up and thus reduces the cost of the power supplies of the reactor. In gyrotron assisted start-up, the radiation is absorbed at the upper hybrid layer, ω_{UH}, and is polarized as an extraordinary wave. It is possible that the gyrotron system, which is designed for bulk heating with the ordinary wave at the cyclotron frequency, Ω, could still be applied to preionization. This is possible if the radiation is reflected from the walls and changes polarization. During preionization, the density is low and $\omega_{UH} \approx \Omega$.

In the plasma expansion phase (.03 sec. < t < 2.0 sec.) the plasma minor radius is expanded from a = 0.25 meter to a = 1.2 meters by moving the plasma center away from the limiter while n and J are held constant. The plasma is then deformed slowly into an ellipse with a shape factor (circumference/$2\pi a$) of S = 1.4 and a cross-sectional area of 8.4 m^2.

In the first bulk heating phase (2.0 sec < t < 3.9 sec), only a total of 12.5 MW of gyrotron output power is activated.

While the ohmic and gyrotron power continue to heat the plasma, the plasma current rises gradually to its final value of 6.7 MA. In the second, major bulk heating phase (3.9 sec < t < 8.4 sec), the full gyrotron power is activated, for a total power of 100 MW. The average density is rapidly increased to 3.1×10^{20} m^{-3}, with the average temperature rising to the final operation value of 8 keV. When β_p is 50% to 75% of its final value, the hexapole field coils deform the ellipse into a D-shape of S = 1.5 while the plasma cross section remains at 8.4 m^2. The variation of n and T_e during start-up are illustrated in Fig. (II.B.3).

Unlike neutral beams which heat both electrons and ions, ECR radiation heats only the electrons. Energy is then transferred to the ions via collisions. The energy deposition of the neutral beams occurs near the plasma center, but it is not highly localized. ECR radiation at frequency ω is absorbed in a local region where the cyclotron frequency, Ω, is nearly equal to ω. Since Ω is a function of major radius R, the possibility exists for control of the spatial location of the heating and thus of control of the temperature profile of the plasma. In fact, the point of energy deposition can be controlled by several techniques. The set of gyrotrons used for heating could be divided into subsets of different frequency in order to heat according to a specified spatial profile. Or the gyrotrons could all have the same frequency but different angles of launch. It might even be possible to vary the frequency electronically on a time scale of order one second in

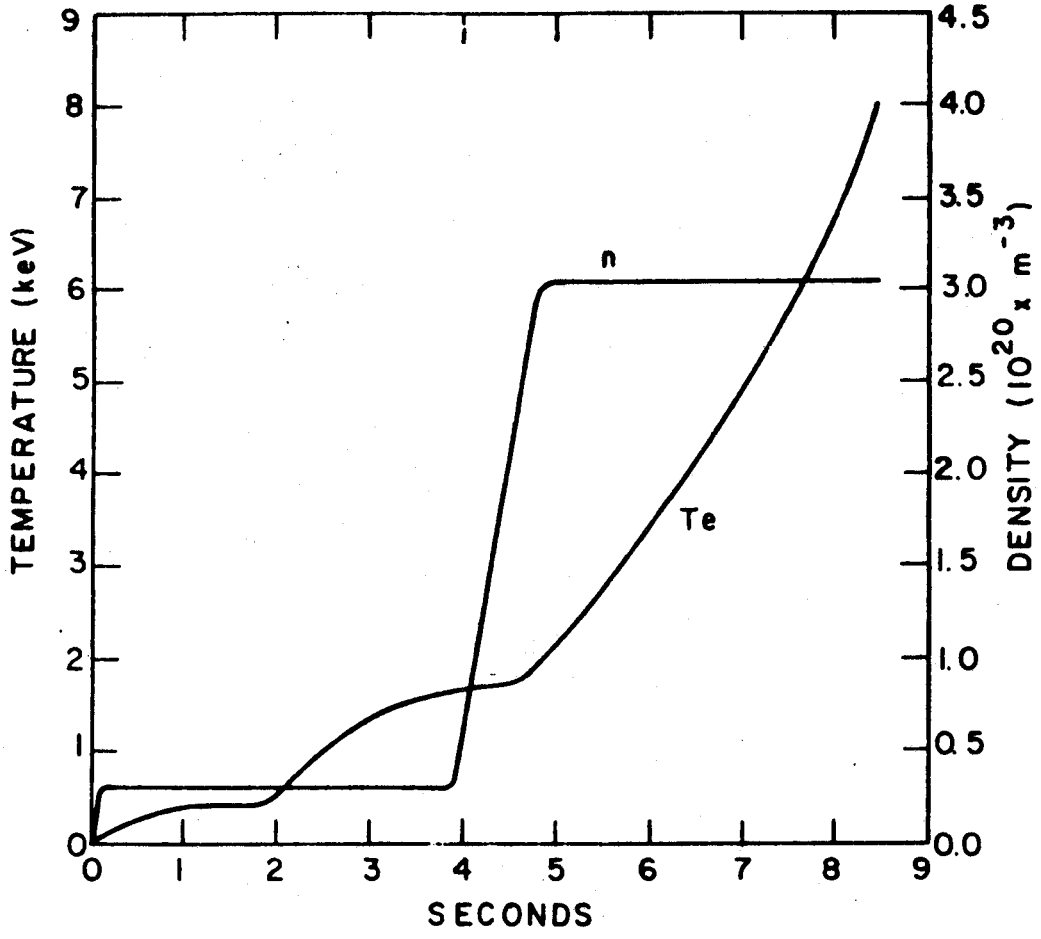

Fig. II.B.3 Average temperature and density during start-up.

order to improve the energy deposition profile. These techniques can lead to improved energy confinement.

After the start-up phase of plasma heating, the plasma will be in the ignition regime. The gyrotron system may be shut off and there is power input into the plasma resulting from alpha particle generation. In the original HFCTR design, the burn control was accomplished in part by use of the ripple field coils. These coils produce a vertically asymmetric toroidal-field ripple of controllable magnitude, which causes an enhanced outward drift of banana-trapped alpha particles. In the present reactor design using ECR heating, the ripple field coils are not needed for neutral beam injection. It would simplify the reactor design if the ripple field coils were also eliminated. However, this can only be allowed if an alternative means of burn control is envisioned. There are many alternative techniques that have been suggested for burn control. We mention here only one technique, namely active control of the burn by stabilization of the thermal runaway using auxiliary heating. This technique is mentioned because it would require additional output from the gyrotron heating system at high power levels during the burn time of 500 secs. The topic of active burn control of nearly ignited plasmas has been analyzed recently by Bromberg et al [BR79]. However, we will not specify active burn control or any specific technique for stabilization of the thermal runaway in the present study. Consequently, the gyrotron heating system will only be assumed to be emitting at full power level (100 MW) for a time

of about 4 sec., during the main plasma heating phase.

II.B.2.4 Modularization of Tokamak System

As an introduction to a later section in this report on the improved modularization of the reactor, we will briefly outline here the modularization system of HFCTR.

The tokamak is divided into 8 modules which can be rapidly and automatically connected and disconnected and removed for replacement by a spare module. It has been estimated that all mechanical operations in a module replacement can be performed in two days. Although one other demo reactor design [MI76] has enunciated a method for rapid, automatic replacement of a blanket and first wall module, this is the first design to incorporate a method for the rapid replacement of a complete 45° sector which includes the TF coils. This approach removes the need to assume that the coil systems will be failsafe and need not be serviceable. It also permits periodic annealing of defects in the matrix of the superconducting cable. The success of an experimental program to establish the reliability of the joining concepts in this design could demonstrate that the tokamak is a topologically acceptable configuration for maintenance in a utility environment.

The reactor is designed so that the exchange of a module is accomplished by built in automatic devices. There are no time consuming hand operations that must be performed with manipulators. All power and coolant connections are made by remotely actuated quick disconnects and only those connections are actuated that are on the module which is to be moved. The waveguide system for the

ECR system is designed so that it also may be rapidly disconnected and reconnected during a module exchange.

II.B.3 Reactor Plant Layout

A plant layout was developed for the ECRH-heated tokamak reactor in order to study whether the propagation of high-frequency radiation imposed significant limitations on the disposition of gyrotron tubes. ECRH, while not as limited as neutral beams, should be relatively close to the plasma load in order to reduce propagation losses. Because of the obvious advantages in both reliability and maintainability, it is desireable to place the gyrotron tubes in a separate, well-shielded building, outside of the reactor cell.

It is difficult to define a conservative design with all of the gyrotrons placed in a single building, because of the relatively low-Q of copper at 200 GHz. Even using greatly oversized waveguides and optical techniques, the transmission losses for the relatively straight runs in the reference design utilizing four gyrotron buildings are 10 - 20%. If only one building were used, the transmission losses to the farthest port would be approximately trebled, or alternatively the diameter of the oversized waveguide would have to be increased, increasing costs through additional width as well as length. The waveguide to the farthest port in a one building design would also be difficult to layout so that it did not interfere with overhead cranes or other devices requiring machine access.

If four gyrotron buildings were permitted for a four port

design, a short and simple run of waveguide would be possible, with only two bends to avoid neutron streaming and allow easy disassembly of reactor modules. This design is shown in Fig. (II.B.4). The compatibility of three additional buildings with competing requirements for space near the reactor design was studied by modifying the plant layout for Rose's actinide burning tokamak reactor [RO77]. Building positions were rearranged, until an effective layout was achieved. The layout recommended for the ECRH-heated reactor has utility runs for all electrical power supplies, and cryogenic, tritium and hydraulic lines which are actually shorter than those for the original layout without the gyrotron buildings. It also accommodates the need for a hot cell and heat exchanger immediately adjacent to the reactor cell.

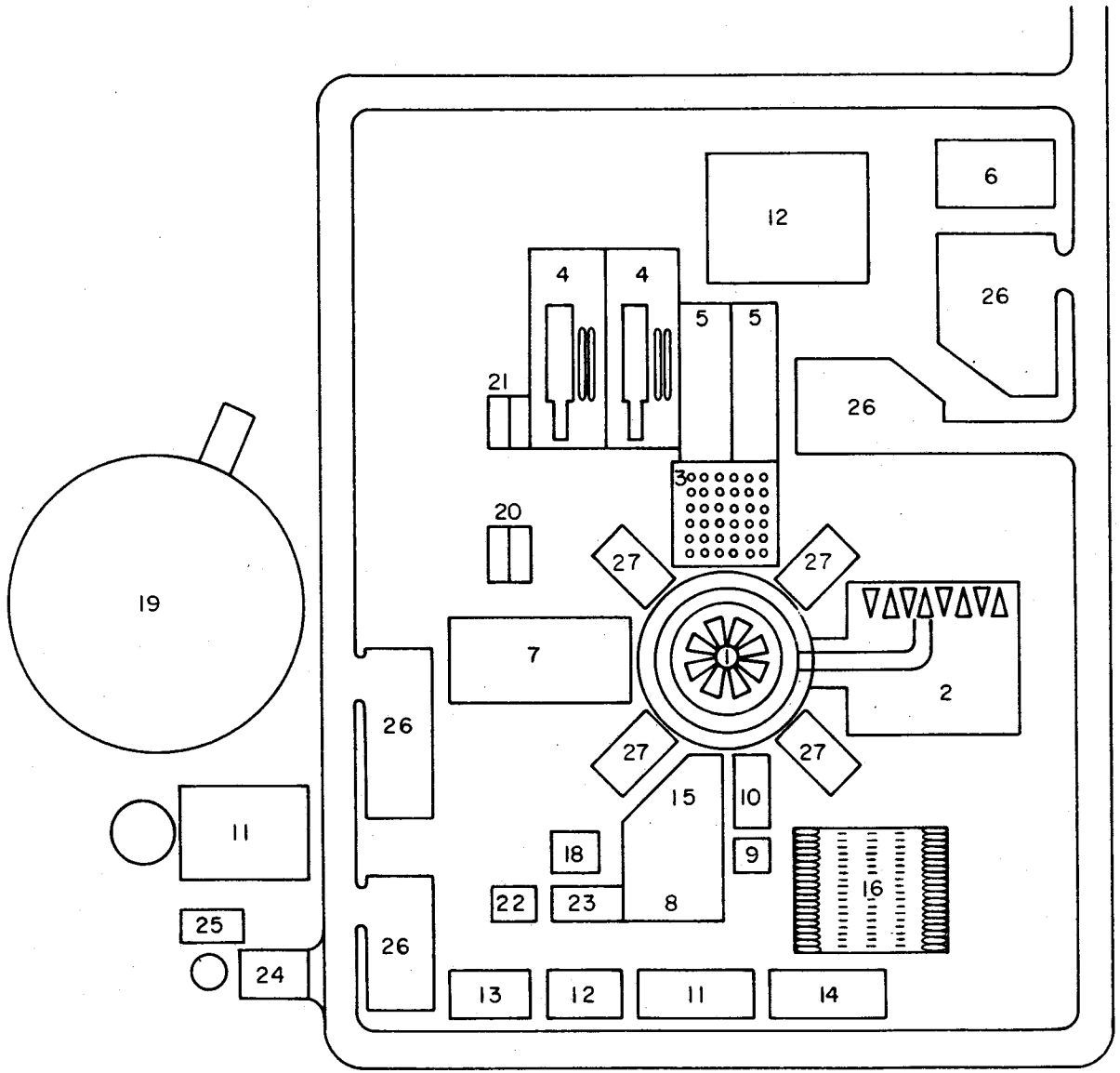

1. Reactor Containment
2. Reactor Service (Maintenance/ Blanket Handling)
3. Heat Exchanger
4. Power Conversion (Steam)
5. Control and Turbine Service
6. Administration/Services
7. Power Conditioning
8. Control/Electrical
9. Nitrogen Processing System
10. Helium Processing System
11. Cooling Water Processing System
12. Tritium Processing System
13. Lithium Processing System
14. Radwaste Storage
15. Electrical Energy Storage
16. Helium Storage
17. Shops/Warehouse/Shipping
18. Emergency Power
19. Heat Rejection and Pumping
20. Input Substation/Switchgear
21. Output Substation/Switchgear
22. Fuel Storage
23. Auxiliary Cooling
24. Waste Treatment
25. Fire Pump House/Tanks
26. Parking
27. ECRH Power Conditioning

Fig. II.B.4 Conceptual Plant Layout for HFCTR Heated to Ignition by ECRH

II.C. DESIGN STUDY OF HIGH POWER, HIGH FREQUENCY GYROTRONS

II.C.1. Introduction

The electron cyclotron resonance maser (ECM) has been investigated extensively over the past two decades, and has been demonstrated to be an efficient, high power source of millimeter and submillimeter radiation [FL77, HI77]. These studies and experiments have identified the important features of ECM's as well as the many technological problems that require a vigorous research and development program. In this section, we analyze the performance characteristics of high power, high frequency gyrotrons using a parametric analysis. By determining the basic design parameters of an ECM as well as analyzing the major technological barriers, a parametric study serves as a useful aid in selecting the most promising path to the utilization of ECRH to heat a commercial, power-producing tokamak.

In a parametric analysis, all the performance characteristics and the complex interrelations among the parameters describing the gyrotron system are modelled in a self-consistent computer code. This algonthm should be kept simple enough that an intentive understanding of the physical processes involved is possible, yet be sufficiently realistic that the important variables of the system are accurately modelled. Studies can then be performed to determine the sensitivity of the operational characteristics of the

gyrotron to variations of its design variables. Tradeoff studies can be conducted to eliminate design options technically not feasible, to explore more promising designs, and to point out the critical technological problems that must be more fully addressed in the future. Such an analysis allows one to determine the most promising design options as well as the regime of operation that is consistent with realistic engineering constraints. Parametric models can also be used to identify attractive new design points that can subsequently be investigated in greater detail, as well as quickly determine the implications fo proposed design changes.

The purpose of this section is to present a summary of the results of our parametric analysis of a gyrotron that is designed to heat a commercial tokamak and that conforms to the physics constraints discussed in the previous section. The major technological problems have been identified as well as their possible solutions always assuming a conservative extrapolation of presently available technology. In our analysis a number of important questions were addressed:

(i) What are the major design parameters of an ECM and how are they interrelated?

(ii) How do the technological and physical constraints limit the parametric space in which an ECM can operate?

(iii) What are the characteristics of an optimized design, and what procedure can be followed to determine the associated device parameters?

(iv) What are the problems associated with operating at high power and high frequency?

Questions (i) and (ii) are discussed in Section II.C.2. A detailed description of the gyrotron model used in our investigation is presented in this section, as well as a discussion of the major constraints imposed by physics and technology. Section II.C.3. explores how the efficiency of the device is influenced by variations of the major design parameters. Questions (iii) and (iv) are addressed in Section II.C.4. An optimization procedure is outlined, and the operating regime available to a gyrotron is established. In addition, the parameters of the reference gyrotron design used in this report are presented and discussed. Section II.C.5. reviews the major conclusions and outlines possible directions for further design study work.

II.C.2. Gyrotron Model

The model used in this analysis of high power, high frequency gyrotrons is based to a large extent on an earlier design study of a 10 kW, 200 GHz gyrotron [TE78]. The appropriate alterations have been introduced into the 10 kW study so that it can be applied to gyrotrons with output powers of hundreds of kilowatts. We will begin the description of the algorithm by discussing the basic assumptions and constants of the model.

We have assumed the gyrotron is operating in a steady state, and that all parameters are independent of time. We have also selected the gyromonotron, a special version of the gyrotron with a single, axisymmetric resonant cavity. We do not rule out the possibility that another device, for example the gyroklystron, may eventually emerge as the optimum device for tokamak plasma heating. However, at the present time the gyromonotron, hereafter to be referred to as simply the gyrotron, is the most widely investigated form of ECM, and also the most powerful source of millimeter and sub-millimeter radiation.

The gyrotron will be operated at the fundamental, that is, $\omega \simeq \omega_c$ where ω_c is the electron gyrofrequency. Operation at the second harmonic, $\omega \simeq 2\omega_c$, would at first seem more attractive as a result of the reduced magnetic field requirements in the cavity. However, our analysis shows that $2\omega_c$ operation is less efficient than ω_c for the present design. This conclusion is based on the nonlinear theory of Nusinovich and Erm [NU72], which will be described later in greater detail. Using their calculations, we find that the overall efficiency, η_T, of a gyrotron operating at $2\omega_c$ is substantially lower than for a fundamental gyrotron. Because of the low transverse efficiency, $\eta_\perp$ (see discussion of efficiency in next section for definition). Although $\eta_\perp$ can be improved for $\omega = 2\omega_c$ operation by increasing the Q of the resonator, this gain is offset by the increased power lossed due to ohmic heating of the cavity walls, so that high total efficiency cannot

be achieved. One can also improve $\eta_\perp$ for $2\omega_c$ operation by increasing the beam current. However, the maximum current is limited by physical constraints of the electron gun, and unless the gun technology is improved, and it may prove impossible to operate at the high currents needed to achieve the optimum values of $\eta_\perp$. Another potential problem with $2\omega_c$ operation is parasitic modes, including modes which oscillate at ω_c. High frequency gyrotrons operating at the fundamental do require high magnetic fields, but those fields are essentially equal to the magnetic fields used to confine the plasma that is being heated and do not represent an unreasonable extrapolation of present technology.

In order to simplify the analysis, we have fixed the frequency and power of the gyrotron. Based on the arguments presented in Section II.A., we have chosen a frequency ν = 200 GHz. This frequency was selected on the basis of the set of constraints imposed by the propagation and absorption of electron cyclotron radiation in the tokamak plasma. The main conclusion reached in Section II.A. was that the need for high density operation (peak density $\gtrsim 4 \times 10^{14}$ cm^{-3}) in moderate size tokamak reactors is likely to lead to the requirement of frequencies in the vicinity of 200 GHz.

The power level of the gyrotron was fixed at 100 kW, which reprerents a compromise value between two conflicting requirements. On the one hand, there is an advantage in achieving high power levels per unit in order to minimize costs. We have estimated that operating with more than one thousand gyrotron units will significantly

increase the cost. Since a total of 100 MS of auxiliary power will be needed to heat the HFCTR, this implies each gyrotron must deliver at least 100 kW. On the other hand, 100 kW is a significant extension beyond present gyrotron technology, and projections to higher power levels may prove unreliable. Fig. (1.B.2) shows the current state of the art of gyrotrons. Based on this data, we can project that a CW device could currently be built to deliver 10 kW at ν = 200 GHz. The Soviets are presently planning to construct a gyrotron for use on T-15 that would operate for 1.5 seconds at 85 GHz and deliver 200 kW. This scales to approximately 25 kW at ν = 200 GHz. Thus, although our choice of P = 100 kW is well beyond the currently available technology, it is in line with the developmental progress anticipated in gyrotron research. As will be shown later, our choice of P = 100 kW is also consistent with limits imposed by the ohmic heating of the cavity walls and the need to operate in low modes in order to reduce mode competition. One should note that P = 100 kW is a representative value, and that the optimum power level may vary about this value.

Another factor which is important in selecting the power level of each gyrotron is the window transmission problem. Although it is not yet certain that a suitable window material can be found for even a 100 kW power level, the window problem is much more severe at higher power levels. It appears likely that, if a 1 MW gyrotron at 200 GHz could be constructed, its output would have to be divided up prior to a window in order to obtain

transmission. Such a division of power is a difficult problem and could negate the advantage of achieving high power from a single unit. Windowless operation might be possible, but it is very unattractive because of the additional requirements of vacuum pumping and the danger of gas leaks into the gyrotron.

The major components of the gyrotron are illustrated in Fig. (II.C.1.), which is a schematic of the λ = 8.9 mm device used by Kisel'et.al. [KI74]. The system consists of three major parts: a magnetron injection gun that creates the electron beam to the left, the resonant cavity in the center, and the collector to the right. The gyrotron is symmetric about the Z axis. The solenoids produce a magnetic field that points in the Z direction and has a profile shown in the graph. As a result of the symmetry, the cathode with its emitter strip is able to produce an intense flow of electrons with rather small velocity dispersion. The electrons, guided by the magnetic field and accelerated by the electrostatic field produced by the anodes, enter a region of magnetic compression. Here, the transverse energy of the electrons increases according to the adiabatic invariant $V_\perp^2/B$ = constant, where $V_\perp$ is the electron perpendicular velocity and B is the magnetic field*. Once within the cavity, the electrons interact with the resonant RF field, and an energy transfer from the electrons to the field occurs. After leaving the cavity, the electrons enter a region of decreasing field (decompression section) and are deposited on a large surface

Fig. II.C.1 **8.9 MM GYROTRON**

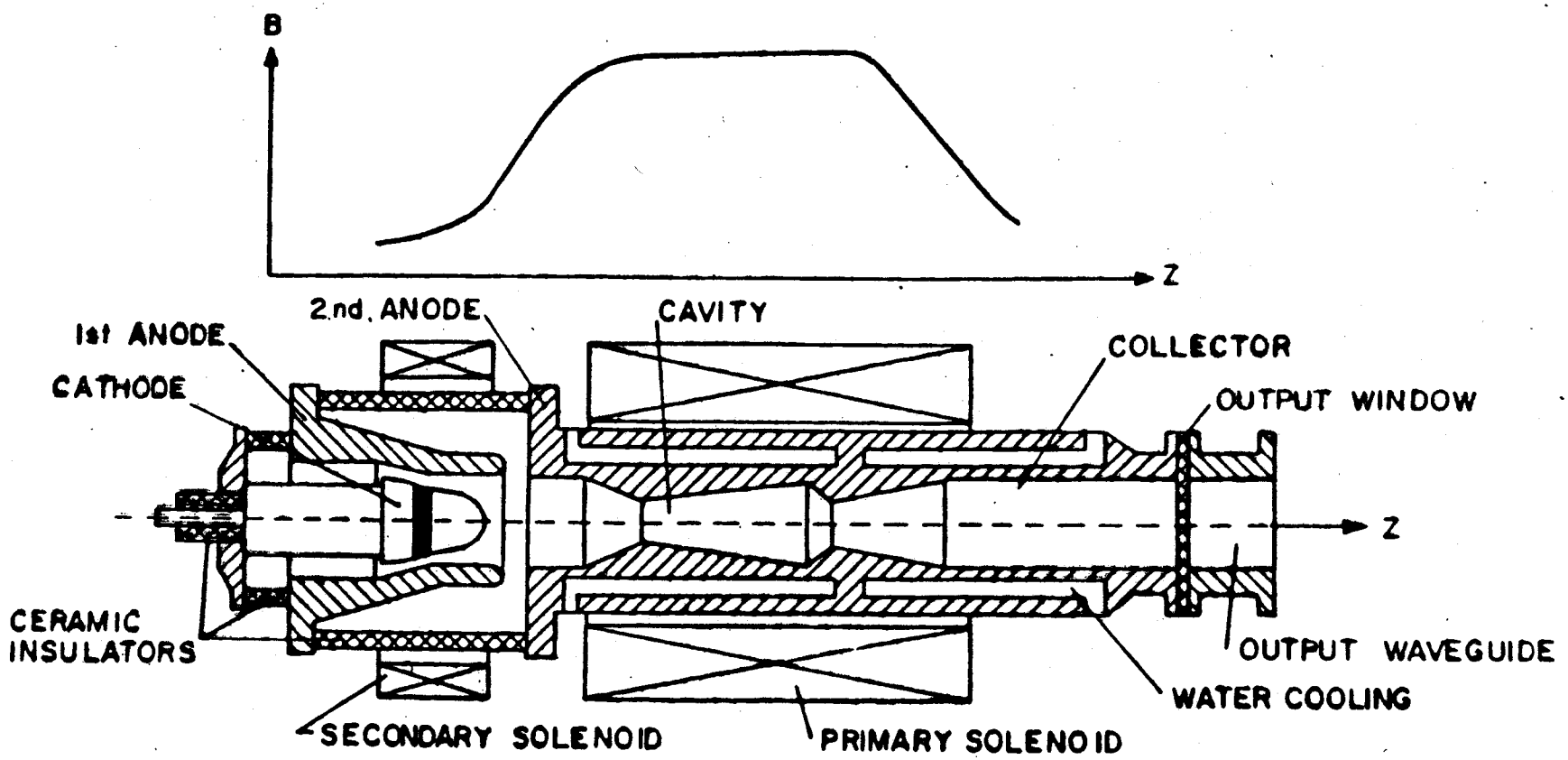

REF.: KISEL' ET. AL., RADIO ENG. ELECTRON. PHYS. 19, No. 4, 95 (1974)

collector. The RF field is transmitted through the output window and down the transmission waveguide to the plasma.

A complete design of a high frequency gyrotron can be carried out using a combination of analytic expressions and numerical results primarily derived from the Soviet literature. The model utilizes an adiabatic electron gun theory [GO73] numerical resonator mode [VL69], and computer calculations of cavity efficiency [GA73, NU72]. These principles may be summarized in a relatively simple analytic model which is very useful for preliminary gyrotron design and for evaluation of technological feasibility, and which serves as the basis of this parametric analysis. It should be recognized that eventually many of the final design parameters must be obtained from computer calculations that more accurately model the physical processes of the device. However, the analytic theories used here do serve to define the approximate value of many parameters and so are of great use in preliminary designs as a result of their simplicity.

The gyrotron design may be divided into two major subsystems, the electron gun and the cavity, which are physically distinct units. However, the analysis of these two subsystems is not independent, and as a result a self-consistent model is required. Fig. (II.C.2.) shows the overall structure of this model. The major components have been related to the six major variables of the design: the cavity radius R_o and length L, the electron beam's parallel and perpendicular velocities, $\beta_{\parallel}$ and $\beta_{\perp}$ ($\beta \equiv v/c$), the beam current I

Fig. II.C.2 Design Constraints of Gyrotron
Frequency and Output Power Fixed

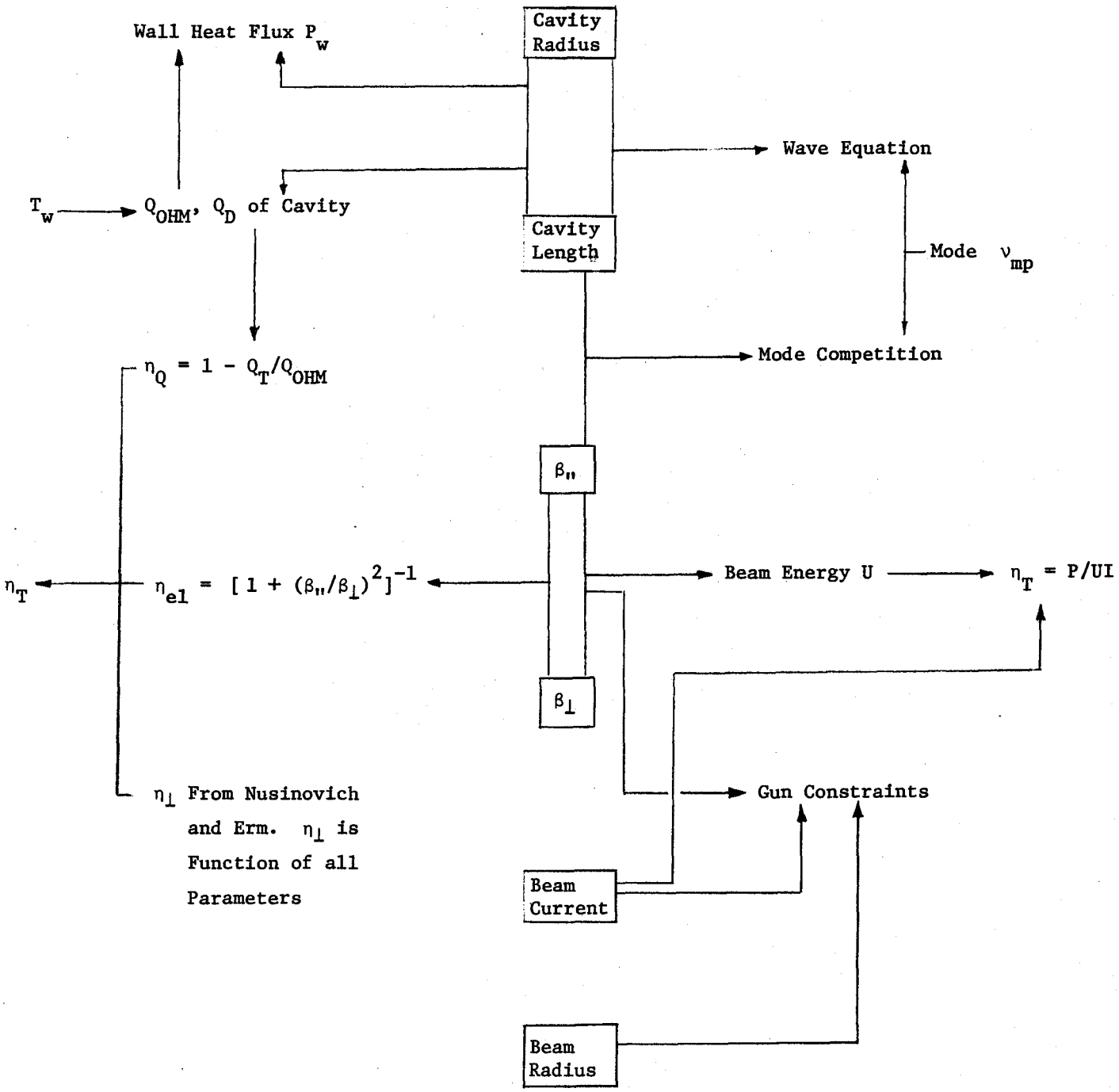

and beam radius R_e. We will now give a brief overview of the model. The wave equation relates R_o and L to the frequency of operation as well as to the transverse mode index ν_{mp}. The vacity radius and length, in conjunction with the wall temperature T_w, also determine the ohmic and diffractive Q's of the system, Q_{OHM} and Q_D. The cavity Q's can in turn be used to calculate the heat flux in the cavity walls due to ohmic currents P_w. The total efficiency of the device η_T can be calculated in two ways. First, it can be related to the beam energy U and current I, $\eta_T = P/UI$. Secondly, it can be derived from its three components, η_Q, η_{el}, and $\eta_\perp$. The main function of our code is to vary the appropriate parameters to obtain a solution in which both definitions of η_T are in agreement. Also included in the algorithm depicted in Fig. (II.C.2.) are limits imposed by mode competition, the appearance of unwanted parasitic modes, as well as constraints on the beam voltage and current due to physical limits of the electron gun.

II.C.2.1 Gyrotron Cavity

We will now describe each component of the gyrotron model in detail. The cavity is illustrated in Fig. (II.C.3.) along with its associated design parameters. The cavity shown is similar to those described and analyzed in the Soviet literature. It is assumed to have no taper, although tapering may improve efficiency and may be included in later designs. The resonance conditions are taken as those for a right circular cylinder, and the mode will be

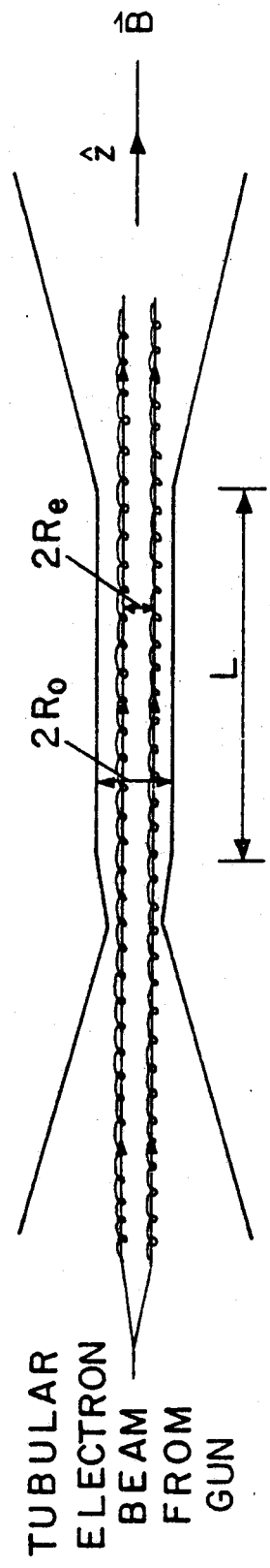

Fig. II.C.3 GYROTRON CAVITY

a cylindrical TE_{mpq} mode. In this case, the transverse mode index ν_{mp} is the p^{th} zero of $J'_m(y) = 0$. Since a gyrotron operates near cutoff, it can be shown that $L >> \lambda$, where λ is the wavelength, and that the wave equation $\omega/c = k$, where $k = 2\pi/\lambda$, can be written as:

$$R_o = \left(\frac{\nu_{mp}}{2\pi}\right) \lambda \qquad \text{(II.C.1)}$$

In order to further simplify the present discussion, we immediately specialize to the case:

$$m = 0,\ q = 1,\ p \text{ arbitrary}$$

The choice $m = 0$ appears to be the optimum for low mode operation at $\omega = \omega_c$. The extension to $m \neq 0$ will be obvious from the treatment given here. The choice $q = 1$ is important for maintaining single mode operation and achieving high efficiency.

The beam radius, R_e, must be matched to a maximum in the transverse RF field distribution. This requires:

$$J_1 (\nu_{op} R_e/R_o) = \text{maximum}$$

or $$J'_1 (\nu_{op} R_e/R_o) = 0$$

or $$\nu_{op}\ R_e/R_o = \nu_{11}, \nu_{12}, \nu_{13}, \cdots \text{ or } \nu_{1p}$$

Let the beam coincide with the r^{th} maximum. Then

$$R_e = \frac{\nu_{1r}}{\nu_{op}} R_o\ ,\ 1 \leq r \leq p \qquad \text{(II.C.2)}$$

The theoretical ohmic Q, Q_{OHM} is given, for a TE_{op1} mode, by

$$Q_{OHM} = \frac{R_o}{\delta} \frac{\nu_{op}^2 + \left(\frac{\pi}{2}\right)^2 r^2}{\nu_{op}^2 + \left(\frac{\pi}{2}\right)^2 r^3} \qquad \text{(II.C.3)}$$

where $r = 2\ R_o/L$ and δ is the skin depth. For $L/\lambda >> 1$, Q_{OHM} is given to high accuracy by:

$$Q_{OHM} = R_o/\delta \qquad \text{(II.C.4)}$$

For a copper cavity at $\lambda = 1.5$ mm, $\delta = 1.85 \times 10^{-5}$ cm at $T_w = 200°C$. It is important to allow for a somewhat degraded Q_{OHM} due to surface imperfections, particularly at short wavelengths. For example, it may be better to assume

$$Q_{OHM} = R_o/\delta \qquad \text{(II.C.5)}$$

$$\Lambda \approx 0.5 - 0.8$$

The diffractive Q of the resonator is given by

$$Q_D = 4\pi \frac{L^2}{\lambda^2} \frac{1}{1 - |R_1 R_2|} \qquad \text{(II.C.6)}$$

where R_1, R_2 are the electric field reflection amplitude coefficients at the two ends of the cavity. The minimum cavity Q is given by:

$$Q_{MIN} = 4\pi L^2/\lambda^2 \qquad \text{(II.C.7)}$$

and we may redefine Q_D as:

$$Q_D = K\, Q_{MIN} \qquad \text{(II.C.8)}$$

In general, the parameter K varies with cavity shape, mode, length and diameter. For the cavity shown in Fig. (II.C.3.), K is not a strong function of cavity mode and a rough value of $K \approx 3$ is obtained. Hence $Q_D \approx 3\, Q_{MIN}$. The total cavity A, Q_T, is given by:

$$\frac{1}{Q_T} = \frac{1}{Q_D} + \frac{1}{Q_{OM}} \qquad \text{(II.C.9)}$$

As will be shown later, it is important to have $Q_D << Q_{OM}$ in order to achieve high efficiency.

The maximum device gain occurs when

$$\omega - \omega_c = k_{\parallel}\beta_{\parallel}c \qquad \text{(II.C.10)}$$

where

$$\omega_c = \frac{eB_o}{\gamma m_o C} \qquad \text{(II.C.11)}$$

and $k_{\parallel} = q\pi/L = \pi/L$. γ is the relativistic increase in rest electron mass, m_o. Since $k_{\parallel}$ and ω are obtained from the cavity design and $\beta_{\parallel}$ from the gun design, Eq. (II.C.10) yields B_o. The value of $k_{\parallel}\beta_{\parallel}C$ is relatively small so as to minimize the importance of the Doppler

effect in maintaining the resonance condition as the electrons lose energy in the cavity. That is,

$$\frac{k_{\parallel}\beta_{\parallel}C}{\omega} = \frac{1}{2}\beta_{\parallel}\frac{\lambda}{L} << 1 \qquad \text{(II.C.12)}$$

The electron gyroradius, r_g, is given by:

$$r_g = \frac{v_{\perp}}{\omega_c} = \frac{c\beta_{\perp}}{\omega_c} \approx \frac{c\beta_{\perp}}{\omega} = \frac{\beta_{\perp}\lambda}{2\pi} \qquad \text{(II.C.13)}$$

The ratio of r_g to the beam radius R_e is:

$$\frac{r_g}{R_e} \approx \frac{\beta_{\perp}\lambda}{2\pi}\frac{1}{R_o(\nu_1/\nu_{op})} = \frac{\beta_{\perp}}{\nu_{1r}} \quad , \quad 1 \leq r \leq p$$

Hence $r_g << R_e$ and the electron beam is in the form of a hollow cylinder.

II.C.2.2 Efficiency

The overall efficiency for conversion of beam power to output EM power is denoted η_T. Only the transverse energy of the electrons may be converted to output power. The transverse efficiency, $\eta_{\perp}$, can be calculated numerically from the motion and RF field equations. This has been done by Nusinovich and Erm [NU72], and their results, modified by Gaponov et.al. [GA75], are shown in Fig. (II.C.4) for first and second harmonic operation. Their calculations are applicable to weakly relativistic, monoenergetic beams

Fig. II.C.4 Gyrotron Transverse Efficiency Based on Nonlinear Theory of Nusinovich and Erm [NU72].

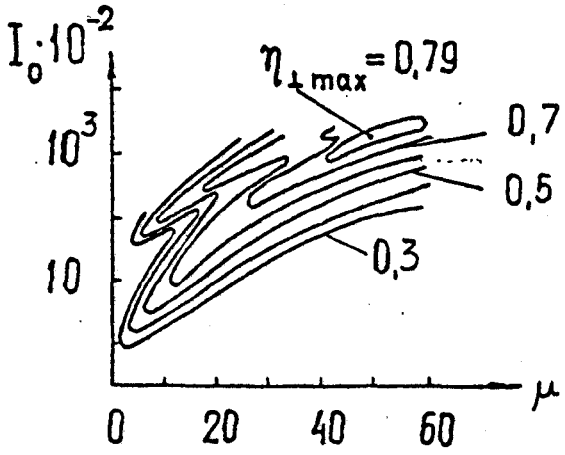

$\omega = \omega_c$

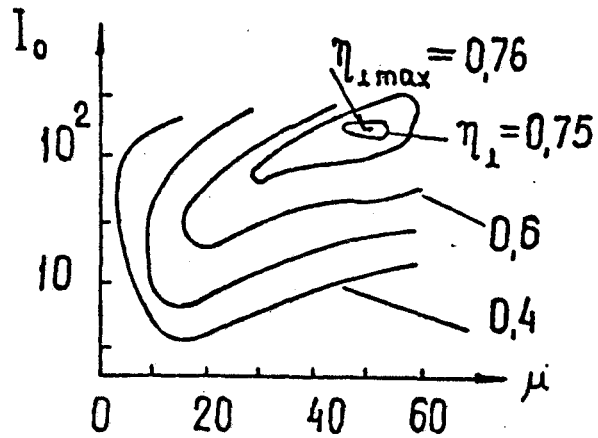

$\omega = 2\omega_c$

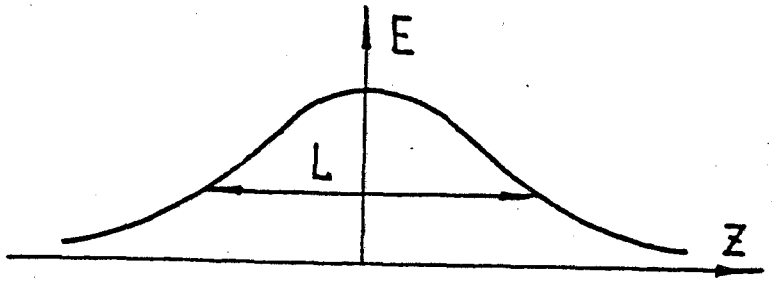

$$I_0 = 0{,}24 I(a)(Q \cdot 10^{-3}) \left(\pi \frac{\beta_\perp}{\beta_{\parallel}}\right)^{2(3-n)} \left(\frac{L}{\lambda}\right)^{5-2n} \left[\frac{(n/2)^n}{n!}\right]^2 G$$

$$G = \frac{J^2_{m-n}(\nu_{mp} R_0/R_p)}{(\nu^2_{mp} - m^2) J^2_m(\nu_{mp})}$$

$$\ell = \pi \frac{\beta^2_\perp L}{\beta_{\parallel} \lambda}$$

with no velocity spread and to an RF field with a Gaussian longitudinal profile. Although our beam is expected to be moderately relativistic ($\beta^2 \simeq 0.2$) and to have a spread in the velocity of the electrons, we believe the results of Nusinovich and Erm can be extended with only a small error to our case as long as the beam voltage U does not become too large (U < 100 kV) and the velocity spread is not excessive [GA75]. The use of a Gaussian to describe the RF field structure has been verified experimentally to be valid in the case of simple open resonators such as the one shown in Fig. (II.C.3) [GA75]. The graphs of Fig. (II.C.4) express $\eta_\perp$ as a function of two parameters, the normalized beam current I_o and normalized cavity length μ.

In addition to $\eta_\perp$, one must also calculate the efficiency for conversion of electron beam power to transverse power, η_{el}. This can be written as:

$$\eta_{el} = \left[1 + (\beta_\parallel/\beta_\perp)\right]^{-1} \qquad \text{(II.C.14)}$$

Finally, the efficiency factor that accounts for ohmic losses in the cavity walls, η_Q, can be expressed as:

$$\eta_Q = 1 - Q_T/Q_{OHM} = Q_{OHM}/(Q_D + Q_{OHM}) \qquad \text{(II.C.15)}$$

The total efficiency can now be written as:

$$\eta_T = \eta_\perp \eta_{el} \eta_Q \qquad \text{(II.C.16)}$$

II.C.2.3 Gyrotron Gun

A typical gyrotron gun is illustrated schematically in Fig. II.C.5. The fundamental parameters of the gun may be defined as follows:

B_k = Magnetic field in the gun region.

B_o = Magnetic field in the cavity region.

$2R_k$ = Diameter of emitting strip.

ℓ_k = width of emitting strip.

d = cathode to first anode spacing.

V_1 = First anode to cathode voltage.

ϕ = Angle between cathode surface and $\overline{B}$

The electron beam must also be defined using the following parameters:

$\beta_{\parallel}$, $\beta_{\perp}$ = velocity components in cavity region.

$\beta_{\parallel k}$, $\beta_{\perp k}$ = velocity components near the cathode

U = total energy of each electron at the cavity.

I = Electron current.

From the above definitions, a number of additional parameters may be defined or calculated. Assume that the electrons have energy U in the cavity region, where U is the potential difference between cathode and ground. Then, γ is given by:

$$\gamma = \frac{1}{\sqrt{1 - \beta^2}} = 1 + \frac{U}{511 \text{ keV}} \qquad \text{(II.C.17)}$$

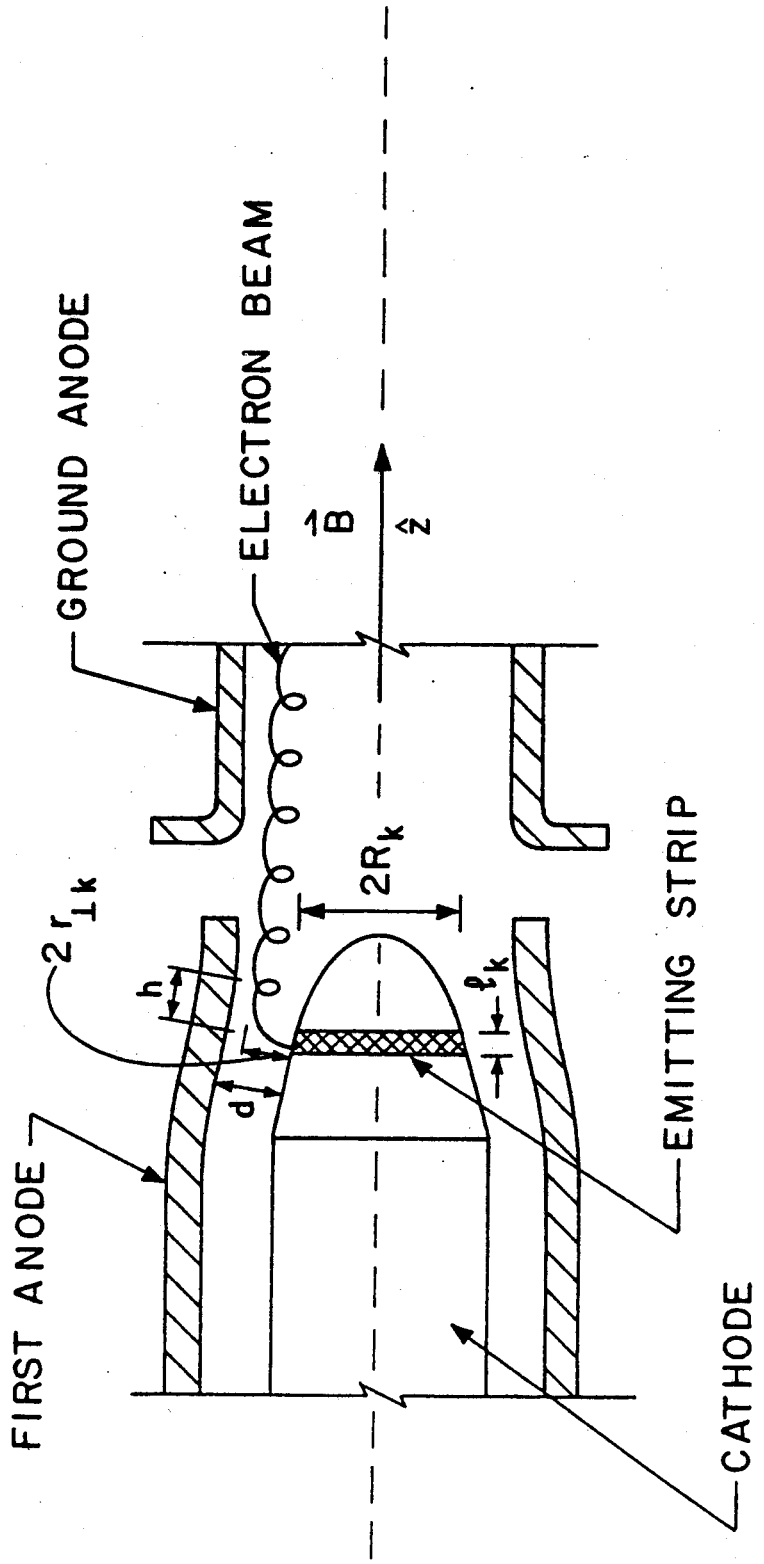

Fig. II.C.5 GYROTRON GUN

The mirror ratio, α, is defined by

$$\alpha = B_o/B_k \tag{II.C.18}$$

The perpendicular electric field near the cathode is given by

$$E_{\perp k} = \frac{V_1}{R_k} \frac{1}{\ell n \left(\frac{R_k + d}{R_k} \right)} \approx \frac{V_1}{d} \text{ for } d << R_k \tag{II.C.19}$$

The electrons coming from the emitting strip travel a distance h along the magnetic field during the time required to make one cyclotron orbit, where

$$h = 2\pi^2 \phi_k r_{\perp k} \tag{II.C.20}$$

for small ϕ_k. The emitter strip area A is given by,

$$A = 2\pi R_k \ell_k$$

and the emitter current density, J_k, is

$$J_k = I/2\pi R_k \ell_k \tag{II.C.21}$$

The initial height to which an electron rises above the emitter strip is $2r_{\perp k}$ where:

$$r_{\perp k} = \frac{\beta_{\perp k} C}{\omega_{ck}} \tag{II.C.22}$$

and ω_{ck} is the cyclotron frequency in the emitter region. The relative width of the emitter strip is defined using the parameter ξ, where

$$\xi = \frac{\ell_k}{2r_{\perp k}} \tag{II.C.23}$$

and $\xi << 1 \Longrightarrow$ narrow emitter

$\xi >> 1 \Longrightarrow$ wide emitter

The perpendicular velocity of the electrons just above the cathode is given by:

$$\beta_{\perp k} = 3.33 \times 10^{-6} \frac{E_{\perp k}}{B_k} \tag{II.C.24}$$

where $E_{\perp k}$ is in V/cm and B_k is in kG.

Some parameters in the gun and cavity regions are correlated via the mirror ratio, α. It is assumed that the electron trajectories between the gun and cavity are adiabatic. Then

$$R_k = \alpha^{1/2} R_e \tag{II.C.25}$$

$$\beta_\perp = \alpha^{1/2} \beta_{\perp k} \tag{II.C.26}$$

$$\beta_{\shortparallel} = (1 - \gamma^{-2} - \beta_\perp^2)^{1/2} \tag{II.C.27}$$

II.C.2.4 Operating Constraints

We will now discuss the major limits that constrain the operating regime of the gyrotron. Our model includes limitations imposed by the cooling requirements, by multimoding, and constraints imposed on the beam parameters by the electron gun. In the case of cooling, the main problem investigated in this report was the removal of heat resulting from ohmic currents in the cavity walls. This heat flux P_W can be calculated from the Q's of the cavity. Since Q_{OHM} is defined as the ratio of the cavity stored energy to ohmic power losses in the walls, and Q_D is the ratio of the stored energy to P, one can express P_W as:

$$P_W = \left(\frac{Q_D}{Q_{OHM}}\right)\left(\frac{P}{2\pi R_o L}\right) \qquad \text{(II.C.28)}$$

P_W can be written in terms of R and L (for fixed P and ω) by substituting Eqs. (II.C.5) and (II.C.8) for Q_D and Q_{OHM}:

$$P_W = \frac{2KPL\delta}{\Lambda\lambda^2 R_o^2} \qquad \text{(II.C.29)}$$

In order to calculate the skin depth δ for Q_{OHM} and P_W, the temperature of the inner cavity wall, T_W, must be known. This requires a detailed analysis of the cavity cooling system. Such an analysis has been done for the reference design, and will be presented at the end of this section. However, within the accuracy of this model, it is satisfactory to choose an approximate value for T_W

and assume it remains constant. The maximum value of T_W can be set by noting that copper alloys cannot be used for prolonged stress service above approximately 250°C. A lower limit can be determined from the temperature of the coolant. This limit is estimated as 100°C. As a result of the high heat fluxes that will occur in the cavity walls, T_W is expected to fall in the upper part of this range. Fig. (II.C.6) shows how Q_D and Q_T vary as a function of T_W for the reference parameters (see Table (II.C.1)). Over the permissible range of T_W, Q_{OHM} varies by about 20%. On the other hand, Q_T only varies by 2.3%, and as a result, η_T is virtually constant. Thus, treating T_W as a fixed constant is a reasonable assumption. In general, Q_T will fluctuate much less than Q_{OHM} as T_W varied because $Q_D \ll Q_{OHM}$ in order to ensure a high total efficiency. For our design study, we have chosen $T_W = 200°C$ as the wall temperature.

We next consider the case of multimode excitation, which is one of the major problems confronting the ECM. This involves the excitation of a number of competing modes in addition to the working mode, thus adversely affecting the efficiency of the device. This problem is exasperated as the cavity size is increased to accomodate higher powers, since one must move to higher order modes, and mode separation decreases. One can derive a simple scaling law that determines if modes will compete from the starting current curves of neighboring modes. Based on the observation that these curves typically have a width of $\Delta X \simeq 2$, where $X = (\omega_c - \omega)/k_{\parallel}\beta_{\parallel}c$, modes TE_{mpq} and $TE_{m'p'q'}$ will not overlap when $|\omega_{mpq} - \omega_{m'p'q'}| \gtrsim (k_{\parallel} + k'_{\parallel})u$.

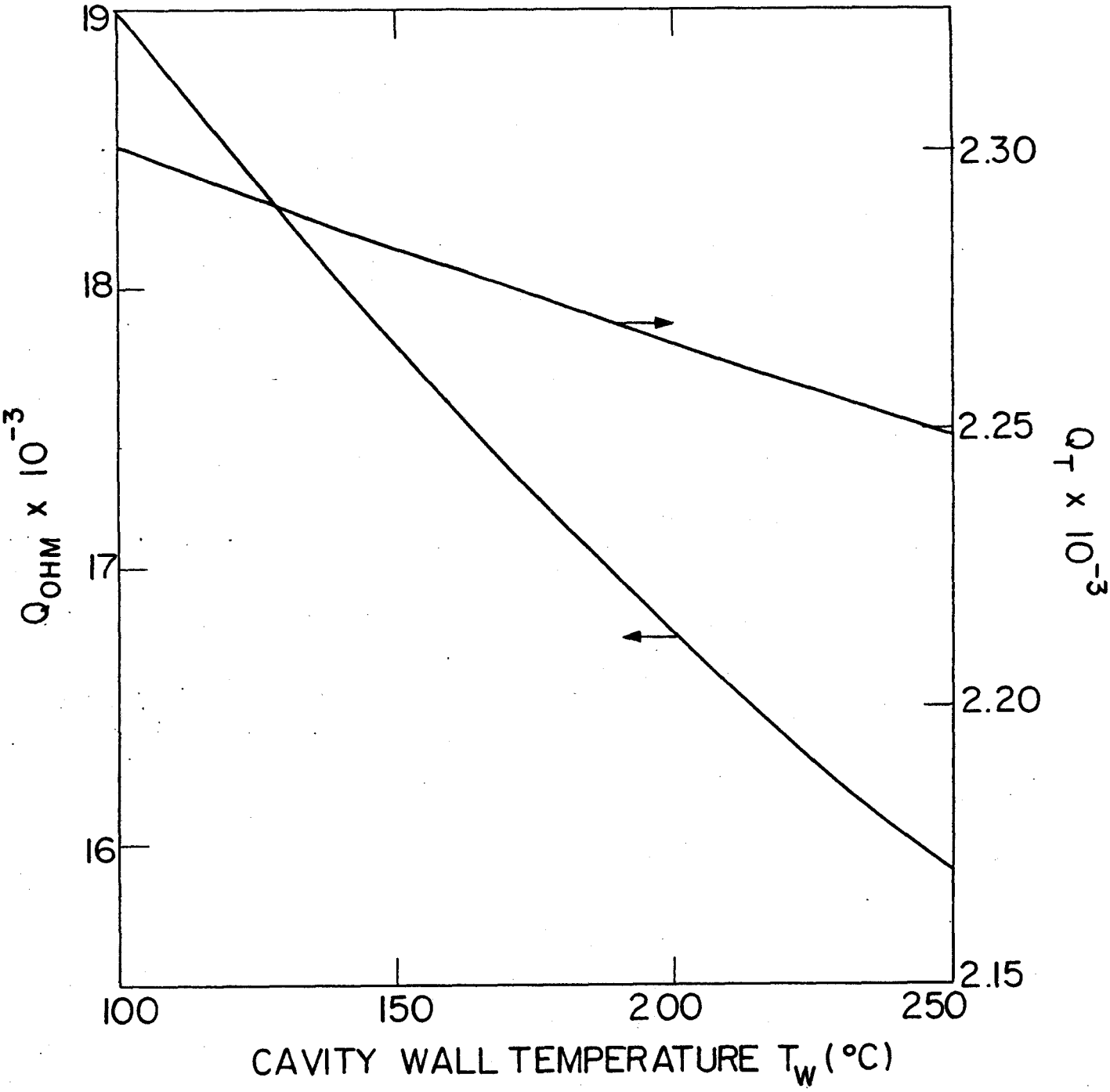

Fig. II.C.6 Dependence of Q_{OHM} and Q_T on cavity wall temperature.

Writing $k_{\parallel} = q\pi/L$ and $\omega_{mpq} \simeq c\nu_{mp}/R_o$ gives:

$$\frac{1}{4} q\Delta q \left(\frac{\lambda}{L}\right)^2 + \frac{\Delta\nu_{mp}}{\nu_{mp}} \gtrsim \frac{1}{2} (q + q')\beta_{\parallel} \left(\frac{\lambda}{L}\right) \qquad \text{(II.C.30)}$$

as the mode separation conditon, where $\Delta q = q - q'$ and $\Delta\nu_{mp} = \nu_{mp} - \nu_{m'p'}$. Here one can see that this equation becomes more difficult to satisfy as one moves to higher modes and $\Delta\nu_{mp}$ decreases. For our case, the TE_{op1} mode being studied here tends to be closely situated to the TE_{2p1} mode, especially for $p \geq 3$. In addition, for gyrotrons which operate near cuttoff, the TE_{mp2} modes are very close to TE_{mp1}.

Mode competition will undoubtedly be one of the major problems confronting the gyrotron as it is extended to higher powers. However, a number of techniques are available that can be used to improve the mode selectivity of the device and decrease the mode density. These include:

(1) Use of a conventional cavity with selective mode suppression using damping on the walls. Here one must avoid introducing higher losses for the wanted mode, and thus reducing the efficiency of the device.

(2) Use of a cavity with tapered walls that enhances mode separation. Vlasov et.al. [VL69] indicate that this can be a very effective technique, and that it does not necessarly lead to a serious reduction in the Q of the wanted mode. The problem

of competition is alleviated here by decreasing the Q's of the unwanted modes as well as increasing the separation of the natural frequencies of the modes.

(3) Use of an unconventional mode that exhibits better mode separation characteristics. One example of this is the Soviet use of the "whispering gallery" modes [BY75] which have their RF fields localized near the cavity walls. One of the difficulties in using an unconventional mode is finding an efficient method for converting the RF power of the resonator to the transmission mode.

We will now outline the procedure followed for selecting the gun parameters, and the subsequent limits on beam current. The magnetic compression factor α is determined either by the maximum electric field allowable in the cathode, or by the need for sufficient clearance for the electrons between the emitter and the first anode. If the breakdown electric field is set at 1×10^5V/cm, Eqs. (II.C.24) and (II.C.26) can be combined and written as:

$$\alpha \geq 1.05\ (\alpha\beta_\perp\omega)^{2/3} \qquad \text{(II.C.31)}$$

where ω is in GHz. The clearance requirement can be written as $d > (2\ r_k + \ell_k\phi_k)$, where $2r_k$ is the electron orbit diameter in the cathode region and $\ell_k\phi_k$ represents a spread in the beam due to the finite width of the emitter strip. This expression yields:

$$\alpha > 1.71 \times 10^3 \left(\frac{\gamma\beta_\perp}{U}\right)(2\beta_\perp + .33) \qquad \text{(II.C.32)}$$

where U is in kilovolts. As a result of the need to keep the magnetic compression as small as possible [SE78], the minimum value of α satisfying both Eqs. (II.C.31) and (II.C.32) is selected. The width of the emitter strip should be made as large as possible in order to minimize the current density at the strip. However, the need to keep the beam width reasonably small sets an upper limit on ℓ_k. If the beam width is restricted to one-tenth the width of an RF field radial peak, this gives:

$$\ell_k \simeq 120 \left(\frac{\sqrt{\alpha}}{\omega}\right) \text{mm}. \qquad \text{(II.C.33)}$$

where ω is in GHz. Here the angle ϕ_k has been fixed at 7.5°. We have also set the first anode voltage $V_1 = 0.3\ U$, which is consistent with past design studies of the electron gun [SE78, VA77]. In practice, the actual value of V_1 is determined by the electron-optics of the gun, and requires a computer simulation of the electron orbits. However, such an analysis is beyond the scope of this paper. Based on this value of V_1, the gap d can be calculated using $d = 0.03\ U$, where d is in millimeters and U is in kilovolts.

We can now calculate the major limits on the beam current. The first results from the need to keep the velocity spread of the beam, $\Delta\beta_\perp/\beta_\perp$, at a reasonably small value in order to ensure that the gyrotron operate at high efficiency. An upper limit on the velocity spread is imposed by the condition that all electrons must have sufficient energy to pass through the high magnetic field

region of the cavity. This implies.

$$\frac{\Delta\beta_\perp}{\beta_\perp} < \left(\frac{\beta_\parallel}{\beta_\perp}\right)^2 \qquad \text{(II.C.34)}$$

This condition is generally less restrictive than that required for high efficiency. An experimental investigation by Taranenko et.al. [TA74] showed that a substantial reduction of efficiency occurred for $\beta_\perp/\beta_\parallel \simeq 3.25$ for a velocity spread $\Delta\beta_\perp/\beta_\perp = 4\%$, well within the limit given by Eq. (II.C.34). In order to determine the maximum velocity spread based on efficiency, a numerical analysis of the beam-RF field interaction would have to be conducted. Such a study is beyond the scope of this report. Instead, we have limited the velocity spread to a fraction $\left(\frac{1}{3}\right)$ to $\left(\frac{1}{2}\right)$ of the value suggested by Eq. (II.C.34). Thus, for $\beta_\perp/\beta_\parallel = 1.8$, the velocity spread cannot exceed 10 - 15%.

The velocity spread of the electron beam arises from several causes, including space charge effects at the cathode, thermal effects, and surface roughness of the emitter. These components are labelled ε_{sc}, ε_T, and ε_a respectively, where $\varepsilon \equiv \Delta\beta_\perp/\beta_\perp$. The spreads resulting from these effects were calculated by Gol'denberg and Petelin [GO73] and Tsimring [TS72]. Based on their results, the limit on I can be written as:

$$I < 104 \frac{R_e \alpha^{3/2}}{\gamma\omega} \left[\varepsilon_{max}^2 - 6.3 \times 10^{-5}\left(\frac{\omega}{\sqrt{\alpha}\beta_\perp}\right)\right]^{1/2} \qquad \text{(II.C.35)}$$

where R_e is in milliteters, ω is in GHz, and ε_{max} is the maximum velocity spread that can be tolerated. It should be noted that this equation is applicable to both narrow and wide emitters, even though ε_{sc} differs for these two cases. This is because the wide emitter case also includes the restriction placed on beam width, which was discussed in conjunction with Eq. (II.C.33). When this requirement is included, both the narrow and wide emitter cases give virtually the same limit on the current for $\phi_k \simeq 7.5°$ and $\beta_\perp$ within the range 0.25 - 0.45.

The second limit on current results from the need to keep the current density at the emitter low in order to ensure that the cathode have a long lifetime. If we choose 4 A/cm^2 as the maximum density, this leads to the condition:

$$I \leq .2513\ \ell_k \sqrt{\alpha}\ R_e \quad \text{Amps} \qquad \text{(II.C.36)}$$

where ℓ_k and R_e are in millimeters.

Finally, a limit can be placed on the current based on the self-potential of the beam. The potential drop in the beam, as well as the voltage between the beam and cavity wall, must be kept small in order to minimize the velocity spread of the beam and achieve high efficiency. Because of the tenuous nature of the beam, its self-potential drop is negligible and the beam can be treated as monoenergetic. However, the voltage drop between the beam and the wall can be quite large. If we limit this voltage to 10% of the beam energy, then the following expression can be derived:

$$I \leq \frac{0.1328\ \beta_{\parallel} U}{\ln(R_o/R_e)} \quad A \qquad \text{(II.C.37)}$$

where U is in kV's. The selected beam current must satisfy the limits imposed by Eqs. (II.C.35), (II.C.36), and (II.C.37).

II.C.3 Parametric Analysis

In this section, we present our analysis of the gyrotron design parameters. The figure of merit for this study was chosen to be the total efficiency, η_T. High efficiency is important for gyrotrons for several reasons. First, it reduces the power supply requirements, which can significantly lower the cost of ECRH power. Second, it reduces the required beam power, which prolongs the collector life and lowers the collector cooling needs. Finally, it reduces the ohmic heating losses in the cavity and helps increase the cavity lifetime.

In order to better understand how the total efficiency of the gyrotron is related to the design parameters, we have plotted η_T as a function of a variety of these parameters. These results are shown in Figs. (II.C.7) through (II.C.11). In all of these graphs, the length L is allowed to very in order to find the highest overall efficiency that can be achieved. Except where indicated, the following parameters have been assumed: ν = 200 GHz, U = 70 kV, I = 4.1A, mode TE_{051}, R_e = 2.07 mm (third radial maximum from cavity center), and $\beta_{\perp}/\beta_{\parallel}$ = 1.8.

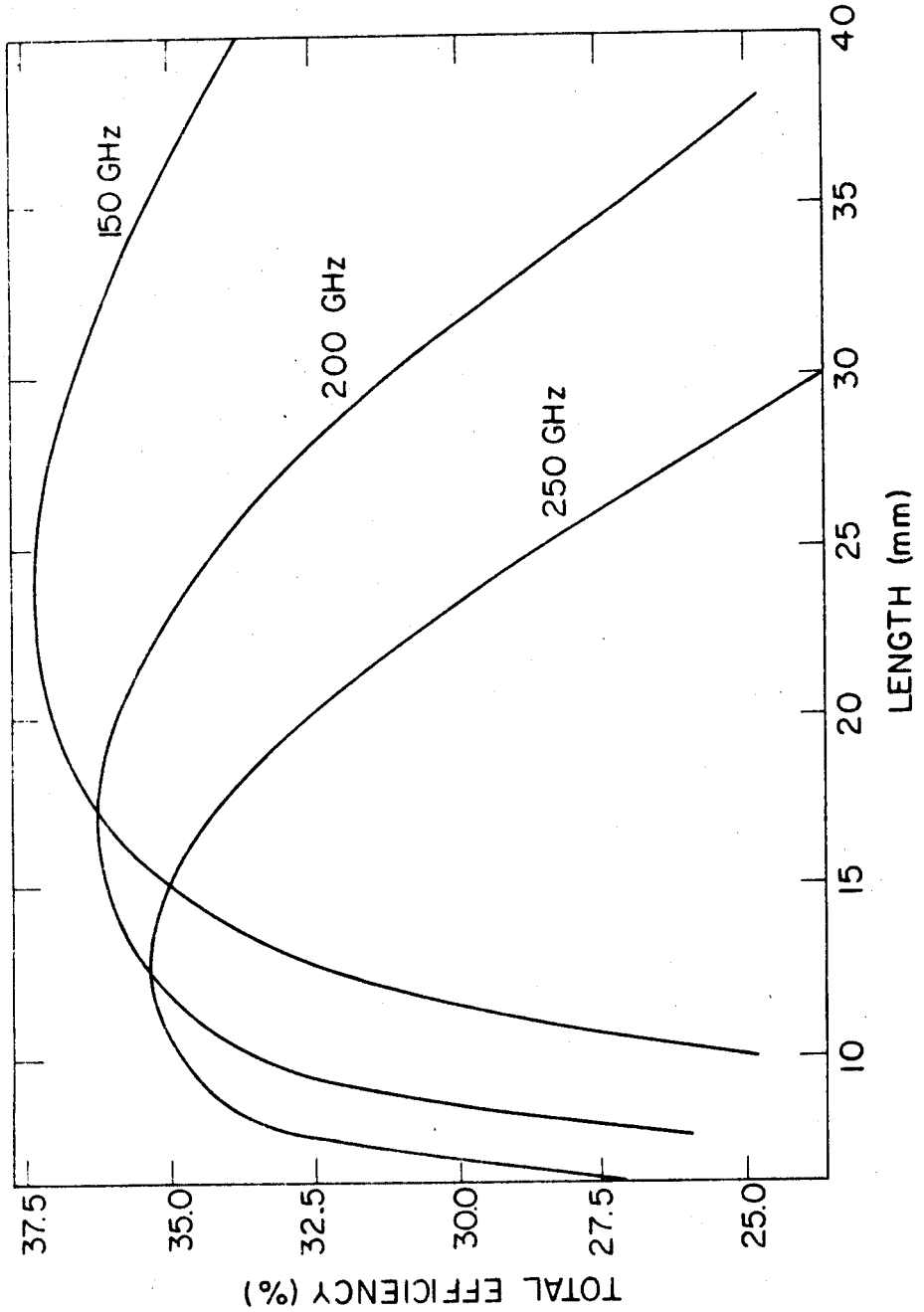

Fig. II.C.7 Total Gyrotron Efficiency vs. Frequency and Cavity Length.

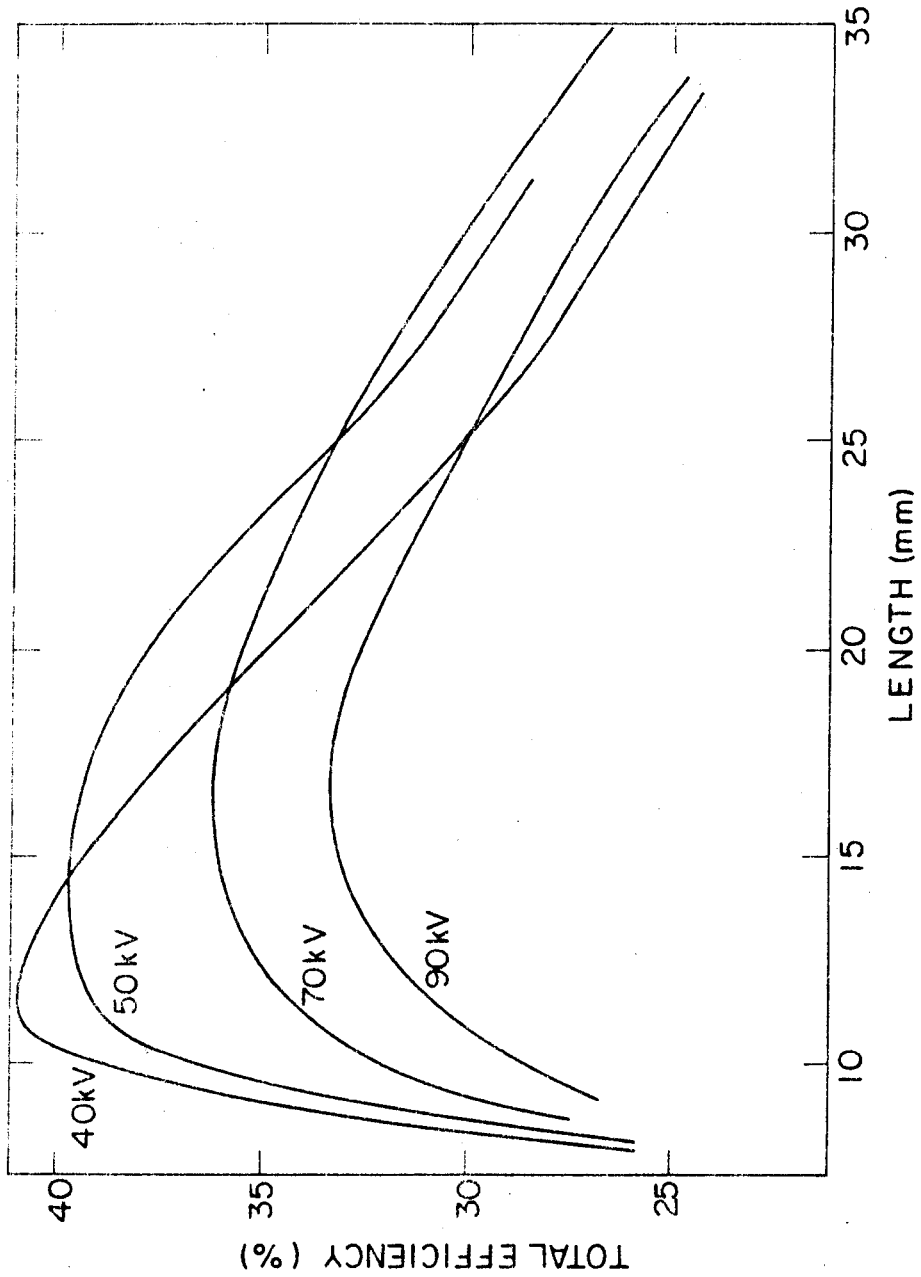

Fig. II.C.8 Total Gyrotron Efficiency vs. Beam Voltage and Cavity Length.

Fig. (II.C.7) shows the effect on η_T of varying the operating frequency of the device. As the frequency is increased, the maximum efficiency will occur at shorter lengths. This is consistent with the calculations of Nusinovich and Erm (Fig. (II.C.4)) in which both I_o and μ, and therefore $\eta_\perp$, can be treated as functions of L/λ, which can be rewritten as $L\omega$. If $Q_D << Q_{OHM}$, then η_T virtually becomes a function of $L\omega$. Fig. (II.C.7) illustrates that this dependence on $L\omega$ is approximately correct, although slightly higher total efficiencies can be obtained at lower frequencies. This dependence allows one to scale η_T to other frequencies by keeping $L\omega$ constant.

In Fig. (II.C.8) the beam voltage is varied from 40 kV to 90 kV. One can observe that operating at too high a voltage can cause a reduction in total efficiency. This is due to the fact that as U is increased, the length must be increased to achieve the optimum η_T, but this causes η_Q and subsequently the maximum η_T to be reduced. Our calculations indicate that for $\beta_\perp/\beta_\parallel = 1.8$, the beam voltage should be between 40 and 60 kV to achieve the highest total efficiencies.

The effect of varying the beta ratio is shown in Fig. (II.C.9). As one can see, the total efficiency is very sensitive to this ratio. In order to achieve the highest η_T, the gyrotron should operate at as high a value of $(\beta_\perp/\beta_\parallel)$ as possible. However, as this ratio is increased, the velocity spread of the beam becomes more problematic [SE78] and can eventually cause a reduction in the

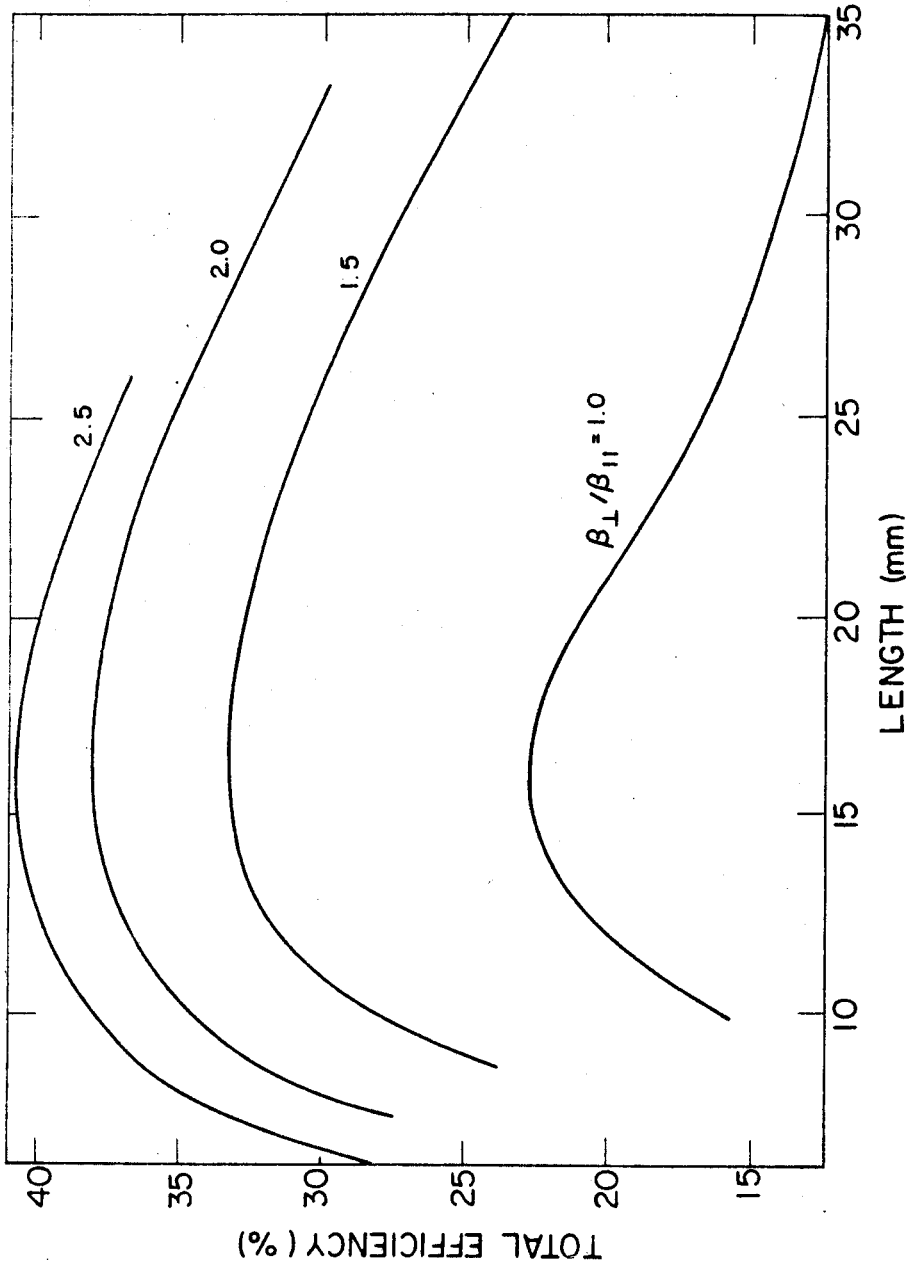

Fig. II.C.9 Total Gyrotron Efficiency vs. Velocity Ratio and Cavity Length.

efficiency of the device [see Eq.(II.C.34)]. Results in Fig. (II.C.9) do not include the decrease of η_T caused by the velocity spread. One should thus select a beta ratio that balances these two opposing influences.

In Fig. (II.C.10) the effect of varying the operating mode, that is, varying ν_{mp}, is shown. For each ν_{mp}, the beam has been adjusted to interact with the third radial maximum of the RF field from the center of the cavity. The choice of mode has a relatively minor influence on the maximum efficiency that can be achieved, suggesting that any mode would be satisfactory if high η_T were the only criterion. However, the operating mode is important because it determines the radius of the cavity for a given ω (see Eq. (II.C.1)). This in turn determines the severity of the mode competition as well as the heat flux P_w. In general, it is advantageous to operate in as low a mode as possible to minimize the number of competing modes.

Finally, Fig. (II.C.11) shows how the K factor in Q_D (see Eq. (II.C.7)) influences the total efficiency. This factor can be interpreted as a measure of RF field trapping by the resonator. The higher K is, the more effectively the cavity traps the field. The graph indicates that the optimum length, as well as the width of the curve, is strongly dependent on K. This suggests a possible procedure for optimizing a gyrotron design. Once the operating mode is selected, a length can be chosen that corresponds to a tolerable heat flux P_w. Then K can be varied until the peak of the efficiency curve occurs at this length. This value of K can then

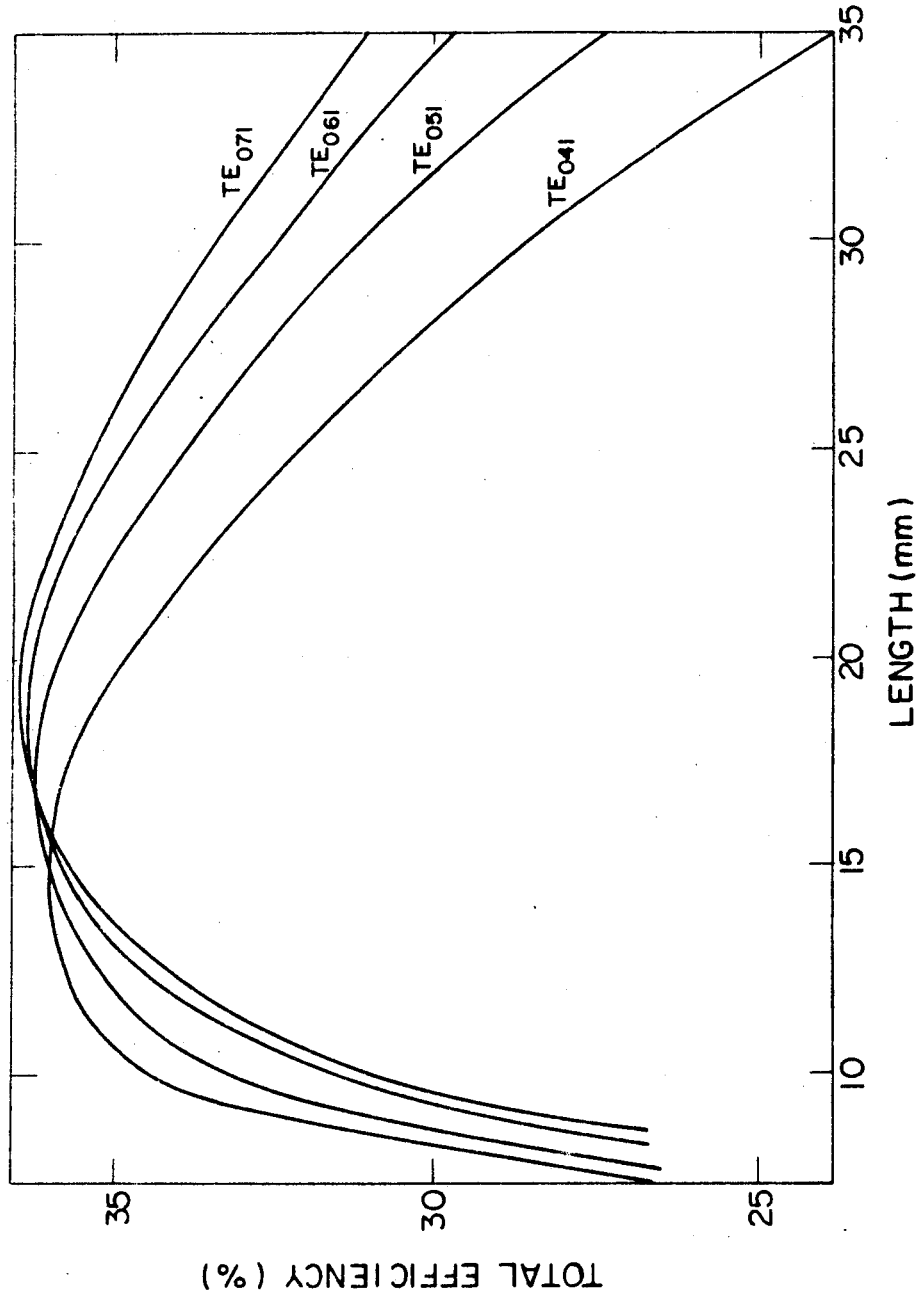

Fig. II.C.10 Total Gyrotron Efficiency vs. Cavity Mode and Cavity Length.

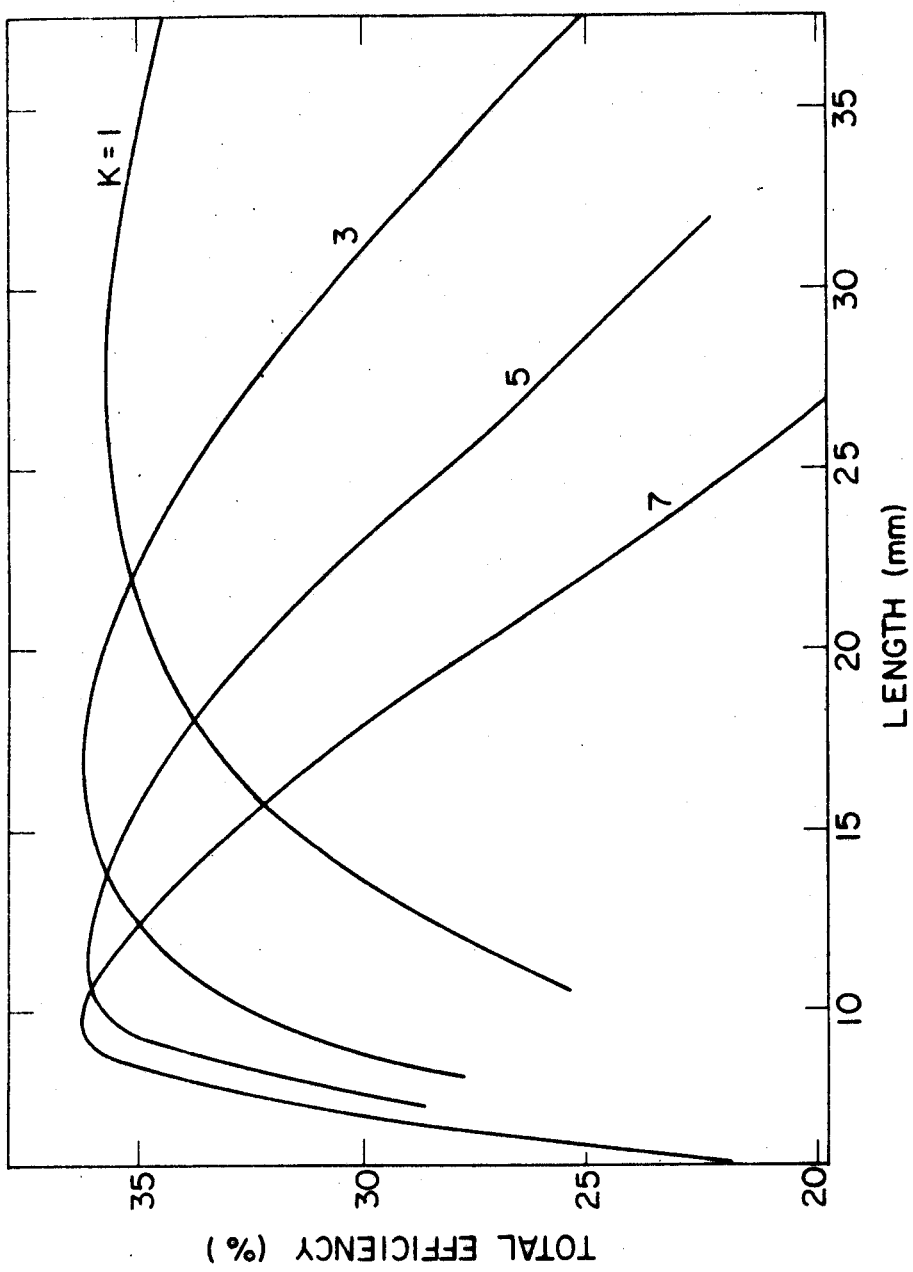

Fig. II.C.11 Total Gyrotron Efficiency vs. the Coupling Factor K and Cavity Length.

be obtained by selecting the appropriate cavity shape and output coupling.

We will now investigate how the constraints imposed by the magnetron gun affect the operating regime of the gyrotron. In the previous section a model for the gun was described in which an upper limit was placed on the current based on the design parameters. This limit on the beam current is illustrated in Figs. (II.C.12) through (II.C.14). Except where indicated, the following parameters have been assumed: ν = 200 GHz, U = 70 kV, mode TE_{051}, R_e = 2.82 mm (fourth radial maximum from center), and $\beta_\perp/\beta_\parallel$ = 1.8.

Fig. (II.C.12) shows the effect of changing the maximum velocity spread of the beam. The characteristics of the operating regime are very sensitive to the choice of ε_{max} when this variable becomes sufficiently small. As ε_{max} is decreased, the limit imposed by Eq. (II.C.35) becomes more restrictive, forcing the gyrotron to operate at higher beam energies and lower currents. The increase in beam energy is beneficial because this causes the velocity spread due to surface roughness and thermal effects to be reduced. As ε_{max} is increased, the maximum current becomes limited by the beam to cavity voltage drop restriction (Eq. (II.C.37)) rather than by the velocity spread criterion. This can be seen for ε_{max} = 12%.

In Fig. (II.C.13), the radial maximum of the RF field involved in the interaction with the electron beam is varied. The gyrotron is operating in the TE_{051} mode with ε_{max} = 10%. This graph indicates that it is advantageous for the beam to be as close to the cavity wall as possible in order to increase the

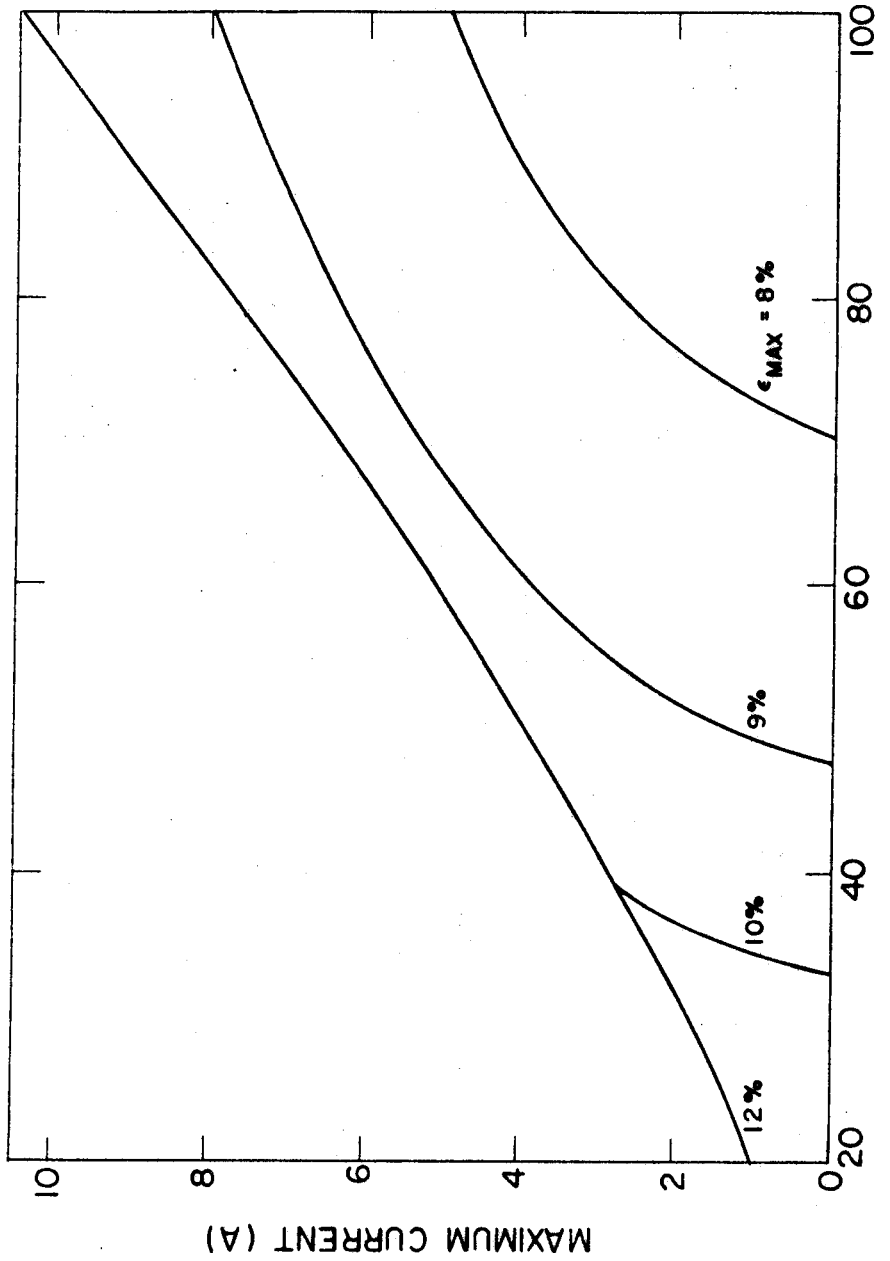

Fig. II.C.12 Maximum Current Based on Gun Constraints vs. Beam Energy and Maximum Transverse Velocity Spread.

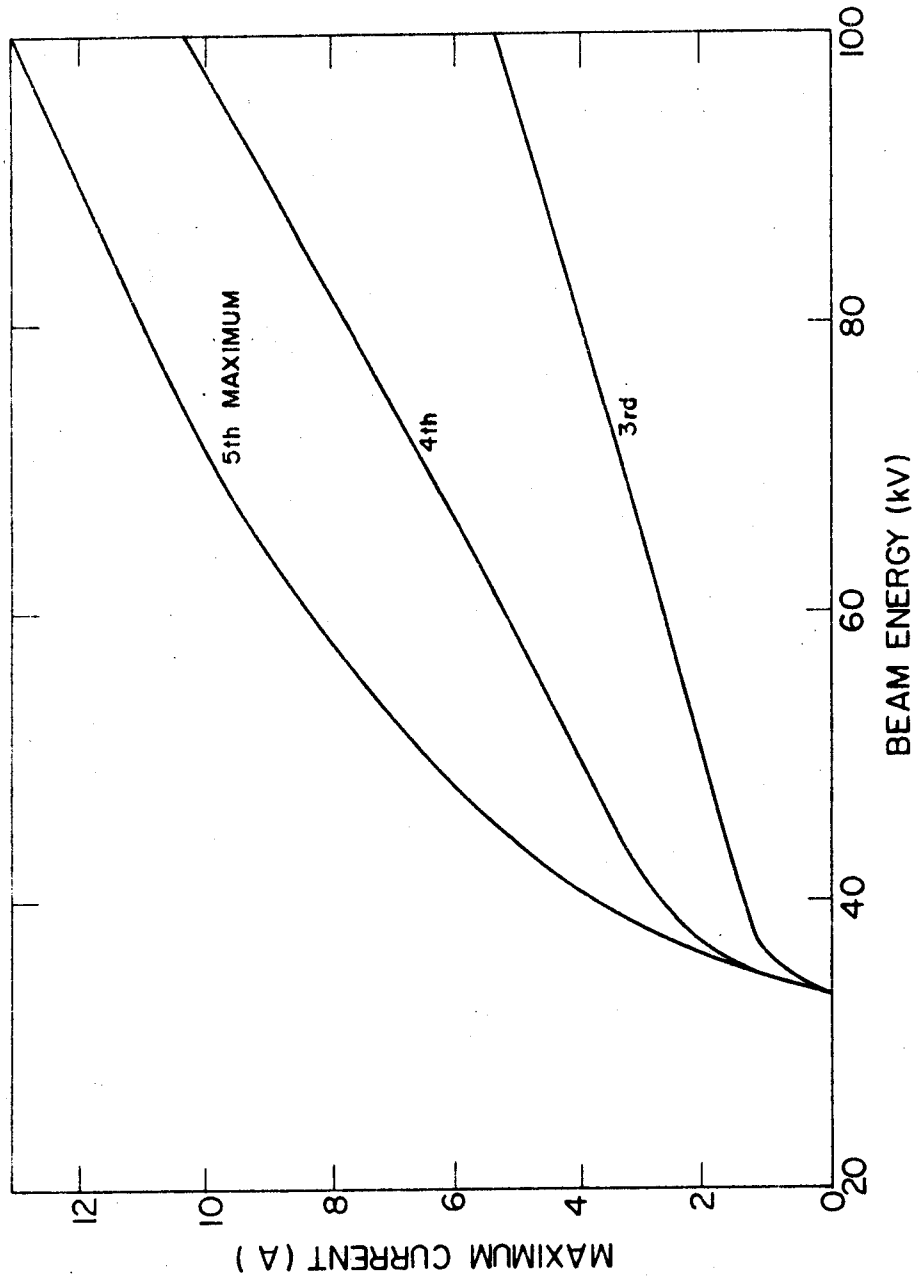

Fig. II.C.13 Dependence of Maximum Current on Radial Position of Electron Beam. Curves Correspond to Radial Peaks of RF Field as Measured From Axis.

current limit. However, one must avoid operating with the beam too close to the wall in order to prevent additional wall heating due to electron bombardment. As in the previous figure, two different limits on the current can be observed. For interactions involving the third and fourth maxima, the current is limited by the cavity-beam voltage, while for the fifth maximum the beam velocity spread sets this limit.

Using the results of Fig. (II.C.13) to choose the beam radius, we investigated the effect of varying the operating mode. This is shown in Fig. (II.C.14) for ε_{max} = 10%. For the TE_{021} and TE_{031} modes, we have chosen to utilize the field maximum closest to the wall, while for the higher modes the second maximum from the wall was used. This selection was based on the criterion $R_e/R_o \lesssim .85$. Here one can see that the limit on the current becomes less restrictive as the p index of the TE_{0p1} mode is increased, suggesting higher modes might prove advantageous since they provide a larger operating regime. However, this finding must be tempered by the fact that mode competition becomes more severe as the gyrotron operates in higher modes. Also of interest in this graph is the transition from a velocity spread limited current to a current limited by the beam-wall voltage as one moves to higher modes.

During the course of our parametric analysis, a number of trade-offs involving major design parameters were found. These trade-offs are important in that they influence the procedure used for choosing these parameters. In the case of the beta ratio, $\beta_\perp/\beta_\parallel$, this involves the opposing requirements resulting from the

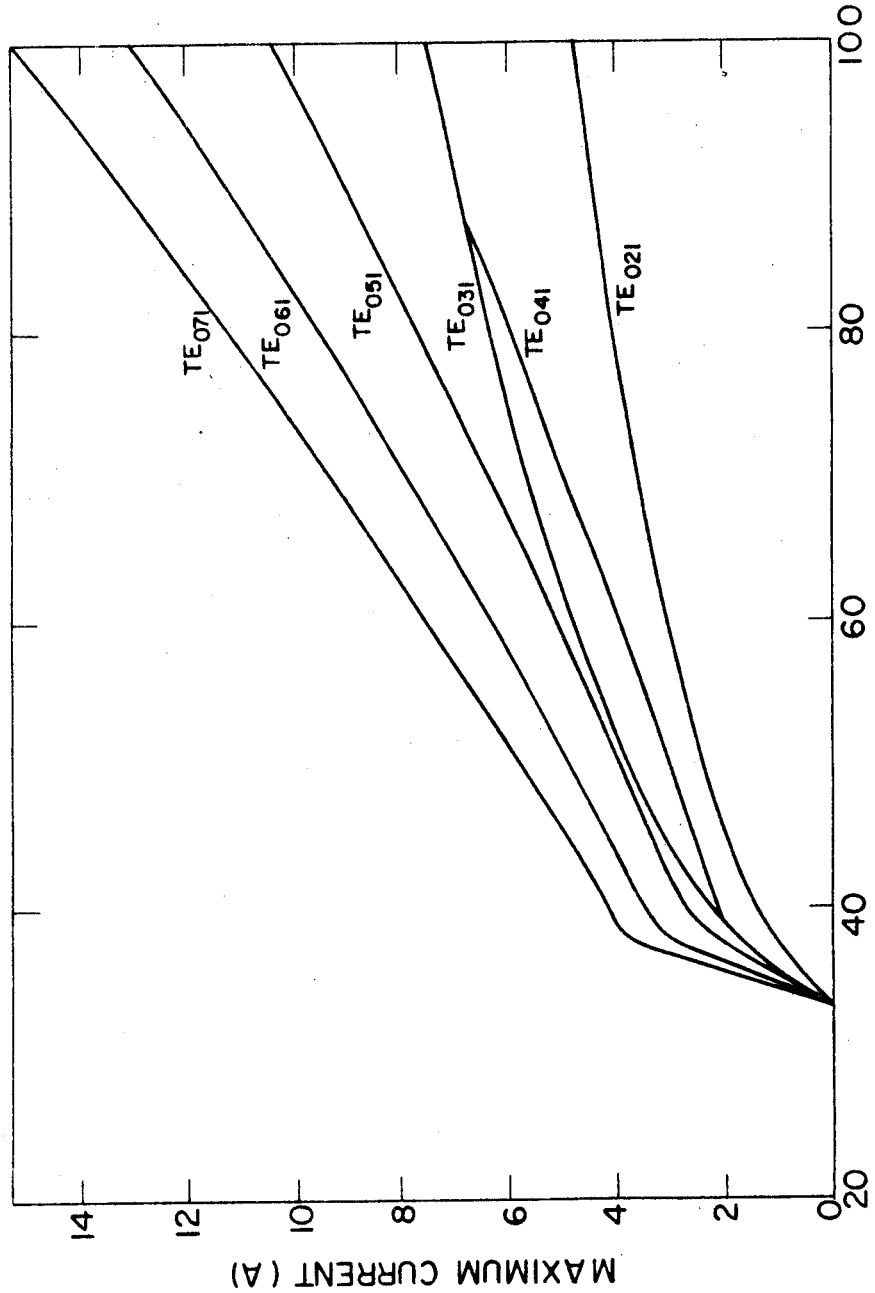

Fig. II.C.14 Dependence of Maximum Current on Cavity Mode.

desire for high efficiency and the need to limit the beam velocity spread. Increasing $\beta_\perp/\beta_\parallel$ enhances η_T but makes Eq. (II.C.34) more difficult to satisfy. In choosing ν_{mp}, one must balance the need for a low wall heat flux with the need to minimize mode competition. As one operates in higher modes and ν_{mp} increases, P_w is reduced but the problem of competing modes becomes more severe. The choice of length often involves the conflicting needs of operating at the highest efficiency possible (see Fig. II.C.7) and keeping P_w at a reasonable level. Finally, as indicated in our discussion of the gun constraint, a large beam radius causes the limit on the current to be less severe but reduces the strength of the interaction between the RF field and beam. As will be shown in the next section, these trade-offs must be balanced in the process of selecting the design parameters.

II.C.4 Selection of Design Parameters

In this section, the procedure followed in selecting the reference deisgn parameters used in this report is outlined. Our goal is to maximize the total efficiency of the device within the constraints discussed in the earlier sections. As mentioned before, we have fixed the power output P at 100 kW and the frequency ν at 200 GHz. We have also fixed the factor K in Q_D at 3 based on the cavity shape shown in Fig. (II.C.3) [VL69]. The electron beam is assumed to pass as close to the cavity wall as possible in order

to ease the gun constraints (radial maximum closest to wall for modes TE_{021} and TE_{031} second maximum from wall for higher modes). We begin by selecting the maximum beam velocity spread that can be tolerated. The discussion in conjunction with Eq. (II.C.34) indicated that a small ε_{max} is desirable because this allows a high beta ratio and thus a high total efficiency. However, Fig. (II.C.12) shows that if ε_{max} becomes too small, then the available operating regime can become severely limited. In order to avoid a restricted operating regime, a maximum velocity spread of 10% was chosen. This leads, via Eq. (II.C.34), to a beta ratio $\beta_\perp/\beta_\parallel$ within the range 1.8 - 2.2. We have chosen to operate at the lower end of this range with $\beta_\perp/\beta_\parallel = 1.8$.

Fig. (II.C.14) can be used to calculate the minimum beam voltages required in order to ensure that the limits imposed on the current by the gun are satisfied. Assuming an optimum efficiency η_T of 30% to 35%, which is consistent with $\beta_\perp/\beta_\parallel = 1.8$, the following lower limits on U were determined:

Mode	Minimum U
TE_{021}	75 kV
TE_{031}	70 kV
TE_{041}	75 kV
TE_{051}	70 kV
TE_{061}	65 kV
TE_{071}	60 kV

As is indicated in Fig. (II.C.8), the gyrotron should in general operate as close to these voltages as possible in order to achieve the highest η_T.

The correct beam current can now be determined by varying I until the two equations containing η_T given in Fig. (II.C.2) have a common solution. This was done for those beam voltages satisfying the above constraint, and the design point giving the highest overall efficiency was selected. The results are shown in Fig. (II.C.15) and (II.C.16). In Fig. (II.C.15) the total efficiency has been has been plotted as a function of cavity radius and length, while Fig. (II.C.16) shows the corresponding value of I. The beam voltage can be calculated from these two graphs by using the equation $U(kV) = 100/\eta_T\ I(A)$. Note that, since ν is fixed, only certain cavity radii represent actual operating points. These points are indicated by the indices Opl of the TE_{opl} mode. Also shown in these graphs is the heat flux P_w, which has been calculated using Eq. (II.C.29).

In order to choose a reference design point, a reasonable value for P_w must be determined. Based on the cavity cooling model given at the end of this section, heat fluxes less than 5 kW/cm^2 appear manageable. The heat flux can be reduced by either increasing the cavity radius (i.e., moving to higher modes), or decreasing the length which results in greater output coupling. In addition, mode competition must also be considered. The mode separation condition, Eq. (II.C.30), can be rewritten in a simpler

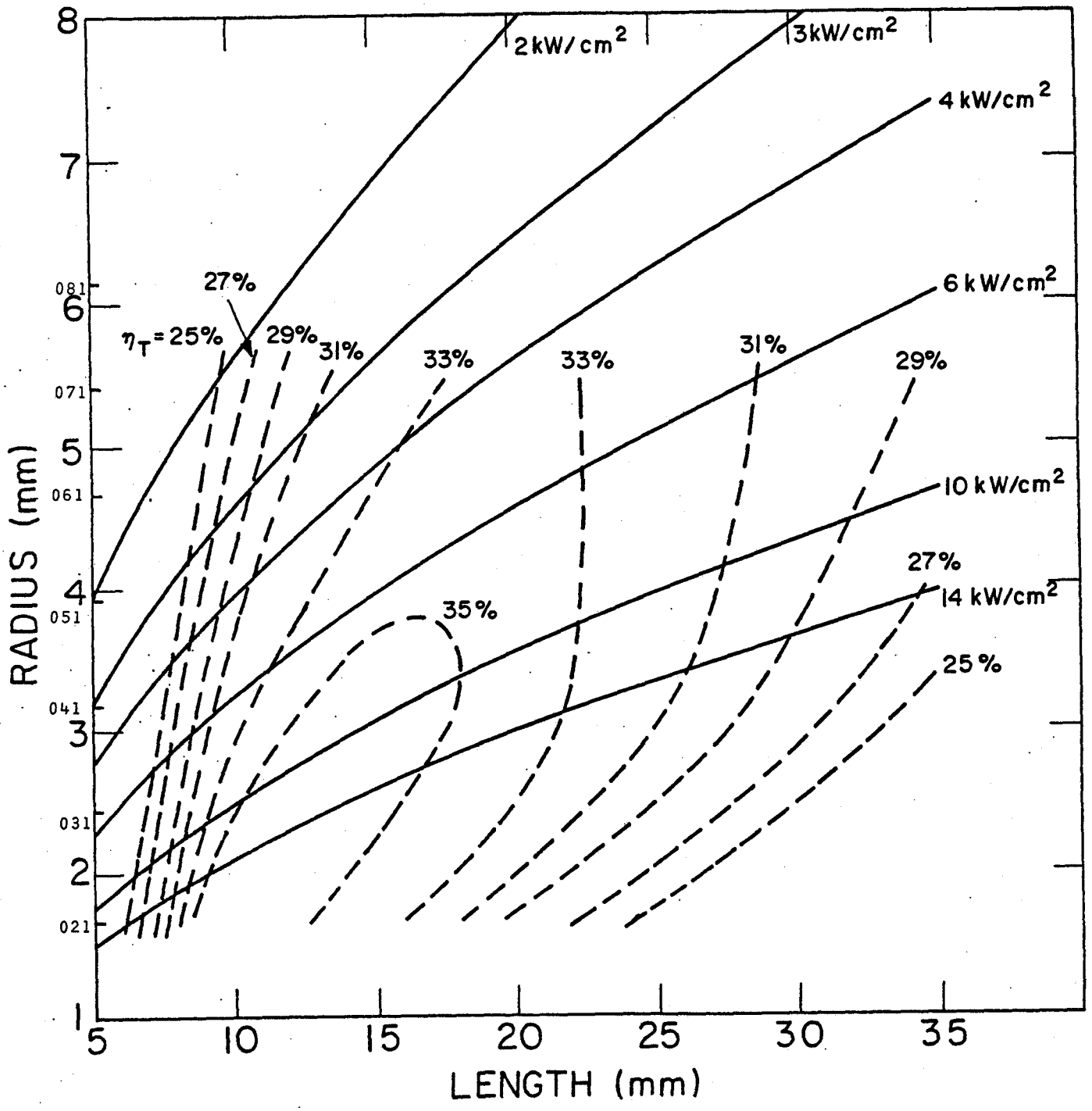

Fig. II.C.15 Optimum total Efficiency of 200 GHz, 100 kW Gyrotron with $\beta_\perp/\beta_{||} = 1.8$.

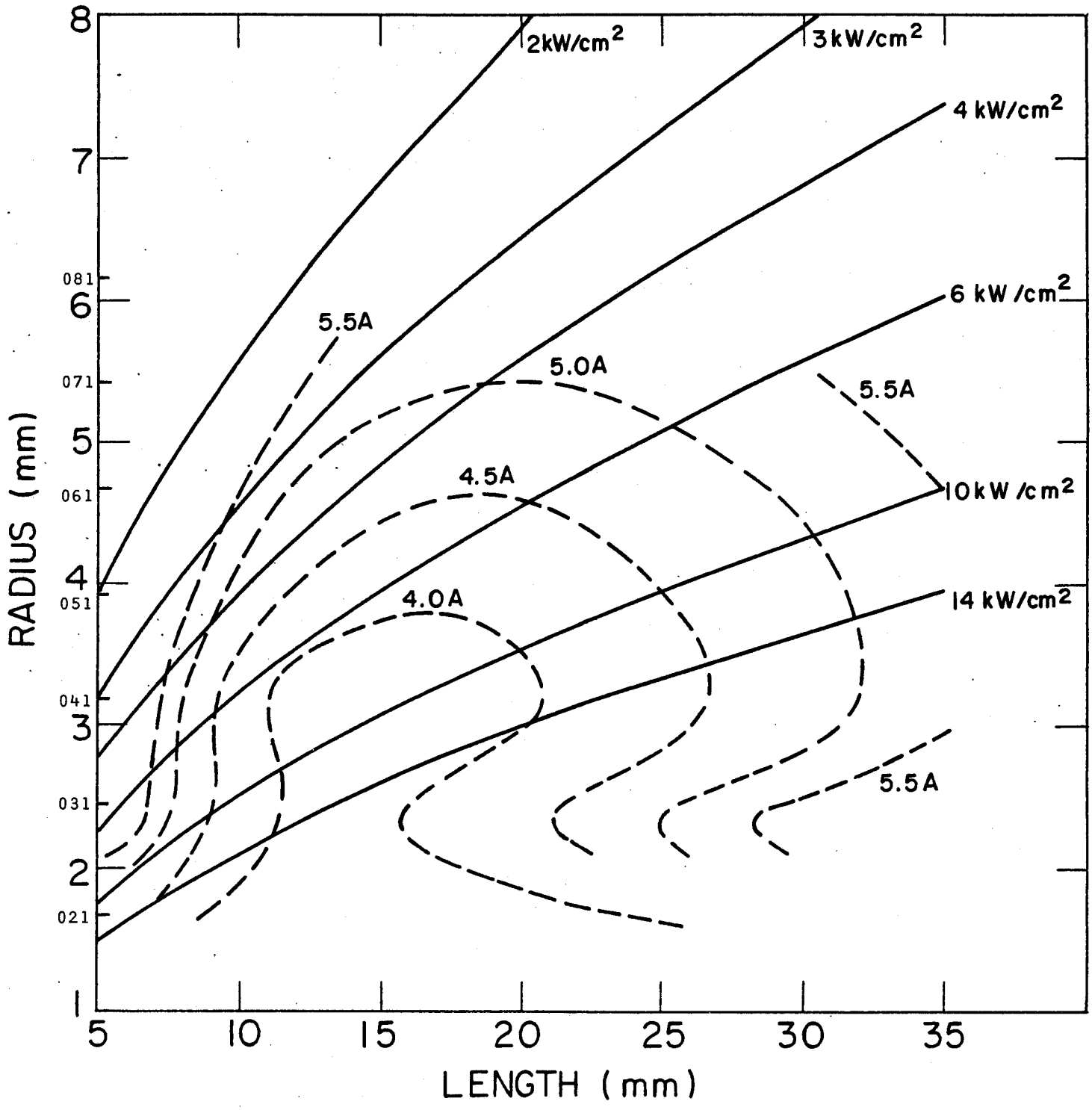

Fig. II.C.16 Beam Currents Associated with Operating Conditions Shown in Fig. II.C.15.

form when determining whether the TE_{op1} and TE_{2p1} modes overlap. Note that, for gyrotrons operating near cutoff, the first term of Eq. (II.C.30) is small compared to the second and can be neglected. Using the fact that $\Delta\nu_{mp}$ scales approximately as $1/R_o$ for the TE_{op1} and TE_{2p1} modes, (this is accurate to within 3% for $3 \leq p \leq 7$) the separation condition becomes:

$$0.116 \gtrsim \beta_{\parallel}\lambda\left(\frac{R_o^2}{L}\right) \qquad \text{(II.C.38)}$$

where all lengths are in millimeters. This inequality scales with respect to R and L in the same manner as P_w. Thus, any attempt to reduce the wall heat flux by varying the length or radius will automatically cause the competition between the TE_{op1} and TE_{2p1} modes to become more severe. Calculations show that for $\beta_{\parallel} = 0.4$, Eq. (II.C.38) will not be satisfied until $P_w > 32$ kW/cm^2, which is well above the 5 kW/cm^2 limit mentioned earlier. It is therefore impossible to simultaneously avoid mode overlap and keep P_w at a reasonable level. In order to alleviate the mode competition problem, it will be necessary to operate at the highest possible P_w and to use some of the mode suppression techniques described earlier in this report. It is possible that these techniques, or the appearance of spurious modes, might lead to a reduction of the overall efficiency of the gyrotron. However, since a multimode treatment is beyond the scope of this paper, we have assumed only one mode exists in the cavity and that the η_T based on the calculations of

Nusinovich and Erm can be achieved.

For P_w = 5 kW/cm^2, modes TE_{051} through TE_{071} provide high total efficiency and can be used as operating points. In order to minimize the number of possible spurious modes by keeping the cavity size as small as possible, we have chosen TE_{051} as our reference design mode. This gives R_o = 3.94 mm and, based on the above value of P_w, L = 12.5 mm. The overall efficiency at this operating point is 33%. The beam voltage is 70 kV, and the beam current is 4.3 A. All other design parameters can be calculated using the equations of Section (II.C.4) and are given in Table (II.C.1). Note that, since $\varepsilon_{TOTAL} < \varepsilon_{max}$ = 10%, $J_k < J_k^{max}$ = 4 A/cm^2 and the beam-wall voltage drop $\Delta U/U$ = 6.8% < 10%, the current is well within the limits imposed by the gun. This reference design is characterized by a very low J_k which ensures that the cathode will have a long lifetime.

If the limits imposed by the gun and wall heat flux could be circumvented, then the power output of our device could be increased dramatically by increasing the current. This is shown in Fig. (II.C.17) where P and η_T have been plotted as functions of I. This figure illustrates that, in general, the output power and total efficiency do not peak at the same operating point. If a wall cooling of P_w = 10 kW/cm^2 could be obtained, then the gyrotron could achieve P = 200 kW with η_T = 39%. The corresponding current would be 7.4 A, giving $\Delta U/U$ = 11.6% and ε_{TOTAL} = 9.8%, both close to acceptable levels. Thus, the wall heat flux is the major

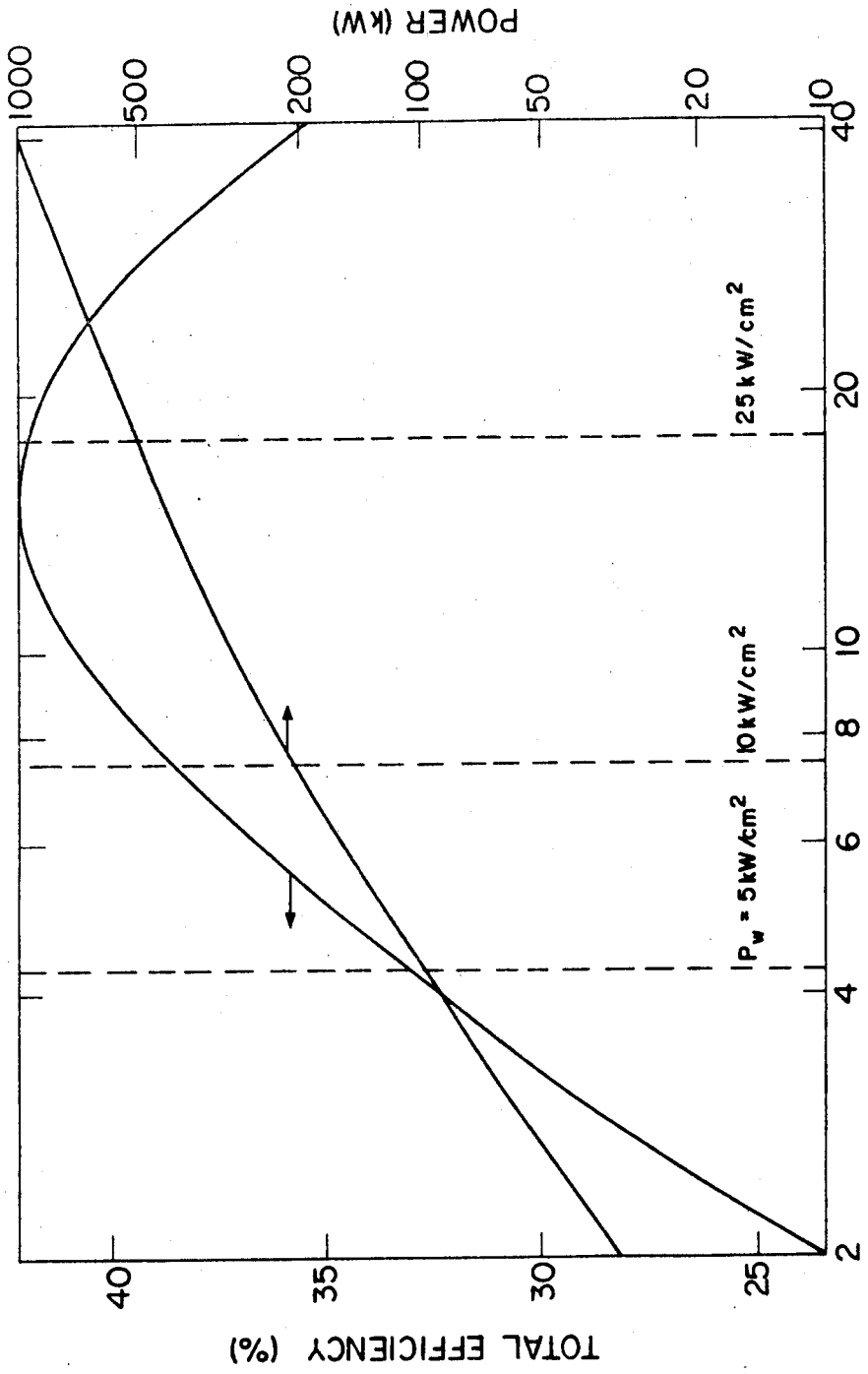

Fig. II.C.17 Total Efficiency and Output Power vs. Beam Current. Also shown are Limits Imposed by Wall Heat Flux.

TABLE (II.C.1)

200 GHz Gyrotron Parameters

ν = 200 GHz	$\omega = 1.257 \times 10^{12}\ 5^{-1}$	ε_{TOTAL} = 8.66%
λ = 1.5 mm	B_o = 75 kG	$\Delta U/U$ = 6.8%
I = 4.35 A	r_g = 0.1 mm	G = 5.16 10^{-3}
U = 70 kV	α = 21.8	μ = 19.66
TE_{051} mode	ξ = 3.0	Q_T = 2264
X_{05} = 16.47	B_k = 3.44 kG	$I_o = 1.79 \times 10^3$
R_o = 3.94 mm	R_k = 13.17 mm	$\eta_\perp$ = 0.50
R_c = 2.82 mm	$\beta_{\perp k}$ = 0.089	η = 0.328
Λ = .8	$r_{\perp k}$ = .467 mm	P = 100 kW
Q_{OHM} = 16,744	$E_{\perp k} = 1 \times 10^5$ v/cm	
K = 3	I_p = 131 A	
Q_D = 2618	ℓ_k = 2.8 mm	
L = 12.5 mm	J_k = 1.88 A/cm^2	
γ = 1.137	V_1 = 21 kV	
β = 0.476	d = 2.1 mm	
$\beta_\perp/\beta_\parallel$ = 1.8	h = 1.21 mm	
$\beta_\perp$ = 0.416	ε_{sc} = 3.3%	
$\beta_\parallel$ = 0.231	ε_T = 1.3%	
$k_\parallel = 2.51\ cm^{-1}$	ε_a = 7.9%	

limit preventing operation at higher powers for the present reference design.

Fig. (II.C.18) shows the effect on η_T of slight variations of the design parameters. We have plotted the change in efficiency caused by the beta ratio, length, beam energy, and beam radius. This graph can be used to determine the expected η_T if the actual design parameters deviate slightly from those values given in Table (II.C.1). Note that the results in this figure do not represent the expected variation of η_T of our device caused by drift of the listed parameters during operation. In such a case, the gyrotron would be detuned (i.e., X would not be at its optimum value), and the efficiency would be likely to vary more than the amount shown. The curves in the figure represent the expected result if X is retuned to its optimum value at each design point. It can be seen that the efficiency is fairly insensitive to parameter variations. Changes in the beam radius cause the largest effect, indicating the need for an accurate electron-optics system that will ensure that the beam will not deviate from a radial peak of the RF field. The variation of η_T with X is described in Section II.C.5.

II.C.5 Gyrotron Cavity Design

Special attention was focused on the gyrotron resonant cavity design, because of the unique and severe conditions under which it must operate. These include high wall loading (5 kW/cm^2), high thermal cycling (> 10^6 cycles), low dimensional tolerances

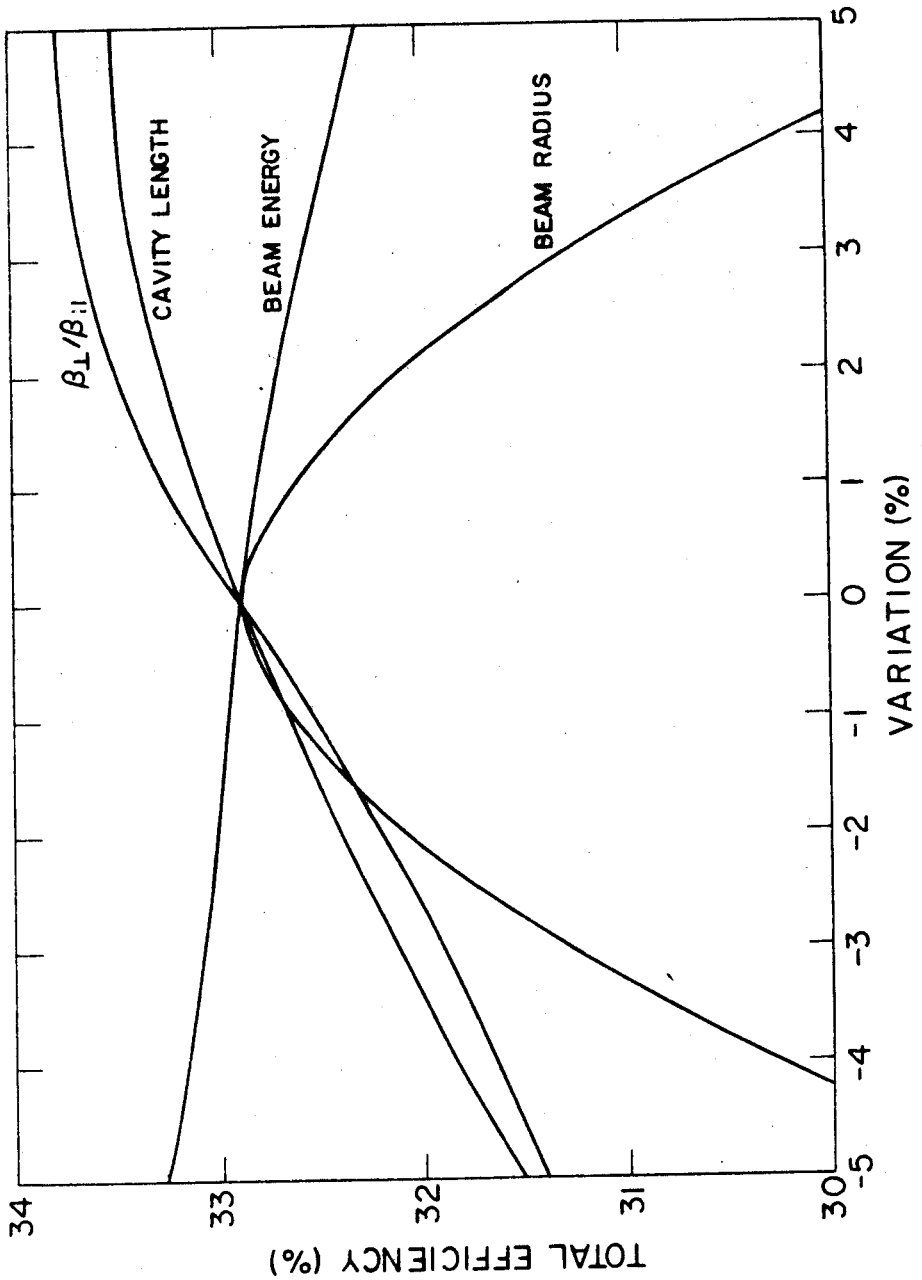

Fig. II.C.18 Changes in Total Efficiency as Design Parameters are Varied. The Detuning Parameter X is Optimized at Each Operating Point.

and small size. A design was selected, incorporating high-velocity water-cooling and a thin, copper sleeve, which was adequate for high-performance and reliable operation.

II.C.5.1 Cavity Description

The gyrotron cavity consists of two types of pieces, as shown in Figs. (II.C.19) and (II.C.20). The outer and larger piece is a casting of electrical grade copper, which includes the resonant cavity, as well as the drift tube and the cavity input and output horns. The casting is connected to the gun and first anode assembly through a metal-to-ceramic seal and is brazed to the collector assembly. Twelve axial-flow coolant holes are machined into the casting with a jeweler's lathe. Four thin copper sleeves, two conical and two cylindrical, are brazed to the outer casting, closing the cooling channels. The inside bores of the cavity, drift tube and horns are then machined to final tolerances.

The water cooling system has a cylindrical, external header on the inlet side and a cylindrical, internal header on the outlet side. Water flows from the collector side of the cavity to the gun side and returns through a hydraulic line, external to the tube. High-purity water flows at a velocity of 75 ms^{-1} through the cavity region, allowing a predicted film temperature drop of only 150 C. A straightforward, single-phase flow design is used, with substantial margins of safety against burnout and cavitation. The

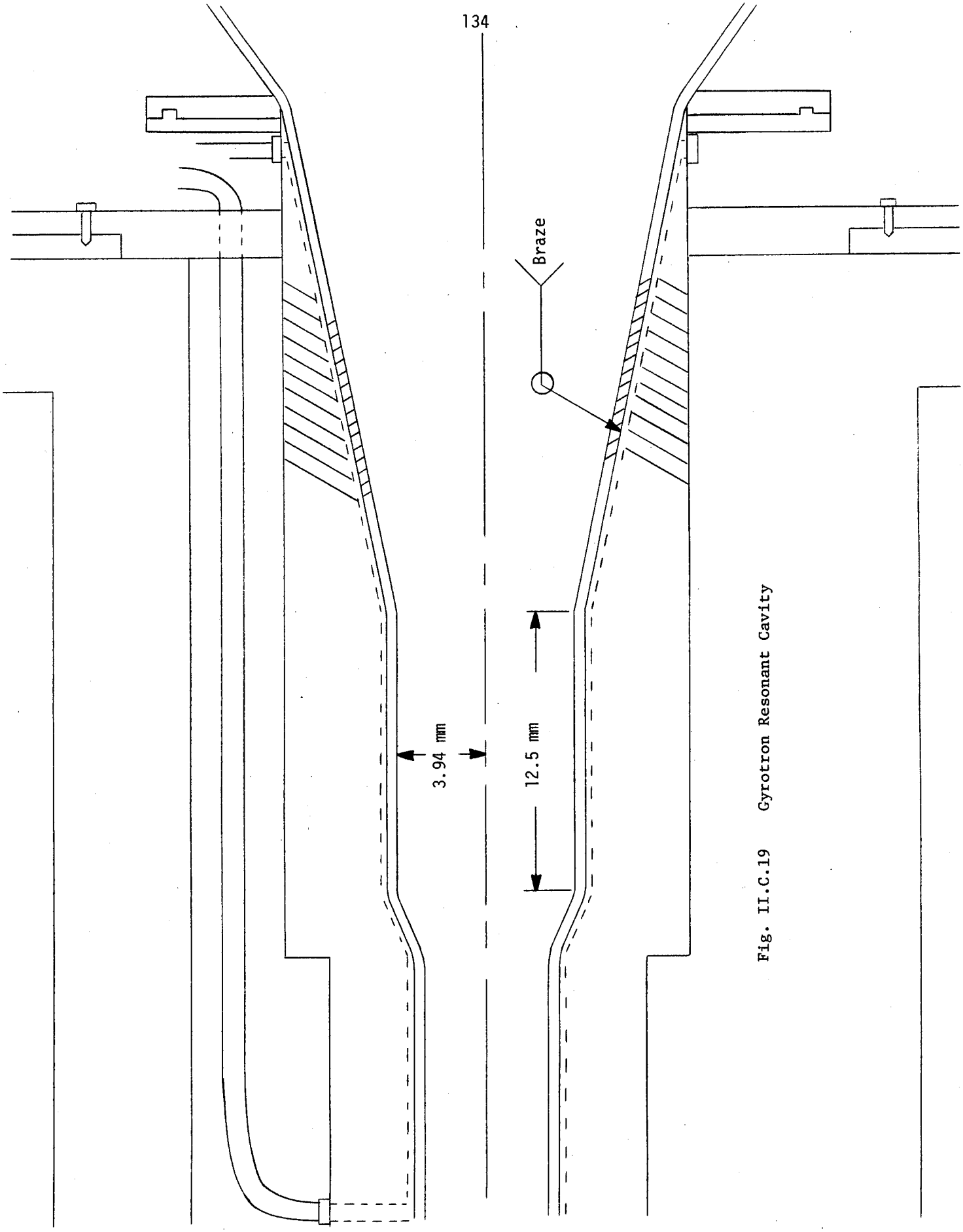

Fig. II.C.19 Gyrotron Resonant Cavity

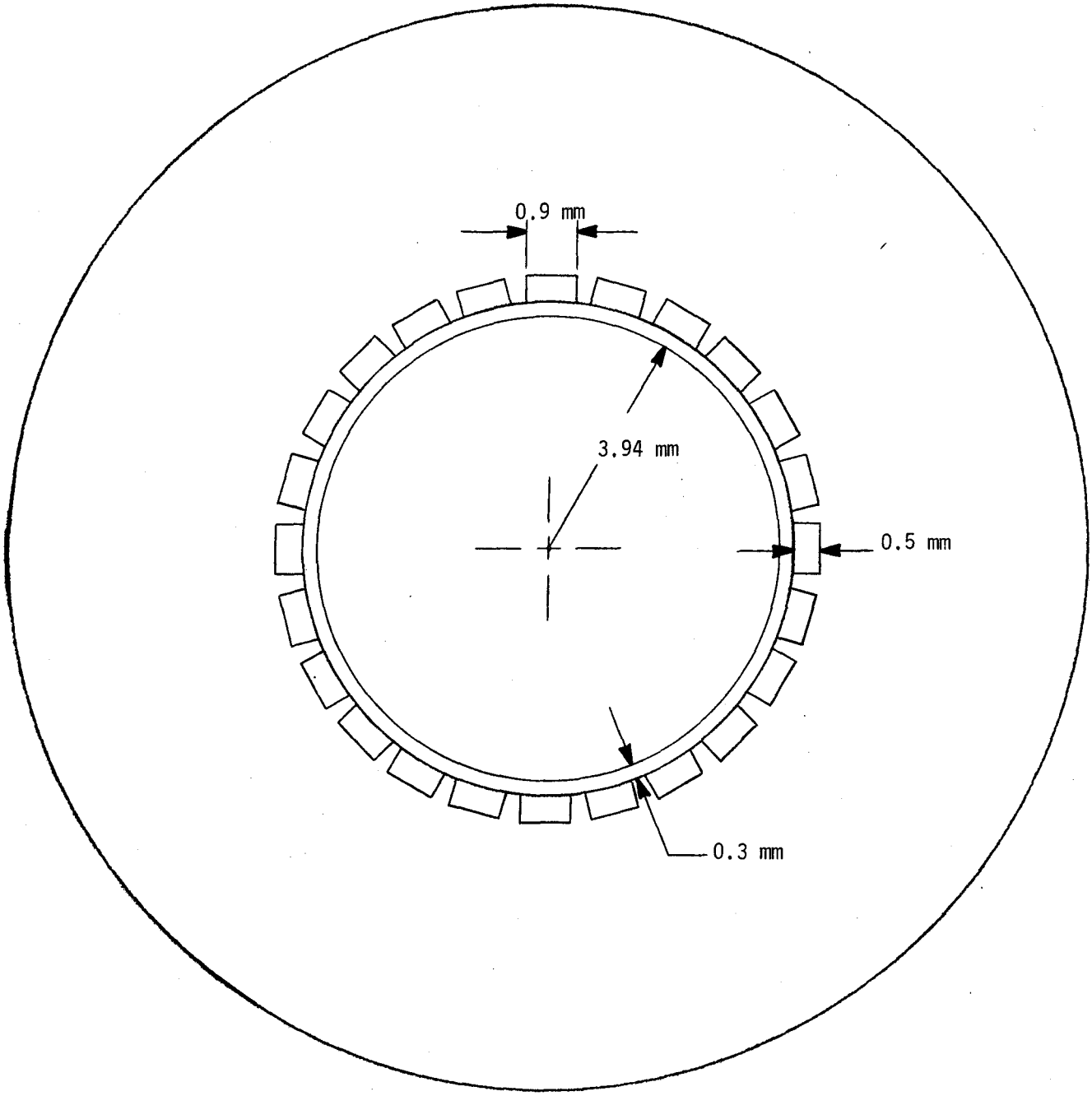

Fig. II.C.20 Gyrotron Cavity Cross Section Showing Cooling Channels.

parameters of the thermal-hydraulic system are shown in Table (II.C.2).

II.C.5.2 Cavity Integrity

The gyrotron cavity must be designed for high reliability versus the combined effect of hydraulic pressure, thermally-induced stresses and cooling channel erosion. Dimensional tolerances must be adequate for positioning of the input electron beam on a radial peak of the electric field, and thermal expansion of the cavity during heating must be limited to avoid detuning of the cavity. Adequate assembly tolerances are assumed to be achievable for the prescribed method of fabrication. While statistical failures will certainly occur in such a large number (> 1,000) of individual tubes, each tube is designed for ultimate fatigue stress limits ($> 10^7$ cycles).

Detuning tolerances can be calculated by relating the gain function of the cavity to its dimensions. The change in the frequency of oscillation due to dimensional changes will only cause a small perturbation in the plasma radius at which the radiation will be absorbed and is of little concern. The key parameter which determines whether the gyrotron will oscillate is the gain bandwidth. The gain bandwidth can be described in terms of the dimensionless parameter X, where

$$X = \frac{\omega_c - \omega}{k_{\parallel}\beta_{\parallel}c} \qquad \text{(II.C.39)}$$

The gyrotron will emit radiation over a gain bandwidth of $\Delta X \simeq 2$ to 4. This predicts an oscillation bandwidth of the order

$$\Delta\omega_G \approx 3k_{\parallel}\beta_{\parallel}c \qquad \text{(II.C.40)}$$

which equals 5.2×10^{10} s^{-1} for the reference design. The variation of X with $k_{\parallel}$ can be shown to be small for all practical cases and is ignored here.

Variations in X can be related to the total efficiency by noting that the efficiency drops to zero when X varies by about 2 from the value of X corresponding to optimum conversion efficiency. Linearizing, a reasonable estimate of the perturbation in efficiency, η_T, is

$$\frac{\Delta\eta_T}{\eta_{opt}} \approx \frac{\Delta X}{2} = \frac{1}{2}\frac{|\Delta\omega|}{k_{\parallel}\beta_{\parallel}c} \qquad \text{(II.C.41)}$$

If $\Delta\eta_T/\eta_T$ is limited to 5%, then for $\omega/k_{\parallel}\beta_{\parallel}c = 72$, $|\Delta\omega|/\omega \leq 1.4 \times 10^{-3}$ and $|\Delta r_o|/r_o$ must be limited to less than 1.4×10^{-3}. Similarly, variations in the magnetic field must be held to $< 1.4 \times 10^{-3}$. The effect of magnetic field variation on gyrotron efficiency is discussed in the literature [KI74] and is consistent with the present analysis. Note that the field variation here is with respect to time and that the sensitivity to field variations in space is much lower. A nonuniformity of as much as 1% should cause only a small change in efficiency [ZA77].

The dimensional tolerances due to cavity detuning can be compared to the dimensional "tolerances" necessitated by fatigue limitations. The temperature drop across the thin 0.3 mm sleeve, from the inside of the cavity to the coolant channel wall is approximately

$$\Delta T = Q'' \rho t \qquad \text{(II.C.42)}$$

where Q" is the surface heat flux of 5 kW/cm^2 and ρ is the thermal resistivity of the sleeve. This predicts a temperature drop across the sleeve of 40 C. 50 C is used here because of the finite thickness of the gaps between cooling channels. The thermal stress in a thin-walled cylinder, heated on the inside and cooled on the outside, and supported on the outside by spines with compliance comparable to that of the inner sleeve is approximately [BE79]

$$\sigma = \frac{\alpha E_{cu}(T_{in} - T_{out})}{2(1 - \nu)} + \frac{\alpha E_{cu}(T_{out} - T_{eff,casting})}{2} \qquad \text{(II.C.43)}$$

where α the linear coefficient of expansion of copper is 1.7×10^{-5} C^{-1}, E_{cu} the Young's modulus of copper is 1.2×10^5 MPa, ν the Poisson's ratio is 0.35, and T_{eff} the effective temperature of the outer casting for thermal gradient calculations is estimated to be about 125°C [BE79]. This predicts a thermal stress of 129 MPa. Since thermal stresses are considerably less likely to lead to

material fatigue than mechanical stresses, the fatigue life criterion is applied to mechanical stresses alone. To determine whether the copper will yield, the thermal and mechanical stresses are added. The yield strength of copper is ambiguous because of the gradual change in the curvature of the stress-strain curve, but is conventionally taken to equal 250 MPa for half-hard OFE copper. Beryllium-doped copper, such as the commercially available GlidCop, achieves a yield strength of 370 MPa at 200°C, with a degradation of electrical conductivity of only a few percent. Since, at the cavity tuning-limited strain of 1.4×10^{-3}, the material stress will equal 172 MPa, the tuning limitation on thermal expansion and the stress limitation on thermal gradients are of comparable severity. The reference design has a substantial temperature margin of safety with regard to either criterion.

The mechanical component of stress, due to hydraulic pressure against the evacuated inner sleeve, will be the principal cause of tube fatigue. While the high-velocity water system could remain on at all times to avoid fatigue problems, the recirculating power due to the high pump power requirements would be excessive. Considering the sleeve beneath a single channel to be a beam of width equal to the channel width and rigidly supported on both ends, the shear stress in the sleeve is

$$\gamma = pw/t \qquad \text{(II.C.44)}$$

where p is the water pressure, w is the channel width and t is the sleeve thickness. The bending stress in the sleeve is

$$\sigma = \frac{3}{2} p \frac{w^2}{t^2} \qquad \text{(II.C.45)}$$

For the inlet pressure of 1.0 MPa, the shear stress is 7.0 MPa and the bending stress is 54 MPa. The combined thermal and mechanical stress must be less than the yield stress. For 10^8 cycles, the fatigue strength for mechanical stresses is 90 MPa for half-hard OFE copper. Becker [BE79] has reworked the manufacturer's fatigue data to take into account the unidirectional character of the stress and correlated the revised curve against independent test samples, as shown in Fig. (II.C.21). The theoretical curve for notched copper implies a fatigue strength of 76 MPa for 10^8 cycles, while the experimental curve implies considerably higher strength.

Erosion of the OFE copper casting can be of concern when the dynamic pressure of the coolant becomes comparable to the yield strength of the channel. For the reference design,

$$\frac{\frac{1}{2} \rho v^2}{\sigma_{yield,cu}} = 1.1\% \quad , \qquad \text{(II.C.46)}$$

so erosion should not be of concern.

Some decrease in the temperature rise in the sleeve during a four second pulse should be provided by the thermal inertia of the relatively more massive casting. However, a first-order calculation shows that 4 kJ could raise the temperature of the entire

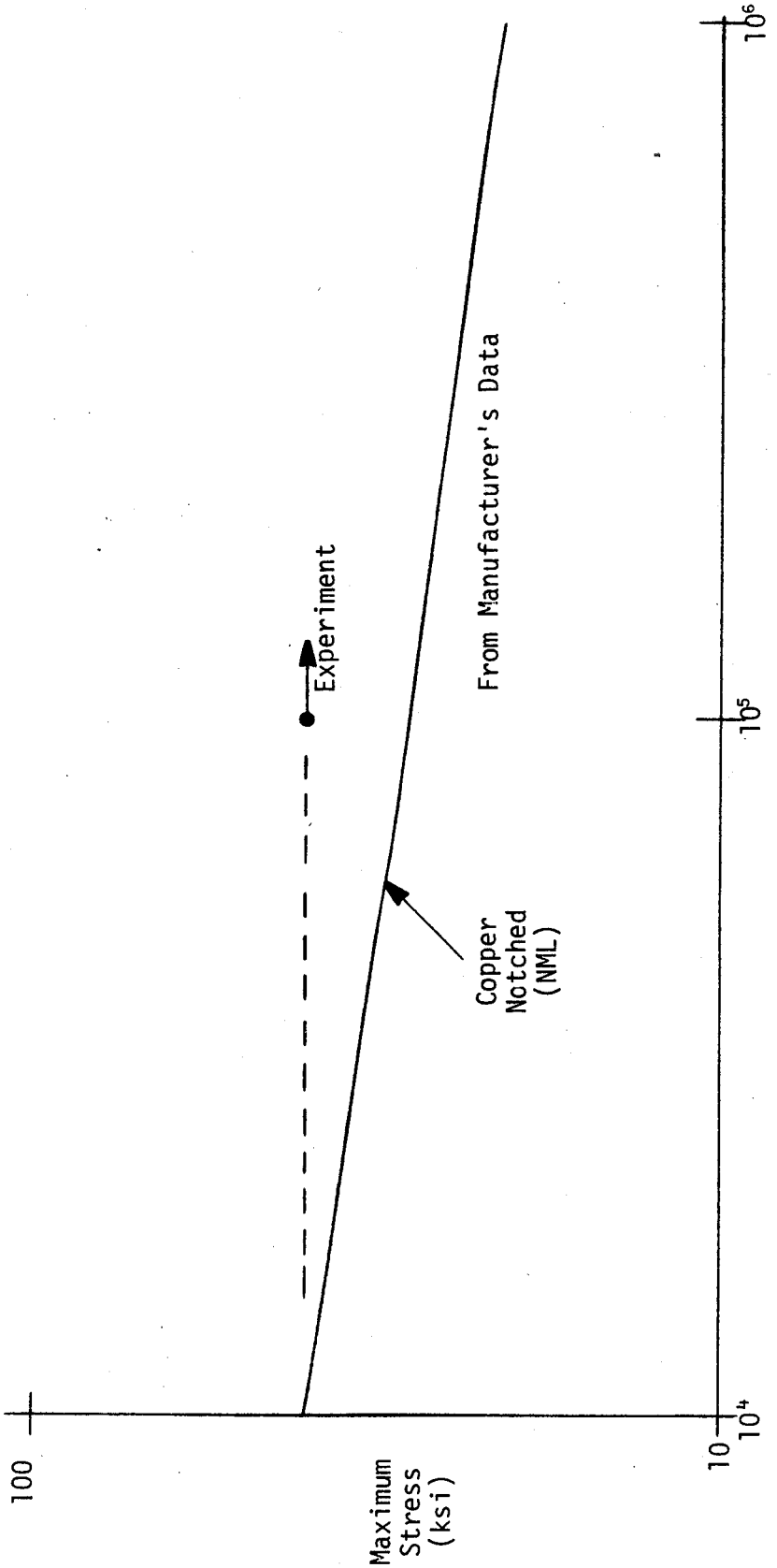

Fig. II.C.21 Fatigue life of OFE Copper Subjected to Unidirectional Stress.

casting by 200°C, while the energy deposited in the cavity during a four second pulse is 62 kJ. The characteristic thermal diffusion time of the casting is approximately 6 seconds, comparable to the pulse length. Therefore, the beneficial effect of thermal inertia appears to be limited to less than a few percent improvement in either temperature rise or gradients.

II.C.5.3 Coolant System Analysis

The principal parameters of the coolant system are shown in Table (II.C.2). The Nusselt number, or measure of effectiveness of the cooling system is determined by the Dittus-Boelter correlation for fully-developed turbulent flow:

$$N_u = \frac{hD}{k} = 0.023\ (R_e)^{0.8}\ Pr^{1/3} \qquad \text{(II.C.47)}$$

where h is the heat transfer coefficient, D the hydraulic diameter, k the coolant conductivity, R_e the Reynolds number and Pr the Prandtl number of the coolant. The channel in the outlet horn has an L/d of 20 so inlet effects can be neglected in the cavity region. Despite their theoretical improvement in the ratio of Nusselt number to pumping power, by about a factor of 1.5, swirl tapes were rejected, because of the small size, noncircular cross-section, added complexity, and low duty-factor pump requirements of the hydraulic system. With straight forward, straight copper channels, the pump power per unit length is 47 kW/m. Over a length of 5.3 cm, including two header drops and three bends, no more acute than 135°,

Table II.C.2

Parameter Table of Gyrotron Cavity Cooling System

No. of cooling channels	12
Channel width	0.18 cm
Channel height	0.06 cm
Flow velocity	75 M/s
Inlet pressure	10^6 Pa
Inlet temperature	25 C
Reynolds number	123,000
Nusselt number	537
Friction factor	0.00613
Heat transfer coefficient	276,000 W/m^2 K
Film temperature drop	156 K
Dynamic pressure	28 MPa
Pressure drop/unit length	52 MPa/m
Pump power/unit length	47 kW/m
Total cavity heating	15.5 kW

a conservatively estimated pump power for the cavity is 10 kW. Head losses external to the cavity are neglected. For a thousand tube system, 10 MW of pumping power would be required, with 15 MW of electrical input to the pump motors. For the reference scenario, the pumps are on for ten seconds of a 500 second pulse and the average electrical recirculating power is only 30 kW.

In addition to the cavity walls, the collector region will also be subjected to high heat fluxes due to electron bombardment. The total power that must be absorbed by the collector walls is:

$$P_c = I U (1 - \eta_\perp \eta_{e\ell}) \qquad \text{(II.C.48)}$$

For the reference design parameters, P_c = 188 kW. Although this is substantially larger than the 15.5 kW absorbed by the cavity walls, it is assumed that the collector radius can be made sufficiently large so that the heat flux on the walls is reduced to tolerable levels. A detailed analysis of the collector will not be given in this report. However, the requirements imposed by the collector design should be comparable to those anticipated for the 200 kW, 28 GHz Varian gyrotron [JO 77], which will operate in a CW mode.

II.C.6. Conclusions

In Section II.C we have presented a parametric analysis of a 100 kW, 200 GHz gyrotron. Our primary goal was to maximize the overall efficiency of the device in order to reduce power supply requirements and enhance the lifetime of the cavity and collector. We also investigated the major technological constraints imposed on the gyrotron by the cooling requirements and electron gun, and determined how the range of the design parameters is limited by these constraints. A self-consistent model of the cavity and gun was developed in Section II.C.2 and subsequently used to determine which design parameters most acutely affect the behavior of the gyrotron. A procedure was outlined for selecting a design point that conforms to the technical and physical constraints and exhibits high η_T, and this procedure was used to select the reference design given in Table (II.C.1).

Our study of the sensitivity of the total efficiency to design variables showed that there is an optimum cavity length for each design point. If L is too short, then $\eta_\perp$ cannot reach its maximum value. If L is too long, then the diffractive Q, Q_D, becomes comparable to Q_{OHM} and η_Q decreases. There is also an optimum beam energy, and for the present design the range of 40 kV to 60 kV was found to give the highest values of η_T. The beta ratio, $\beta_\perp/\beta_{||}$, has the largest impact on the efficiency and should be made as large as possible. However, as $\beta_\perp/\beta_{||}$ increases, it becomes more difficult to control the quality of the electron beam, and eventually the velocity spread of the beam becomes so severe that a net reduction of the overall efficiency occurs. Finally, we found that the optimum length could be altered by changing

the degree of output coupling, and that such a change did not greatly affect the maximum η_T that could be achieved.

Our analysis of the electron gun indicated there are three major limits on the maximum beam current. These limits involve the highest allowable velocity spread [Eq. (II.C.35)], the current density at the cathode [Eq. (II.C.36)], and the beam-wall voltage drop [Eq.(II.C.37)]. It was found that operating in a higher mode and having the beam interact with a radial maximum near the cavity wall helped to alleviate these constraints on I. A detailed design for the cavity coding system was also developed, and a wall heat flux $P_W \lesssim 5 kW/cm^2$ was found to be acceptable.

A number of trade-offs were encountered during the course of our analysis that influenced the procedure used in selecting the design parameters. The choice of $\beta_\perp/\beta_\parallel$ involved the opposing requirements resulting from the desire for high efficiency and the need to limit the beam velocity spread. When selecting the operating mode, one must balance the need for a low wall heat flux with the need to minimize mode competition. The difficulties associated with wall heating and spurious modes become more acute as the frequency and power level of the gyrotron are increased, and it was found that for the present design the requirements imposed by these two problems could not be satisfied simultaneously, necessitating the use of additional mode suppression techniques. Finally, when choosing the beam radius, it is desirable to have R_e as large as possible in order to ease the gun constraints on the current, but this reduces the strength of the interaction between the beam and RF field.

Although the gyrotron model we developed was found to realistically describe the physical processes of the device, one should understand the limitations of our analysis. We restricted our attention to a simple design only, and did not include efficiency enhancement techniques such as magnetic field [FL77] and RF field [BY75] profiling. The model is based on the present understanding of the gyrotron, and our conclusions might be altered somewhat as the technology of the device improves. Our basic purpose was to demonstrate that a 100 kW, 200 GHz gyrotron appears feasible based on a reasonable extrapolation of present state of the art technology, and to determine a representative set of design parameters that might characterize such a device.

A parametric study is also useful in pinpointing major problems that must be investigated in greater detail in the future. On the basis of our analysis, we recommend the following areas be examined closely:

(1) Electron gun - find ways of increasing $\beta_\perp/\beta_\parallel$ without introducing a velocity spread in the beam. Increase the breakdown voltage limit so that the mirror ratio α and the velocity spread due to space charge might be reduced.

(2) Cooling - investigate the problems associated with the development of hot spots.

(3) Multimoding - develop mode suppression techniques that will not adversely affect the efficiency of the gyrotron.

(4) Profiling - determine how magnetic and RF field profiling affect the efficiency and operational characteristics of the device.

Finally, we should point out that the gyrotron design presented here is based on the single cavity oscillator, or gyromonotron. Our conclusion is that a 100 kW, 200 GHz gyromonotron represents a significant extension of present day technology, but that such a device should be possible. However, we recognize that major improvements in gyrotron technology are possible and that alternative versions of the gyrotron, such as the gyroklystron and gyro-twystron [FL77] or even totally new devices, may be developed with improved output power, efficiency and/or reliability. Such improvements in electron tube technology would result in a more favorable outlook for ECR heating of a tokamak power reactor.

II.D GYROTRON POWER AND MAGNET SYSTEMS

II.D.1 Gyrotron Power Systems

The gyrotron cathodes and first anodes require high voltage, moderate current power supplies. A high degree of voltage regulation and cathode protection is required. The power supply design considerations are similar to those of state-of-the-art klystron supplies and near state-of-the-art neutral beam power supplies. A standard series regulator configuration was selected, with protection of gyrotrons and regulator tubes provided by crowbars, as shown in Figure II.D.1.

The most important and expensive circuit is the cathode supply. The second anode or collector is ground for both the cathode and first anode supplies. Six cathodes are supplied by a single switch/regulator tube, rated at a current of 40 A and a stand-off voltage of 120 kV, such as the commercially available X2062K. The nominal operating parameters of the regulator are 25.8 A with a plate-ground voltage of 70 kV and a plate-cathode voltage of 5 kV. The tube dissipation of 129 kW, and plate dissipation and (for the X2062K) screen dissipation of 3 kW are within the maximum allowable steady-state ratings of the tube. For a pulse longer than two seconds, no benefit can be derived from the thermal inertia of the tube, and both plate and screen dissipation ratings become power rather than energy dependent.

In order to stay within the dissipation limits of commercially-available tubes, the voltage regulation at the modulator cathode must be high. Traditionally, as in the Alcator C klystron supplies [ME79], this is accomplished with a large high-voltage capacitor bank which prevents

excessive droop in the voltage at the tube cathode. However, for a pulse as long as 4 s, this method can be overly expensive. For example, in order to keep plate dissipation of an X2026K within maximum allowed limits, a voltage droop of about 3 kV would be permitted. For a typical high voltage rectifier-transformer reactance of 0.125 p.u. (desired in order to limit rectifier fault currents to no greater than 8 p.u.), the regulation from no load to full load is $\sim$ 0.088. Therefore, the time behavior of the capacitor voltage after tube turn-on is dominated by the low "equivalent resistance" for voltage-drop calculations of the transformer reactance. For a four second pulse, a capacitance of 26 mF would be needed to limit the droop to 3 kV. If all the current were drawn from the capacitor bank, a capacitance of 34 mF would be needed. This would require a capacitor bank with an energy storage capacity of 73 MJ and an approximate cost of \$10.0 M, perhaps a hundred times higher than that of the tube being protected. The alternate design, proposed here, uses two switched resistors in order to greatly enhance regulation in exchange for a small penalty in energy dissipation, as shown in Figure II.D.1. Before the beginning of a gyrotron pulse, the fast ac breaker is closed and the capacitor bank of only 25 μF is charged to 75 kV in 0.15 s, through a 4 kΩ resistor. Rectifier terminal voltage remains close to the open circuit value of 82 kV. After 0.15 s, the dc switch S1 is closed and the rectifier voltage drops rapidly to its full load value through a small 40 Ω resistor. While the tube must stand off 82 kV, which it is rated to do, the voltage droop while it is carrying current and dissipating power is now negligible.

While the use of dropping resistors may seem inelegant for an electrical generating facility with severe design constraints on re-

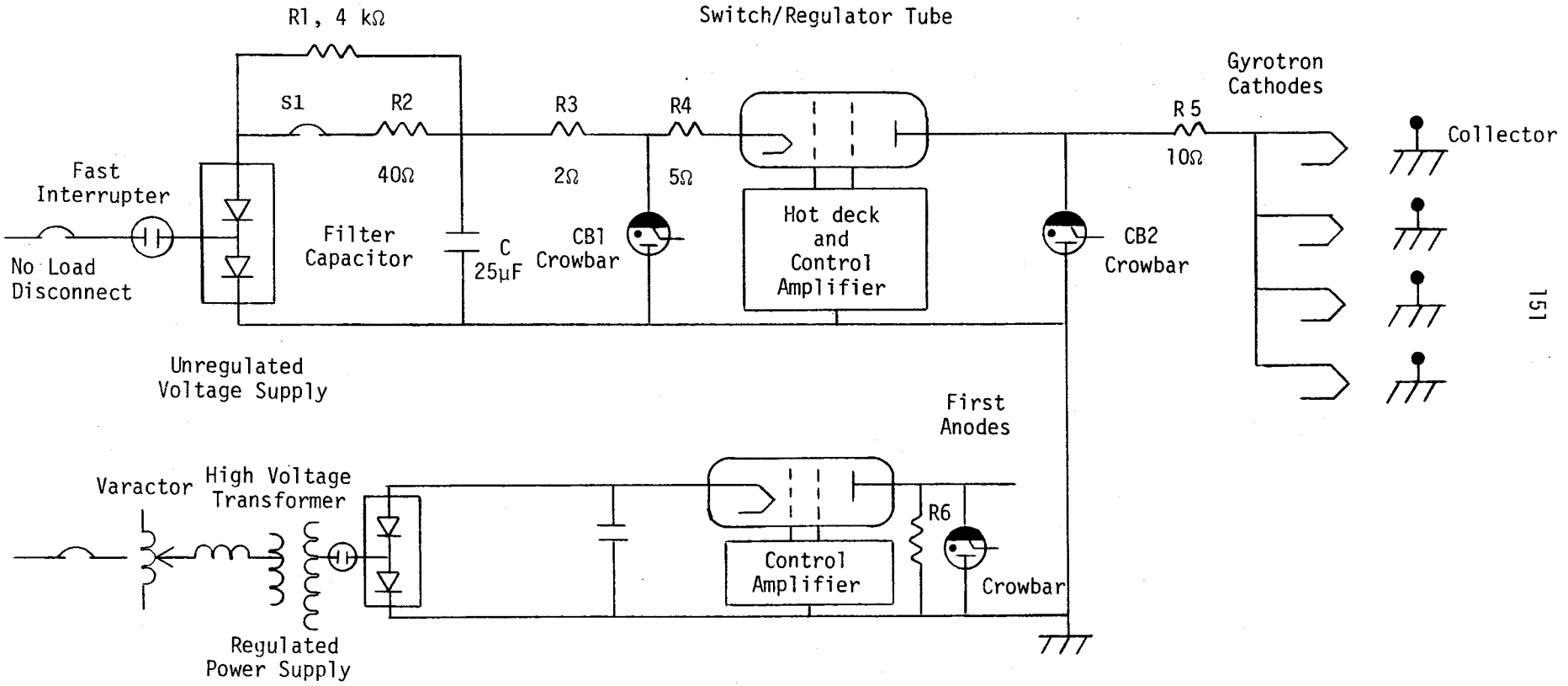

Figure II-D.1
Regulated Power Supply for
Four ECRH Gyrotrons

circulating power and net energy balance, they have many advantages for this specific application and negligible disadvantages. The loss of power supply efficiency due to the four series resistors R_1, R_3, R_4, and R_5 is 1.8%. Since the duty factor of the gyrotron heating circuit is 4 s out of 500 s, the average power dissipated by the resistors is 2 kW over a cycle, which is negligible. Tube and capacitor costs are substantially reduced, while rectifier ratings increase by less than 1.8% since the resistors permit the tubes to separate at a lower plate-cathode drop. For a 12-pulse rectifier, the main dropping resistor R_2 reduces the 3.4% peak voltage ripple at the rectifier to 0.6% ripple. This relieves the tubes of any ripple reduction requirement and allows slower grid control circuits or lower gain in the grid feedback control circuits with substantially lower possibility of unwanted tube oscillations. R_2 also snubs the deposition of energy from the capacitor bank, when the ac breakers are opened on faults. R_3 limits the energy deposition from the capacitor bank into the series crowbars CB_1, while R_4 and R_5 provide the negative voltage necessary to fire the crowbars and remove arc current rapidly on arcs of the modulator and gyrotron respectively. This saves the cost of negative bias supplies.

Because of their small size, gyrotron cathodes are probably limited to a few joules of arc dissipation per arc before voltage holding degradation begins, similar to the degradation observed on neutral beam grids. The combination of dropping resistors prevents damage to the cathodes. Unlike neutral beams, gyrotrons can be placed in close proximity to their power supplies. If R_5 is physically adjacent to each gyrotron cathode, for a typical arc voltage of 30 V, it would attenuate

the arc energy due to stored energy in cable and modulator parasitic capacitance by a factor of 2,000.

Since cable runs will be short, the dominant source of stored energy is the 10,000 pf plate capacitance of the modulator. Without resistor R_5, it would deposit 25 J in the arc or require building expensive, biased saturable snubbers similar to those used for all large sources made at the Lawrence Livermore Laboratory. R_5 reduces the energy deposition from stray capacitance to negligible quantities. In the case of a simultaneous gyrotron and modulator arc, R_3, R_4 and R_5 attenuate the energy deposited by the capacitor bank by a factor of about 3,000 to 24 J, even if both crowbars fail. For a sensor and crowbar response time of 50 μs and stray loop inductance of 3 μH, the deposited energy is limited to 0.1 J.

The adequacy of 0.6% voltage ripple can be justified by the following electron optics considerations. Since the first anode power supply draws negligible current, it is assumed that first anode-cathode voltage can be controlled to a high degree of accuracy with little cost penalty. A "keep-alive" resistor, R_6, is shown at the regulator plate to allow the desired high degree of regulation. Voltage droop and ripple requirements on the cathode-grounded cavity voltage can be expressed in terms of the dimensionless detuning parameter X, where

$$X = \frac{\omega_c - \omega}{k_{||} v_{||}}$$

as described in Section (II.B).

The variation of the cathode voltage V will cause both the cyclotron frequency ω_c and the parallel velocity $v_{||}$ to change. The relativistic cyclotron frequency is $\omega_c = \omega_{co}/\gamma$, where ω_{co} is $eB_o/m_e c$

and

$$\gamma = 1 + \frac{V(kV)}{511} \quad .$$

Since $V \approx \frac{1}{2} m_e (v_{\parallel}^2 + v_{\perp}^2)$ one can write:

$$\frac{\Delta v_{\parallel}}{v_{\parallel}} = \frac{1 + g^2}{2} \frac{\Delta V}{V} \quad \text{where} \quad g \equiv v_{\perp}/v_{\parallel} \, .$$

Solving for ΔX,

$$\Delta X \cong -\left[\frac{\omega}{k_{\parallel} v_{\parallel}} \frac{V(kV)}{511} + \frac{(1 + g^2)}{2} X\right] \frac{\Delta V}{V} \quad .$$

Using the reference values of $\omega/k_{\parallel} v_{\parallel} = 72$, $V = 70$ kV, $g = 1.8$ and $X = -2.5$, and applying the previously derived (Section II.C) requirement that $\Delta X < 0.1$ for a 5% loss in efficiency due to detuning,

$$\frac{\Delta V}{V} < 0.022$$

is the design requirement for ripple and droop voltage. This limit is consistent with the specifications for the power supplies for gyrotrons in the Soviet Union, which have a droop of less than 2%. An analysis by Seftor et al [SE78] indicates that the variation of electron beam velocity due to a voltage droop can be neglected.

II.D.2 Gyrotron Magnets

The solenoid magnets used to create an electron cyclotron resonance of 200 GHz in the gyrotron cavity are long, superconducting NbTi solenoids with graded current density to enhance field homogeneity. Field uniformity of better than 1% can be achieved in the cavity region.

The NbTi conductor is edgewound on an inner bobbin in layers. Insulating spacers are used to achieve graded current density. No internal structure is necessary. Magnet parameters are listed in Table II.D.1.

TABLE II.D.1

Parameter List for Gyrotron Cavity Magnets

Superconductor Type	NbTi
Matrix material	Copper
Maximum field	7.6 T
Conductor current	562 A
Stored Energy	40 kJ
Radius, Inside Bore	2.0 cm
Radius, Outside Bore	8.0 cm
Length, magnet winding	20.0 cm
Turns	2200
Conductor dimensions	0.4 cm × 0.1 cm
Ampere - turns	1.21 MAT
Hoop force, total	0.182 MN
Maximum stress in copper	56 MPa

The field, energy, and homogeneity requirements of the solenoid bore are unexceptional, and, with the exception of a requirement for microwave and x-ray shielding, present no significant design problems.

II.E Microwave Transmission System

Once the RF power is generated in the gyrotron cavity, a suitable transmission system must be designed that transmits this power to the plasma with relatively small losses. A variety of techniques are available for millimeter wave propagation [PO59, YO68, YO69, OK68, BE69]. In this section we will investigate the advantages and disadvantages of several approaches and select the one that appears most suitable for high frequency, high power transmission. A detailed design based on this approach will then be given, including discussion of the loss mechanisms, filters, mode transducers, and windows.

When designing a transmission system, a number of requirements must be satisfied. These include the following:

(1) The system should be compact in order to satisfy space limitations. This suggests the use of a guiding structure that keeps the power concentrated.

(2) Attenuation due to ohmic heating in the guiding structure, diffraction, and conversion to lossy or unusable modes should be small. This simplifies the problem of cooling the structure. This also provides design flexibility since the gyrotron sources can be placed relatively far from the reactor without excessive power losses.

(3) The system should operate well below breakdown voltage, yet be able to support a high power density in order to ensure that

the dimensions of the system do not become excessively large.

(4) Power transmission should not be overly sensitive to system irregularities such as surface roughness, misalignment, joint offsets, etc.

(5) Any mode transformations that are required should be accomplished with minimal conversion to unwanted modes.

(6) If windows are needed, they must withstand vacuum and thermal stresses, and result in minimal insertion losses.

(7) The transmission system should be easy to assemble, disassemble, and align.

Research in the area of high frequency microwave transmission has increased recently as the result of renewed interest in utilizing centimeter and millimeter waves for long distance, trunk communication [KA65, YO69, IN76]. A major reason for this interest has been the need for additional communication channels, and at these wavelengths enormous bandwidths can be made available. The results presented in this section represent to a large extent an extrapolation of this research to our regime of operation. Our emphasis will differ somewhat from that of microwave communication. Whereas in communication signal distortion represents a major problem, our primary goal is to minimize power losses, and signal variations do not play a crucial role. Interest in millimeter wave transmission has also increased in conjunction with weather and surveillance radar, and radio astronomy.

II.E.1 Comparison of Transmission Techniques

A variety of methods are available for millimeter wave propagation, and a number of these techniques are described in Table (II.E.1). For each method of propagation, the advantages and disadvantages are given, as well as typical power and attenuation values based on a frequency of 200 GHz. These approaches can be categorized into three basic classes of waveguides:

(1) Beam waveguides, where the cross-sectional field distribution of the microwave beam is reconstituted at periodic intervals. Free space transmission, which involves no reconstitution of the beam can also be included here. Beam waveguides are of greatest interest at wavelengths below a few millimeters where conventional waveguides become inefficient for long distance transmission and the required mechanical precision poses severe technological problems.

(2) Surface waveguides, where the field is essentially on the outside of the guiding structure.

(3) Closed waveguides, where the entire field is enclosed by a metal container and shielded from the environment.

High power microwave transmission is hampered primarily by the relatively large transmission losses in the guiding structure. This loss is due to ohmic heating caused by currents flowing in the structure. Efficient power transmission thus requires either a mode which is associated with very low current, or a technique which

TABLE (II.E.1) COMPARISON OF TRANSMISSION TECHNIQUES

TYPE OF PROPAGATION	EXAMPLE	ADVANTAGES	DISADVANTAGES	POWER	ATTENUATION
Free Modes	Free Space	No metal attenuation No connection to reactor Design Flexibility	Safety problems Aperure losses Beam spread	$\lesssim 1$ MW/cm^2	1.5×10^{-2} dB/m for R_r = 50 cm R_e = 4.5 cm
Beam Modes	Reflecting Mirrors	Minimal attenuation Reduced material requirements No connection to reactor	Alignment Window Safety problems Lack of Experimental results	25 MW/beam	3.3×10^{-4} dB/m
Surface Wave	Cylindrical copper Line	Simple design	Support problems Interference between lines Radiation losses	2500 kW/line	0.1 dB/m (1 cm. diameter line)
Closed waveguide - Multimode	TE_{01} in circular waveguide	Adequate size Self alignment Lower attenuation as ω increases Experimentally tested	Spurious modes More structural material required	800 kW/waveguide	6.8×10^{-3} dB/m (14 mm. diameter pipe)
Closed waveguide - Fundamental mode	TE_{11} in circular waveguide	No spurious modes Known technique Flexibility Self-alignment	High attenuation Low power Rotating polarization	4.2 kW/waveguide	6 dB/m (1.2 mm diameter pipe)

POWER AND ATTENUATION VALUES BASED ON FREQUENCY OF 200 GHz

utilizes very little guiding structure. More favorable are the limitations imposed by electric breakdown on the power-carrying capacity of these waveguides. Most of the waveguides that were investigated could theoretically support the power levels we require with a sufficient margin of safety.

Free space transmission [BE69, OK68] involves the transmission of power from an emitting to a receiving antenna. The antenna may be a microwave type of receiver, such as a horn, or an optical component, such as a reflecting and/or focusing mirror. This approach offers the advantage of not using a guiding structure with its inherent losses. Attenuation is due to diffraction and to the intervening air, and as long as the air is kept dry it should cause a negligible attenuation of about 3×10^{-5} dB/m. The lack of waveguide connections to the tokamak reactor results in design flexibility and simplifies the assembly and disassembly procedures. The power carrying capacity of 1 MW/cm^2 [OK68], based on the breakdown of air at room temperature and one atmosphere pressure, is more than adequate for our needs. Potential problems include alignment difficulties, beam spread due to the lack of a mechanism for reconcentrating the beam power, and losses due to mismatches and inefficiencies at the horns/antenna. There is also a safety problem associated with the lack of shielding and the possibility of accidental irradiation of neighboring equipment due to misalignment.

One possible free space transmission system would consist of

a focusing reflector as the emitting antenna and a microwave horn as the receiving antenna. One might also utilize a reflector at the receiving end that would focus the incoming power into the horn. For our design we have assumed each gyrotron will have a separate transmission system in order to avoid problems associated with combining power from different sources. Theory [BE69] shows that transmission efficiencies greater than 90% can be obtained if $R_e R_r/D\lambda \gtrsim 0.5$, where D is the pathlength, λ is the wavelength, and R_e and R_r are the radii of the emitting and receiving antenna respectively. Using R_r = 50 cm., which is based on space limitations within the reactor building, D = 30 m based on the plant layout discribed in Section (II.B), and λ = 1.5 mm, then one requires $R_r \geq 4.5$ cm in order to achieve high transmission efficiency. Such a design appears feasible. However, the safety problems and difficulties associated with alignment tend to reduce the attractiveness of this system. These problems could be reduced if the gyrotrons were placed closer to the tokamak reactor.

In order to avoid losses due to beam spread, one can utilize quasi-optical techniques to periodically reconcentrate the beam power [BE69, OK68, YO68]. The prefix "quasi" is used to indicate that the transmission is governed by a combination of geometric optics and diffraction optical relations. We have investigated a reflecting mirror, rather than a lens, arrangement, because of the low losses of mirrors, and the results are shown on the second row of Table (II.E.1). As with free space transmission, the reflector system offers the advangages of no waveguide connections to the reactor and lower costs due to the reduced material requirements (as

compared to a closed waveguide system). It also suffers from the same alignment and safety problems as free space transmission.

In order to reduce the complexity of a beam waveguide system, we have assumed in our design that all the power of an ECRH station (~ 25 MW) can be combined into a single beam. Problems involving the adverse interaction of RF radiation from individual gyrotrons can be avoided by allowing each gyrotron to operate at a slightly different frequency. This will not greatly alter the absorption process in the plasma since the frequency bandwidth will remain narrow. The beam is assumed to have a Gaussian cross-sectional profile since this distribution has the highest energy concentration on the beam axis. Studies [OK68] indicate that Gaussian beams can be obtained with sufficiently high launching efficiencies using conical horns. The mirrors consist of elliptical copper plates shaped to give the appropriate focal length and of sufficient size that the diffraction losses become negligible. Based on the voltage breakdown criterion, these mirrors must be separated by at least 6 meters in order to support a 25 MW beam with λ = 1.5 mm. The choice of reflection angle (the angle between the mirror surface and beam) involves a trade-off between the need for a small angle in order to minimize attenuation due to ohmic losses in the reflectors, and the desire for a large angle to simplify the alignment problem. As indicated by Table (II.E.1), beam waveguides appear capable of transmitting high power levels in a low-loss efficient manner. The major

problem facing the quasi-optical approach in our design is the difficulties associated with transmitting a 25 MW beam through the vacuum window at the reactor. We assume that a window will not be able to transmit more than about 5 kW/cm^2. For a 25 MW beam, the total window area must then be about 5×10^3 cm^2, i.e. 0.5 m^2. It appears unlikely that any single window of that size will be able to withstand the thermal stresses due to internal beam attenuation as well as the stresses resulting from the pressure differential. One possible solution is a division of the main beam into a number of smaller beams just before the vacuum wall, and then transmitting each of these beams through a separate window. This would allow the use of thinner windows, thus reducing the beam losses, but would add to the complexity of the system. The necessity of locating such a complex structure, which will require precise alignment, at the reactor site is a negative feature of this transmission system.

Surface waveguides [OK68, BE69] are defined as transmission systems in which the power is transmitted along the outer surface of a guiding structure. A large variety of surface wave techniques have been developed involving both dielectric and metallic media. These systems offer the advantages of design simplicity. However, as with beam systems, the lack of shielding causes safety problems. Surface waveguides are also hampered by radiation losses near guide supports, bends, and the launching and receiving horns. There is

also the possibility of field interference between neighboring lines if they are too close. We have investigated the use of a cylindrical copper transmission line running from each gyrotron to the reactor. For a 1 cm diameter line, the power carrying capacity is more than adequate, but the attenuation due to ohmic losses of 0.1 dB/m is too high for our design. Surface waveguides appear to be best suited for high power transmission over very short, straight paths that require minimal structural support for the guide.

The final transmission scheme we studied was the closed waveguide [OK68, BE69]. The most common types are the rectangular and circular waveguides. We have limited our attention to two versions of the circular guide; a small diameter tube in which only the fundamental mode, TE_{11}, can propagate, and an oversized tube in which the power is transmitted in the form of a TE_{01} mode but in which a variety of spurious modes can exist. Closed waveguides, because of their inherent shielding, pose a less severe safety problem than open systems, and are less susceptible to misalignment. However, closed guides require more structural material, and this will tend to augment the cost of such a system.

As indicated by Table (II.E.1), a circular guide supporting only the fundamental mode is not a viable transmission method. High frequency operation requires a very small diameter pipe, and this causes the attenuation to be too high and the power level to be too low. Thus, an oversized tube is the only kind of closed guide that can be used in our design. The choice of TE_{01} as the

propagation mode is based on an attractive feature of TE_{op} modes in circular guides. Their attenuation due to ohmic losses decreases as frequency increases. Thus, at 200 GHz, it is possible to transmit high power levels in a reasonably small diameter pipe and sustain less than a 5% ohmic loss over a 30 m distance. The major difficulty facing oversized guides is losses resulting from coupling between the TE_{01} mode and unwanted modes. Such coupling is caused by a variety of factors, including guide irregularities, surface roughness, and bends.

Another problem with a transmission system utilizing the TE_{01} mode in oversized circular waveguide is the necessity to linearly polarize the radiation at the reactor for ordinary wave plasma heating. This problem could be avoided if linearly polarized radiation were produced near the gyrotron and then transmitted with low loss and low conversion to other modes. This might be possible using TE_{op} modes in a rectangular guide or TE_{11} mode in an elliptical guide. In these cases, the problem of matching the gyrotron output to the guide mode appears to be more severe than in using TE_{01} mode in circular guide. Improved technology of mode conversion, however, could make the other approaches more attractive.

Based on our broad investigation of transmission schemes, the oversized waveguide and reflecting mirror systems are the most attractive methods for our design. Of these two techniques we have chosen to use the oversized waveguide. Although the quasi-optical

approach doesn't require the high mechanical precision of waveguides and can negotiate bends more easily, the problems associated with the need to break up the beam in order to transmit it through a vacuum window severely penalize this method, as well as the need to provide some shielding of the beam and the difficulty of aligning the optical structure. The oversized waveguide was also chosen based on past communications research in which total attenuations as low as 1 dB/km were achieved experimentally for a frequency range of 40 to 100 GHz over a distance of several miles [AL77]. A detailed design based on the oversized waveguide will be given in the next section. Although the reflecting mirror system was not selected for our design, it should be noted that our work indicates that this approach is a viable alternative.

II.E.2 Detailed Transmission Design

In this section the major features of a transmission system based on the oversized waveguide concept will be described. Each ECRH station will deliver 25 MW of RF power to the plasma. Based on a transmission efficiency of approximately 80%, which will be justified later in this section, each station must produce 31.25 MW of power. With each gyrotron producing 100 kW, and assuming an individual oversize circular waveguide transmission run for each gyrotron, this implies a set of 313 pipes running to the reactor. We envision an 18 x 18 array of transmission waveguides, where the additional tubes over 313 will be used for diagnostics or as spare channels in case working channels are lost. This array of tubes will be encased in

a larger container that will provide support. This larger tube might also be used to contain a forced air (or inert gas) flow that would carry away the heat generated in the walls of the waveguides.

Fig. (II.E.1) shows the major features of the individual transmission waveguides. Since the operating mode of the gyrotron will be TE_{051}, a converter will be necessary to transform a TE_{05} mode to a propagating TE_{01} mode. Such a component must be able to accomodate the high power that will be transmitted and at the same time not introduce a large insertion loss in comparison to other loss mechanisms. We will assume that such a device can be constructed. One possibility is the use of quasi-optical techniques similar to those used in a design proposed by Vlasov et al. [VL74, VL75] for transforming circular waveguide modes into polarized, highly directional wave beams or into the principal modes of a rectangular waveguide. In their experimental investigations, they achieved a somewhat low power transformation coefficient of 70 - 75% for λ = 5.1 mm, but expected that this coefficient could be increased if more exact transformer parameters were chosen based on the consideration of diffraction effects.

One potential problem facing the gyrotron is the possibility of RF power being reflected at some point along the transmission path back into the resonant cavity, causing a severe power load and subsequent damage. Such a reflection could occur at the plasma,

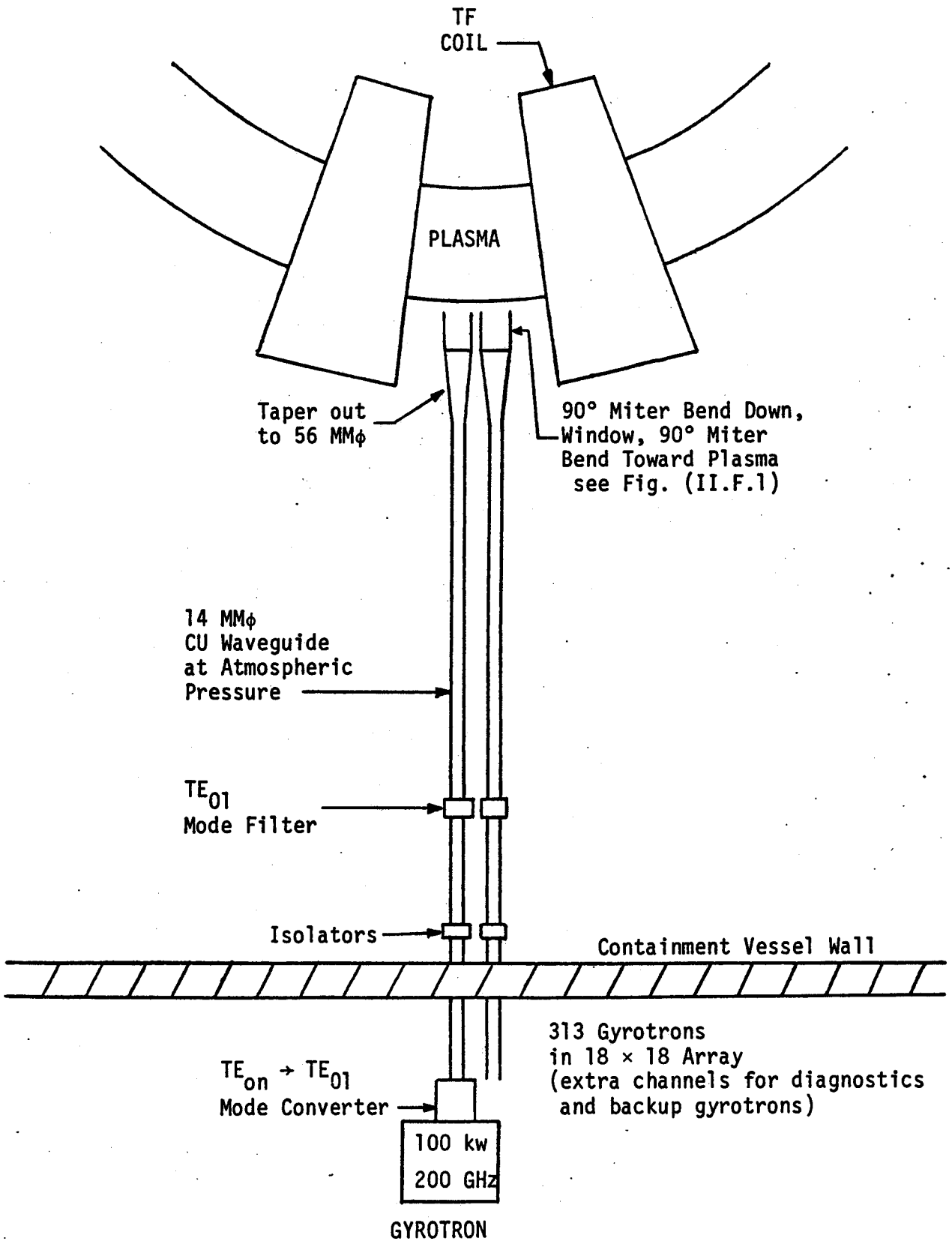

Fig. II.E.1 ECRH POWER TRANSMISSION

or might result from an accidental transmission failure caused, for example, by breakdown in the waveguide. Reflected waves might also result from mode conversion at waveguide irregularities. Reflections due to the plasma or mode conversion should not pose major problems, since the power levels associated with these processes should be small, and this power will be in the form of higher order modes which will be severely attenuated by the waveguide. A transmission failure, which conceivably could cause 100% reflection, would be a more serious difficulty, especially if it occurred near the gyrotron. Thus, it may be necessary to protect the gyrotron with an isolator which would allow power transmission only in the forward direction. This component might be in the form of a directional coupling, based either on multiple hole coupling between two waveguides [OK68] or on quasi-optical techniques [BE69]. As with the mode transducer discussed earlier, further research is required in order to design an isolator with high power capabilities and a low insertion loss at the required high frequencies.

A mode filter may be necessary in order to suppress spurious modes that are excited by irregularities in the transmission system. Such modes, if reconverted back into the TE_{01} mode, might adversly interact with the original mode, causing such problems as local heating or breakdown if unwanted resonances occurred. A mode filter should provide low loss for the TE_{01} mode and high losses for

unwanted modes. One possibility is the helical waveguide [BE68], which has the property of high loss for TM modes and TE_{mp} modes with $m \neq 0$. This guide takes advantage of the fact that TE_{op} modes have wall currents only in the azimuthal direction, and provides high resistance to axial currents. Unfortunately, higher order TE_{op} modes with $p > 1$ cannot be suppressed with a helical type mode filter, and at present effective attenuation of these modes requires further research.

The transmission guide will be composed either of high strength copper, or will consist of a steel tube with an inner layer of copper. The inside surface must be polished to a very smooth finish in order to minimize ohmic losses. Two 90° miter bends will be needed at the reactor end in order to gain access to the plasma. This configuration will allow for easy replacement of the reactor modules without removing the overhead transmission guides. Another miter bend will also be needed in the ECRH building in order to provide sufficient room for each gyrotron. A gradual taper will be necessary just before the vacuum window in order to reduce the power density to approximately 5 kW/cm^2, which is consistent with present-day microwave window experience (at lower frequencies).

The choice of guide radius is based on limitations imposed by voltage breakdown and attenuation due to the walls. The radius should be kept as small as possible in order to minimize coupling

between the TE_{01} and spurious modes and keep the transmission system compact, but should be large enough to accomodate 100 kW with a sufficient safety margin and have small ohmic losses. Calculations show that power attenuation is the most limiting criterion for our design. Based on our desire to keep ohmic losses at less than 5% of total power, a waveguide radius of 7 mm was selected. The theoretical power capabilities of such a guide, using 2.9×10^4 V/cm as the breakdown voltage, is 800 kW. In reality, environmental conditions and the presence of waveguide components will lower this maximum level. However, we believe that a safety factor of 8 should be adequate if the transmission system is carefully constructed. If it becomes necessary to increase the system power capacity, one might use a gas other than air, such as SF_6, or pressurize the waveguide.

Table II.E.2 gives the major design parameters and operating characteristics of the transmission system. The waveguide tolerances and losses are based on pipe qualities that can presently be obtained for communication systems [IN76]. These tolerances are more precise than those typically associated with commercially produced waveguides. However, it has been shown that they can be achieved utilizing special techniques. The loss mechanisms can be classified into two major groups: losses due to the finite conductivity of the structure, and losses due to the conversion of energy to spurious modes. We will now discuss these individual loss processes in detail.

Table II.E.2 Transmission System Parameters

DIMENSIONS:	Wavelength	1.5 mm	
	Inner radius	7.0 mm	
	Wall thickness	1.0 mm	
POWER:	Operating	100 kW	
	Theoretical maximum	800 kW	
	(based on breakdown of air at one atmosphere)		
WAVEGUIDE TOLERANCES:	Ellipticity	10 μm	
	Curvature	800 m	
	Diameter	10 μm	
	Joint Offset	20 μm	
	Joint Tilt	3'	
LOSSES:	Theoretical ohmic	$(6.8 \times 10^{-3}$ dB/m)	2.0×10^{-1} dB
	Estimated realistic ohmic	$(2.7 \times 10^{-3}$ dB/m)	8.1×10^{-2} dB
	Mode conversion-curvature	$(2.8 \times 10^{-4}$ dB/m)	8.4×10^{-3} dB
	Mode conversion-diameter deviations	$(3.2 \times 10^{-4}$ dB/m)	9.6×10^{-3} dB
	Taper (3 m long, 14 mmϕ → 56 mmϕ)		2.3×10^{-2} dB
	Miter Bends (3)		1.4×10^{-1} dB
	Mode Filter (Helix)		3.0×10^{-3} dB
	Mode Transducers (at gyrotron and at reactor)		1.3×10^{-1} dB
	Windows (2)		1.9×10^{-1} dB
	Joints (3)		1.7×10^{-1} dB
	Total		9.6×10^{-1} dB
			(80% transmission)
TEMPERATURE:	Average	31°C	
	ΔT	16°C	

As mentioned earlier, one of the major advantages of using the TE_{01} mode is the reduction of attenuation as frequency increases. For a copper waveguide operating far above cutoff, the theoretical attenuation for TE_{op} modes can be written as:

$$\alpha \simeq \frac{8.69}{r} \sqrt{\frac{\omega\varepsilon_o}{2\sigma}} \left(\frac{\omega_{cut}}{\omega}\right)^2 \quad \text{dB/m} \qquad \text{(II.E.1)}$$

where ω_{cut} is the cutoff frequency and r is the guide radius in meters. This equation was used to calculate the guide radius required for a power loss of 5% or less (7.4×10^{-3} dB/m for a 30 m length). In reality, surface roughness and minute surface irregularities tend to increase the effective resistivity of the walls and cause attenuation to become more severe. Tischer [TI79] observed that a major contribution to the excess losses of copper guides at millimeter wavelengths was due to an anomaly of the skin effect at room temperature. These effects result in an increase of the attenuation on the order of 40%. This is also in agreement with empirical observations on the WT4 waveguide system [AN77], where steel pipes were electrolytically plated with copper on a production basis, yielding a waveguide that was found to be stable over a three-year testing period. Based on these findings, we anticipate an additional attenuation of 2.7×10^{-3} dB/m.

Mode conversion results whenever the geometry of the waveguide departs from a perfectly true right circular cylinder. Such

departures distort the field configuration of the propagating mode, resulting in the coupling and transfer of energy to spurious modes. These unwanted modes tend to be higher order modes which are quickly dissipated in the waveguide. Since approximately 200 modes can propagate in our guide, mode conversion represents a potentially severe problem.

The mode conversion problem can be modeled by m coupled transmission line equations where m denotes the number of possible modes of propagation. Approximate solutions have been obtained for continuous coupling due to random imperfections using first-order perturbation theory [R062]. It has been shown [CA77] that the mode conversion losses can be written in the following general form:

$$\alpha_{MC} = 4.34\ C_{a,b}^2\ S_x\ (\Delta\beta_{a,b}/2\pi) \qquad \text{(II.E.2)}$$

Here α_{MC} is the expected attenuation of mode a in dB/m, $C_{a,b}$ is the coupling coefficient between modes a and b, and S_x is the power spectral density, which describes the magnitude of a particular type of irregularity. S_x is evaluated at the beat frequency of the coupled modes, $\Delta\beta_{a,b}/2\pi$, where $\Delta\beta$ is the difference between the propagation constants of the two modes. Equation (II.E.2) must be evaluated for each coupling process. We have determined α_{MC} for our system based on deviations of straightness and diameter, utilizing the power spectral densities achieved on the WT4 system. Our

calculations indicate that mode conversion losses should be small in comparison to ohmic losses for pipe qualities that can presently be obtained.

One potential problem is the degeneracy that exists between the TE_{01} and TM_{11} modes. This raises the possibility of strong coupling between these two modes, especially if any unintentional bends exist along the waveguide run. One technique that might be used to circumvent this problem is the use of a dielectric liner to break the degeneracy. However, such a liner might not be feasible in a high power environment. If a pure metallic waveguide is utilized, great care will have to be taken to ensure that straightness tolerances are met.

In addition to pipe imperfections, joint discontinuities will also cause coupling between modes. We envision each waveguide to be constructed of three, ten-meter sections. Based on typical errors found in communication waveguides, we assumed an average offset of 20 μm and a tilt of 3 minutes. Of these two factors, the tilt is by far the major difficulty, coupling power primarily into the TE_{12} mode. As Table (II.E.2) indicates, joint irregularities represent one of the major loss mechanisms.

The losses associated with mode transformation from the gyrotron output mode to the TE_{01} mode and from the TE_{01} mode to a linearly polarized mode are difficult to estimate. The quasi-optical techniques suggested by Vlasov et al., as previously mentioned, have been successfully applied but with a power transmission of only 70 - 75%. These high losses, however, could very likely be

reduced by using more complex mirror shapes and/or by reflecting from two or more mirrors. By these techniques, diffraction losses and mode mismatch could, in principle, be greatly reduced. Since the loss per mirror reflection should be of order 1% or less, mode transformation losses in principle can be reduced to a very small value. In the present study, we will assume a very small contribution ($<1.3 \times 10^{-1}$dB) to the total loss due to mode transformation.

If the waveguides are kept at atmospheric pressure, then the RF power will have to propagate through two vacuum windows, one at the gyrotron output and one at the reactor. Candidates for window materials include:

(1) Ceramics - this includes alumina, Al_2O_3, and beryllia, BeO.

(2) Mica - has been used successfully by the Soviets in a high frequency CW gyrotron.

The basic difficulty in evaluating the performance of these windows is a lack of information concerning loss characteristics at frequencies near 200GHz. For our analysis, we have assumed a beryllia window with a loss tangent of 1×10^{-3}. Calculations indicate that for a 60 mm diameter window, a thickness of 2 mm should be adequate to withstand stresses due to the pressure differential. Based on this thickness, a total loss of 0.19 dB is anticipated. Table (II.E.2) indicates that this is one of the major transmission loss mechanisms. One possible way of avoiding the use of windows is to evacuate the waveguides. However, this will augment the com-

plexity of the system, and might necessitate the placement of the gyrotrons closer to the reactor. If windows are utilized, there are a number of alternative schemes other than the use of a single, flat window that could reduce thermal stress problems. One of these schemes may prove to be successful for high power, high frequency transmission.

In order to gain access to the plasma, as well as provide room for the gyrotrons, a minimum of three bends will be required. Two methods have been used in overmoded circular waveguide systems to accomplish a rapid change in direction: a constant-curvature bend, and a miter bend based on quasi-optical principles. We have chosen the miter bend because of its compactness and low loss characteristics. The loss in dB is equal to $2.4(\lambda/r)^{1.5}$ for bends with $\lambda/r<<L$ (OK68). For our system, the total loss is expected to be 0.14dB. This value should be reduced in the future as bend designs become more refined (SP76).

The final two loss mechanisms that we have considered are those associated with the taper and mode filter. The taper is employed to reduce the RF power density in the window. The losses associated with the taper can be kept small by making the transition sufficiently gradual. Thus, the longer the taper, the less mode conversion one would expect. Assuming a 3 m. straight taper, the loss (primarily to the TE_{02} mode) is calculated to be 2.3×10^{-2}dB. This loss, or the taper length, could be reduced by employing a variable taper in which the waveguide shape is chosen to minimize abrupt discontinuities. We modeled the mode filter theoretically

with a one meter section of helical waveguide, which will damp out the TEmp, $m \neq 0$, modes. The increased loss in the helical guide as compared to the ohmic losses of a pure copper pipe is approximately 25% (KA65). Based on this value, the mode filter will add 3×10^{-3}dB to the total attenuation, and therefore represents a small factor. Summing all the individual losses, we obtain a total attenuation of 0.96 dB, which translates into an expected power transmission of 80%. Based on the assumption that this heat (except that generated at the window, which will presumably have its own cooling system) will be distributed evenly along the pipe, a temperature fluctuation of 16°C is anticipated for gyrotrons that will be operating for 5 seconds of a 500 second power cycle. The average temperature will be 31°C based on the dissipation of heat by free air convection. Of course, localized heating due to design imperfections could drastically affect the temperature in those areas.

Our conclusion based on our analysis of a transmission system utilizing the TE_{01} mode in an oversized waveguide is that such a design appears feasible. A total loss of about 20% was calculated, with the potential for lower losses as designs become more refined. Since a fixed frequency is involved, phase and delay distortions as well as bandwidth and coherence considerations, associated with information transmission systems, are less important. The major goals for a power transmission system are low attenuation, low reflection, reliability, and long life. At present, the primary unknowns include the deleterious effect of spurious modes, as well as the lack of microwave components that can accommodate both high

power and high frequency. As mentioned earlier, our use of an oversized guide scheme does not exclude other concepts, such as quasi-optical techniques or a beam waveguide, as viable transmission systems.

II.F. Wave Launching and Port Design

In this section we will deal specifically with the reactor end of the microwave transmission system. In particular, we will describe the polarizer needed to convert the circular TE_{01} mode into a beam of linearly polarized radiation, and will discuss the problems associated with transmitting RF power in a high neutron, high temperature environment. The constraints imposed on the transmission waveguide can be classified into two categories: those resulting from the plasma absorption process, and those associated with the constrained reactor geometry. Requirements due to the plasma include the need to launch the power at a specified angle with respect to the toroidal magnetic field, and to keep diffractive losses at a minimum. Geometric considerations involve the need for sufficient clearance for the waveguide between the magnet coils, as well as adequate access so that microwave components may be replaced when necessary.

Fig. II.F.1 shows the ECRH port design. The RF power is transmitted from the gyrotron buildings to the reactor in straight, horizontal waveguides that are supported at an elevation slightly higher than the reactor modules. This allows replacement of the modules without removing the horizontal portion of the guides. After a 90° miter bend, the radiation propagates through the vacuum window to the polarizing and focusing mirrors. The position of the vertical portion of the waveguides is determined by the poloidal coils, and as a result the mirrors are located approximately 3.2 meters from the plasma center. The mirrors transform the circular TE_{01} modes

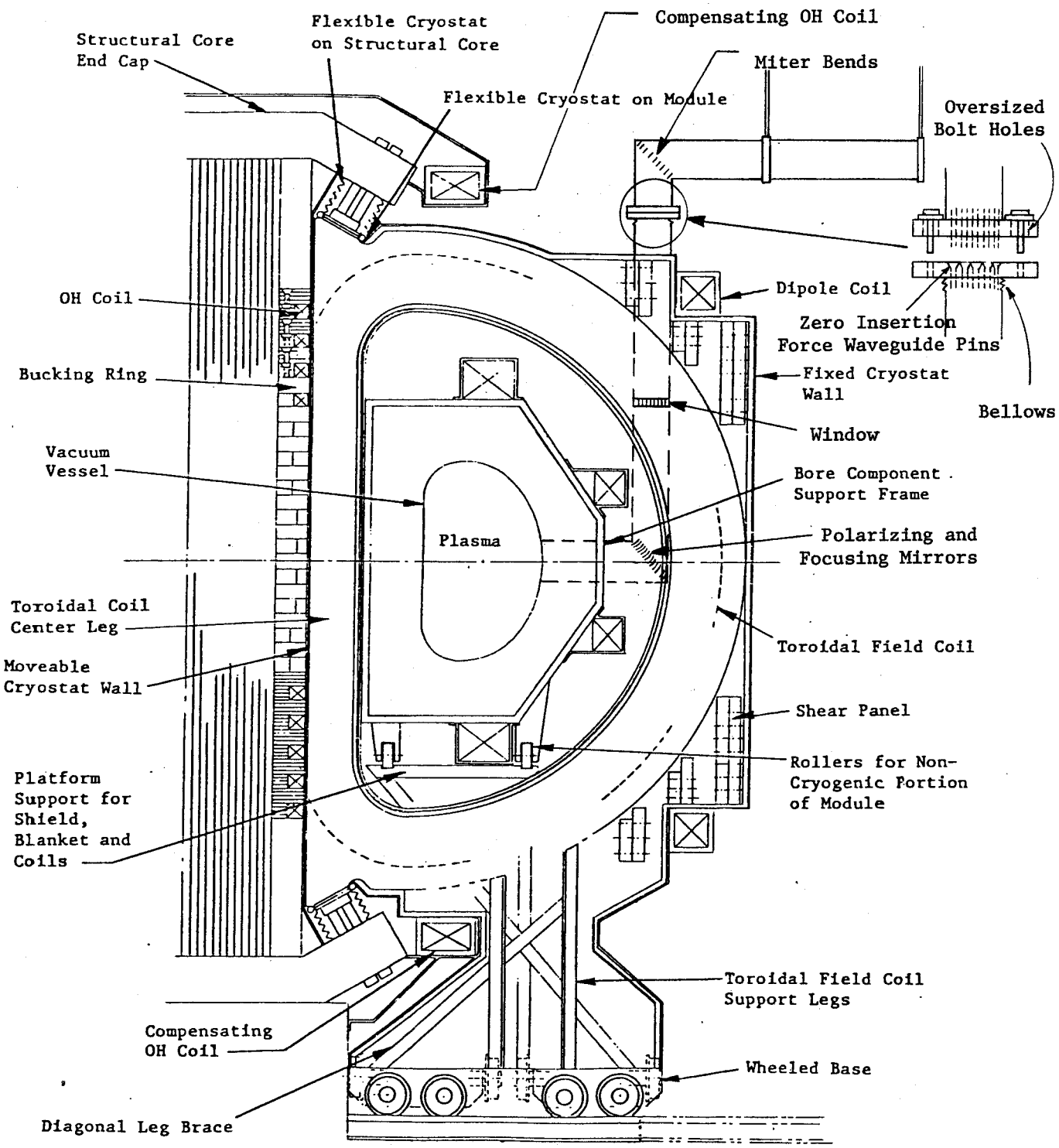

Fig. II.F.1 ECRH Port Design

into linearly polarized modes and focus the RF power into the plasma.

In order to allow for the removal of a module, a disconnection joint will be necessary. At this joint, the outer support pipes are held together by a series of bolts fitted through oversized holes in the two mating flanges. When the flanges are properly matched, the internal array of waveguides are aligned in the correct manner. These internal guides need not be individually bolted because of the unique current distribution of TE_{01} modes. Since these modes are supported by wall currents with no longitudinal component, azimuthal breaks will not affect their propagation, and therefore a tight fit at the joint for electrical contact is not necessary. However, care must be taken to ensure that the joint offset and tilt are kept as small as possible in order to minimize mode conversion losses. For our design, the diameter of the outer support tube is determined by the relative positions of the dipole coil and the poloidal coil just outside the blanket. The maximum diameter is 70 cm., which will provide adequate clearance for an 18 x 18 array of 14 mm. diameter waveguides.

Past experiments have shown that simple open-ended oversized waveguides are quite effective in launching the power into the plasma. Power densities of $5kW/cm^2$ per port have been used with no major problems (DA77). There should be minimal interactive coupling between the four ECRH ports as a result of the efficient power absorption that is anticipated. Based on a power density of $5kW/cm^2$, 100 MW will require 2.0 m^2 of port area, which compares favorably with the 4-5 m^2 required for neutral beam heating of the HFCTR. Thus, the

access required for ECRH, which consists of 0.4% of the total first wall area, should have a relatively minor effect on the breeding ratio of the blanket.

The major difficulty associated with launching the ECR power will involve the conversion of the waveguide mode to linearly polarized radiation. Direct launching from the end of the oversized waveguide will not be satisfactory because of the circular polarization of the radiation. A mode transducing mirror has been developed by Wengenroth (WE78) which utilizes phase and polarization shifting techniques at a reflecting surface. This approach has been demonstrated at 33 GHz. In order to convert the TE_{01} mode, a twist reflector plate is utilized. The angular spread of the beam is approximately λ/D, where D is the diameter of the output waveguide. For our configuration, this gives a spread of 1.5°, which implies an 8.6 cm. diameter beam once it reaches the plasma center. Thus, the beam will be sufficiently narrow to be used for localized heating. The RF power will be launched at close to 90° with respect to the toroidal field, and there will be no variation of launch angle during a shot. The angular spread of 1.5° should have a relatively minor effect on the absorption process. At present, it is not possible to calculate the losses associated with these mirrors, but they should be kept under approximately 5×10^{-2} dB in order to avoid heat dissipation problems.

In addition to the RF power, the polarizers will also be subject to a neutron flux that will degrade their performance. This degradation will include an increase in the resistivity of the copper from which they are constructed as well as the possibility of surface erosion. Although the lifetime of these mirrors

cannot presently be calculated, provisions must be made for their easy removal in case of failure. Our design provides sufficient access through the vertical portion of the waveguide so that, after the internal array of pipes is removed, the mirrors can then be lifted out and replaced. A laser beam can then be used to realign the transmission system. We have also investigated the possibility of increased ohmic losses due to the higher temperature of the final stretch of waveguide. We believe this effect should be minimal. First, the losses are relatively insensitive to the wall temperature, with an increase from 30° to 200°C resulting in a 20% rise in ohmic losses. Secondly, the heating should involve only a small portion of the waveguide, since the blanket protects the entire transmission path prior to the polarizers. If this heating of the waveguide proves problematic, then a cooling system for the final section of guide might be required.

II.G. WAVE ABSORPTION IN THE PLASMA

II.G.1 Introduction

There have been a number of recent theoretical treatments of ECR heating in a tokamak plasma [see, for example, AL76a, AL76b, AL77, MA79, LI77, FI78, MA78, MA79, OT79, WO79, EL77, TA78]. The general results of these theoretical treatments were summarized in Section II.A. There, the qualitative features of ECR heating were reviewed and applied to the design of an ECR heated reactor. In this section, we investigate additional properties of the ECR heating process and review previous studies of tokamak ECR heating. In later parts of this section we will present some specific results for ECR heating of the HFCTR plasma.

There have been several detailed studies of the deposition profile for ECR heating of specific tokamaks. For example, Alikaev et.al. [AL76ab, AL77] have performed wave trajectory and absorption analyses for the T-10 and T-20 machines; Litvak et.al. [LI77] have obtained results for T-10; Fidone et.al. have performed calculations for TFR [FI78]; Ott et.al. [OT79] for Versator II, PLT and UWMAK III; Eldridge et.al. [EL77] for ISX; and Maekawa et.al. for JFT-2 [MA78, MA79]. We have not performed a wave trajectory and absorption analysis in the present study because such an analysis is beyond the scope of this report. Instead, we will review the results of the previous analyses and obtain some specific results

for HFCTR in the nonrelativistic, quasi-transverse limit. This approach should give a good qualitative picture of ECR heating of HFCTR. However, for accurate quantitative results, a treatment including dispersion and relativistic effects, such as [OT79], is necessary.

II.G.2 Review of ECR Heating Theory

The formulation of the analysis of wave trajectories and absorption at ECR in a tokamak plasma is described in detail elsewhere [AL76ab, AL77, LI77, OT79]. We will review a few results for ordinary wave heating at Ω. We assume that the wave is incident from the low field side of the tokamak. The absorption coefficient, k_2, for the field amplitude in a warm plasma is [AK74], [LI77]:

$$k_2 = k_o \beta_T \phi_2(\theta,q) f(z) \qquad \text{(II.G.1)}$$

$$f(z) = \exp(z^2)\left(1 + \frac{4}{\pi}\left(\int_0^z \exp(t^2)dt\right)^2\right)^{-1}$$

$$\begin{aligned}\phi_2(\theta,q) = \cos\theta \{ & n_2^4(1 - q + \tfrac{7}{4} q \sin^2\theta) \\ & + n_2^2 \left[(1 + q)\left(\tfrac{1}{2} q - 1\right) \sin^2\theta \right. \\ & \left. + \tfrac{1}{4} q^2 \tan^2\theta(1 + \cos^2\theta) - (1 - q)(1 - \tfrac{1}{4}q)(1 + \cos^2\theta)\right] \\ & + (1 - q)(1 - \tfrac{1}{2}q) + \tfrac{1}{4}(q - 2) q^2 \tan^2\theta\} \\ & \times \left(\sqrt{\pi}\, q(2 \sin^2\theta n_2^2 + 2q - 2 - \sin^2\theta)\right)^{-1}\end{aligned}$$

$$\beta_T = \sqrt{2T_e/mc^2}$$

$$z_2 = (\omega - \Omega)/\omega n_2 \beta_T \cos\theta$$

$$q = \omega_p^2/\omega^2$$

θ = angle between k and B

Eq. (II.G.1) is derived from a nonrelativistic Vlasov equation. Consequently, it does not apply when θ is too close to $\pi/2$, i.e. it is assumed that $n_2 \cos\theta >> \beta_T$. Otherwise, the velocity dependence of Ω must be taken into account. Results in the relativistic limit have been obtained by [FI78, OT79]. The form of Eq. (II.G.1) can best be appreciated if quasi-transverse propagation ($\sin^2\theta >> 2(1 - q)\cos\theta$) is assumed. Then

$$k_2 \cong \frac{k_o \beta_T}{4\sqrt{\pi}} \frac{q}{\cos\theta} f(z_2) \qquad \text{(II.G.2)}$$

Integration of Eq. (II.G.2) along the wave path in the plasma, assuming no refraction, yields an optical depth, Γ_2,

$$\Gamma_2 = \frac{\pi}{4} \beta_T^2 \, q \, k_2 \, R_o \qquad \text{(II.G.3)}$$

which is related to the absorption, A, and transmission, T, by:

$$1 - T = A = 1 - \exp(-\Gamma_2) \qquad \text{(II.G.4)}$$

since no reflection is predicted [see MA79].

The form of Eq. (II.G.3) is identical to that of Fidone et.al. [FI78] in the nonrelativistic limit for $n_2 \cos\theta > \beta_T$. In the weakly relativistic limit, the absorption spectrum is somewhat asymmetric about $\omega = \omega_H$. However, the changes are not too severe [see FI78], and Eqs. (II.G.2) and (II.G.3) can still be used for $n_2 \cos\theta \sim B_T$. For angles $\theta \gtrsim 80°$, the nonrelativistic theory is not applicable. Calculations in the weakly relativistic regime have been carried out by Fidone et.al. [FI78] and Ott et.al. [OT79].

II.G.3 Results for Reactor ECRH

Wave trajectory and absorption calculations for ECR heating have been carried out for two reactor-size tokamak plasmas. Alikaev et.al. [AL76a, AL77] have analyzed the T-20 machine using a nonrelativistic theory and Ott et.al. [OT79] have analyzed UWMAK III using a relativistic theory. A comparison of these two machines with HFCTR is given in Table II.G.1.

There is a qualitative difference between the ECR heating of a reactor size plasma and that of a smaller machine. This difference arises because of the very large optical depth in the large machines. The optical depth for ordinary wave heating at Ω, Γ_2, is listed in Table II.G.1 for T-20, UWMAK III and HFCTR at temperatures $\langle T_e \rangle$ = 2 and 7 keV. The large optical depth actually results from the large value of R_0/λ in these machines. This may be seen by rewriting Γ_2 as:

Table II.G.1 Comparison of ECR Heating of Reactor Size Plasmas

MACHINE	T-20	UWMAK III	HFCTR
$\langle n \rangle$ 10^{14} cm^{-3}	0.5	0.65	2.4
B_o T	3.5	4.05	7.4
$\alpha = \omega_{po}^2/\Omega_o^2$	0.84	0.81	0.9
a (cm)	200	270	120
R_o (cm)	500	810	600
R_o/a	2.5	3	5
R_o/λ 10^3	1.6	3.1	4.0
λ (mm)	3.1	2.6	1.5
$\langle T_e \rangle$ keV	3,5,10	2 - 7	1 - 7
θ ($\measuredangle \vec{B},\vec{k}$)	53° - 84°	85°	---
Reference	[AL76a,b]	[OT79]	This paper
Γ_2, $\langle T_e \rangle$ = 2 keV	21	43	45
Γ_2, $\langle T_e \rangle$ = 7 keV	73	150	156

$$\Gamma_2 = \frac{\pi^2}{2} \beta_T^2 \, q(1 - q)^{1/2} \left(\frac{R_o}{\lambda}\right) \qquad \text{(II.G.5)}$$

Since the quantity $q(1 - q)^{1/2}$ is slowly varying, Γ_2 is primarily a function of (R_o/λ). This quantity is approximately the same in UWMAK III and HFCTR. Physically, R_o enters into the optical depth because the toroidal magnetic field varies as R^{-1}.

The large optical depth in reactor-size machines has several implications. The ordinary wave radiation is effectively absorbed when the integrated optical depth along the trajectory is about two. For large machines, a value of $\Gamma_2 = 2$ is achieved early in the tokamak start-up cycle, even though the temperature and/or density are low. Even during the plasma expansion phase of the start-up (cf. Section II.B.2.3), when the density is a few times 10^{13} cm^{-3} and $\langle T_e \rangle$ is a few hundred eV, Γ_2 will be of order one and the ordinary wave would be highly absorbed. However, at lower $\langle T_e \rangle$ and $\langle n_e \rangle$, the ordinary wave radiation might still be absorbed after reflecting from the walls and converting to extraordinary wave radiation.

A second implication of the large optical depth is that the ordinary wave radiation will be absorbed rather far from the resonance point $\omega = \Omega(z_2 = 0)$. That is, the radiation is fully absorbed in the tail of the absorption spectrum and in a zone whose spatial width is significantly narrower than the full width of the absorption profile. This point may be illustrated using results in the quasi-transverse limit.

In the quasi-transverse limit, we may estimate the spatial location of the wave absorption using Eq. (II.G.2). Let the radiation be incident in the R direction from $R = - R_o - a$. Then the integrated absorption at the major radius R' is given by $\Gamma_2 (R')$, where

$$\Gamma_2 (R') = \int_{-\infty}^{R'} \frac{k_o \beta_T}{2\sqrt{\pi}} \frac{q}{\cos\theta} f(z)\, dR \qquad \text{(II.G.5)}$$

$$z \cong \left(R - \frac{\Omega R_o}{\omega}\right) (n_2 \beta_T \cos\theta\, R_o)^{-1} \qquad \text{(II.G.6)}$$

where we have approximated the limit $- (R_o + a)$ as $- \infty$ in the integral in Eq. (II.G.5) since $\omega \approx \Omega$. Obviously.

$$\Gamma_2 (\infty) = \Gamma_2$$

where Γ_2 is given by Eq. (II.G.3). In this analysis, we ignore the variation of density and temperature with R and also the effects of refraction. This may be done if the absorption is localized and refraction is small.

We may now define the radii R_1 and R_2 (as well as z_1 and z_2) by:

$$\Gamma_2(R_1) = 0.1 \qquad \text{(II.G.7)}$$

$$\Gamma_2(R_2) = 2.0$$

Then the transmission at R_1 is 0.90 and at R_2 is 0.14, so that 76% of the absorption occurs between R_1 and R_2. Using Eq. (II.G.6), we may rewrite

$$\Gamma_2(R') = \frac{k_o R_o}{2\sqrt{\pi}} q\, n_2 \beta_T^2 \int_{-\infty}^{-z'} f(z)dz \qquad \text{(II.G.8)}$$

where z' and R' are related by Eq. (II.G.6), or:

$$\frac{\Gamma_2(R')}{\Gamma_2} = \frac{2}{\pi^{3/2}} \int_{-\infty}^{z'} f(z)dz \qquad \text{(II.G.9)}$$

where Γ_2 is $\Gamma_2(\infty)$ and is given by Eq. (II.G.3). Eq. (II.G.9) has the following significance. Since

$$\Gamma_2(R') \ll \Gamma_2$$

for both $R' = R_1$ and R_2 in a reactor-size tokamak plasma, therefore the integral of f(z) dz will only be over large values of z, i.e. $z > 1$. This is equivalent to, and verification of, the statement made earlier that the absorption will occur in the tail of the absorption profile.

As an example of the above analysis, results, obtained for T-20 and HFCTR in the quasi-Transverse theory, are presented in Table (II.G.2). Results obtained by Alikaev et.al. are also presented for comparison. The results in the table are for an incidence angle of $\theta = 70°$, for which $n_2 \cos\theta \sim \beta_T$ and the nonrelativistic theory

Table (II.G.2)

ECR Absorption Calculations, T-20 and HFCTR

	T-20 [AL76a,AL77]	T-20 (This theory)	HFCTR (This theory)
$\langle T_e \rangle$ keV	5	5	5
α	0.84	0.84	0.9
θ	70°	70°	70°
z_1, z_2	--	2.9, 1.9	2.7, 2.0
$(R_1 - R_o)/a$	--	0.18	0.22
$(R_2 - R_o)/a$	--	0.12	0.15
$(R_a - R_o)/a$	(0.2)	0.15	0.18
r_a/a	0.32	--	--

still applies [LI77, FI78]. As predicted, both z_1 and z_2 are larger than one, indicating absorption in the tail of the absorption profile. We may define a value of the major radius, R_a, as that value at which the maximum wave absorption occurs (and not the maximum of the absorption coefficient). Then the values of R_a in Table (II.G.2) indicate that the wave absorption is relatively far from the plasma center for $\theta = 70°$ in both T-20 and HFCTR. When refraction is taken into account, the absorption occurs at a value of minor radius r_a such that $r_a > (R_a - R_o)$. When θ is closer to 90°, absorption occurs nearer to the plasma center. The results in Table (II.G.2) also show that, although the present approach is reasonably accurate, it should only be used for order of magnitude estimates and not for exact analysis.

Because wave absorption occurs in the tail of the absorption profile, it is necessary, in order to heat the center of the plasma, to use a microwave frequency ω which exceeds Ω by an amount $\Delta\omega$, such that

$$\frac{|\Delta\omega|}{\Omega} = \frac{|R_a - R_o|}{R_o}$$

For reactor-size plasmas, $|R_a - R_o|/R_o$ is less than 10% so that the change in frequency is not very significant.

For reactor-size tokamaks, the absorption occurs at a major radius for which z is between about 2 and 3. This means that we may give an approximate expression for this case:

$$\left| \frac{R_a - R_o}{a} \right| \approx 3 \frac{R_o}{a} (1 - q)^{1/2} \beta_T \cos\theta \qquad \text{(II.G.10)}$$

Eq. (II.G.10) predicts that absorption occurs farther from the plasma center as the angle θ decreases from 90°. It also predicts that the location of the absorption varies as the temperature of the plasma changes during the heating cycle. Both of these effects are observed in the calculations of Alikaev et.al. [AL76a, 77]. There might also be a potential problem if the location of the heating zone were to move to the plasma edge as the temperature rises to the ignition point. The absorption point will, in fact, move in major radius location by an amount ΔR_a in heating from $\langle T_e \rangle$ = 2 keV to $\langle T_e \rangle$ = 8 keV, where ΔR_a is given approximately by:

$$\frac{\Delta R_a}{a} \approx (0.27) \frac{R_o}{a} (1 - q)^{1/2} \cos\theta \qquad \text{(II.G.11)}$$

The value of ΔR_a is, therefore, comparable to the value of $(R_a - R_o)$ for $\langle T_e \rangle$ = 2 keV and should not be a major problem for $\theta > 70°$.

Finally, we note that the electrons heated are those which satisfy the Doppler condition

$$\frac{\omega - \Omega}{\omega} \approx k_{\parallel} v_{\parallel} \qquad \text{(II.G.12)}$$

If the absorption is far from resonance, then only those electrons with large values of $v_{\parallel}$ and large energy E_{res} will be heated. Values of E_{res}/T_{max} of up to four are predicted in T-20 by Alikaev et.al. [AL77]. However, the resonant electrons should lose their

energy through collisions in a time short compared to the energy confinement time in reactor size tokamaks, so that bulk heating will still result.

II.G.4 Conclusions

The nonrelativistic, quasi-transverse theory of ECR heating of a tokamak plasma has been applied to the absorption of ordinary wave radiation in the limit of a reactor-size tokamak with large optical depth. Simple calculations demonstrate that the radiation will be absorbed in the central region of the plasma for $\theta \gtrsim 70°$. The absorption occurs in the tail of the absorption profile, at a location where ω is not equal to Ω. However, the absorption can be forced to occur in the center of the plasma by tuning ω to be slightly larger than Ω_o, i.e. ω resonant toward the inside (high field side) of the tokamak. The location of the heating zone is a function of plasma density and temperature and the angle of launch of the radiation. As the plasma heats up, the location of the absorbing zone shifts. The magnitude of this shift is not negligible, but absorption will still occur in the central region of the plasma. It would be useful to have calculations of absorption for a tokamak reactor such as HFCTR in the relativistic limit. Ott et.al. [OT79] have calculated in the relativistic limit the ordinary wave absorption for UWMAK III, but only for a wave incident at $\theta = 85°$. They find good absorption of the radiation in the center

of the plasma. These results indicate that ordinary wave heating of a reactor-size tokamak plasma is a feasible technique for bulk heating of the plasma to ignition temperatures.

II.H. IMPROVED MODULARIZATION OF THE REACTOR

II.H.1. Description of Improved Modularization

HFCTR presented an advanced, fully automated, modularized reactor design which permitted rapid replacement of modules for either scheduled or unscheduled maintenance [CO79]. Its superiority over unautomated designs, using manipulators, was that the downtime due to mechanical operations in a module replacement could be reduced from several months to two days, as shown by Sniderman's parallel design studies [SN79], [CO79]. The HFCTR approach differed from other automated designs, such as Mitchell's disassembly technique for the Culham Mark II [MI76], in that all the magnet systems were also modularized so that a magnet module suffering unexpected damage could be rapidly replaced. However, the HFCTR modularized approach was limited by time delays due to nonmechanical operations such as detritiation of the vacuum vessel prior to disassembly and reestablishment of high vacuum after reassembly. Realignment of the finger joints in the internal poloidal field coils and of mechanical vacuum seals in the vessel flanges and the avoidance of frozen bellows in the flexible cryostats were all deemed feasible, but introduced a measure of uncertainty in the timing of mechanical operations.

A comparison between the reliability of a gyrotron and neutral beam heated tokamak is shown in Table (II.H.1). The gyrotron system is clearly superior in every aspect to the neutral beam heated tokamak. The number of elementary operations involved in the dis-

TABLE (II.H.1)

Comparison in Reliability Between Gyrotron and NB Heated Tokamaks

	Gyrotrons	Neutral Beams
1) Elementary Operations in disassembly	3	6
2) Types of utility disconnects	0	6
3) Motion of complex structures	No	Yes
4) Assembly/disassembly time/minutes	34	590
5) Cost of redundancy (operation with failed components)	<1%	33%

assembly of the four waveguide flanges, described in Section II.F, is only three: position the bolt torquing device, loosen the flange bolts and remove the torquing device. The disassembly of the reference neutral beam system requires six [C079]: uncouple the utility connections, position the bolt torquing devices, remove the flange bolts, remove the bolt torquing device, retract the neutral beam injector to the temporary storage location and raise the floor cover plate over the floor opening. The neutral beam has six types of utility disconnects: water, liquid helium, liquid nitrogen, gas handling, vacuum and electric. The microwave system has none, since the disconnect flange interrupts transmission in air at atmospheric pressure. Since one-half of the flange is bellows mounted, no movement of complex structures is needed in order to allow an entire TF module to be removed. However, in the case of the neutral-beam heated system, the entire beam line must be retracted beneath the floor of the reactor cell, then raised and realigned during reassembly. The total disassembly/assembly time for the microwave system is only 34 minutes, as compared to 590 minutes for the neutral beam system, as timed by Sniderman [C079]. Of course, for an unautomated disassembly procedure, the difference in disassembly/assembly time would be much greater, favoring the microwave system.

A final difference in reliability is the low cost of redundancy in the ECRH-heated tokamak. Since an entire neutral beam line can easily fail and will routinely be out of commission frequently during cryopanel regeneration, at least 33% redundancy had to be built into the four arm neutral beam system. This still gives no margin

if a single large component should suffer an unexpected failure. In contrast, the output of each gyrotron is intrinsically paralleled and independent of all other gyrotrons in the system. A single tube failure reduces the system output by only 0.1 %. Thus, with only 10 % redundancy, about 100 tube failures would be permitted before unscheduled maintenance became necessary.

The second innovation is simply a decision to remove all modules at once. As shown in Figure (II.H.1), it is possible for all old modules and replacement modules to move simultaneously to their desired positions without any "traffic jams". The symbols O and N represent the old and new modules, respectively, while the numbers correspond to the clockwise toroidal position of each module, when assembled. While the previous HFCTR replaced a single module in only two days, it did not attempt to define the fundamental time limitations necessary for detritiation of the vacuum vessel prior to disassembly and reestablishment of high vacuum after reassembly. These are typically estimated to require several days apiece. For example, if the total downtime of a module replacement is no less than two weeks and a first-wall replacement is necessary every two years, the downtime for the replacement of eight modules would equal 16 weeks, for a maximum availability of 85 %. By replacing all modules at once, scheduled downtime can be reduced to two weeks. Furthermore, the impact of uncertainties is greatly reduced. Another major benefit of simultaneous replacement is the substantial reduction of the activation of the reactor cell resulting from the removal of all used modules to a separate hot cell. This permits the possibility of some form of human entry into the reactor cell if any critical alignment problems should arise in the process of automated reassembly. A final benefit of simultaneous

Fig. II.H.1 Module Replacement

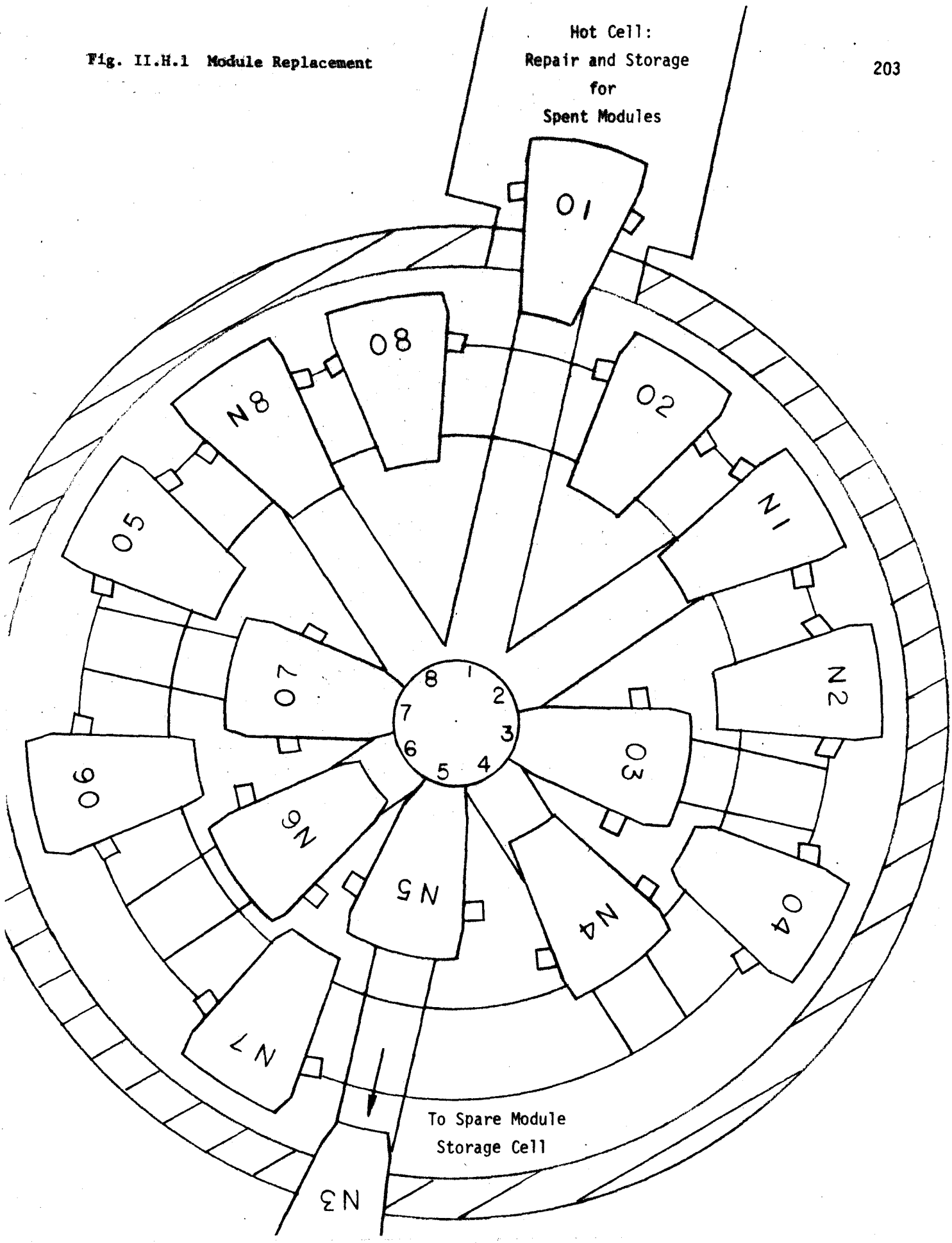

disassembly of all modules is that the first generation of modules need not be replaced at a fraction of their useful service life. Simultaneous replacement increases the service life of the first generation of modules by a factor of $2N^2/N(N+1)$, where N is the number of modules.

Responses to specific inquiries concerning the need for a long time for detritiation and the incompatibility of simultaneous module replacement with the conclusions of a previous study [FU78] are contained in the next two sections.

II.H.2. Detritiation of Plasma First Wall and Blanket Walls Prior to Module Disassembly

If large amounts of tritium are released to the reactor cell subsequent to opening modular vacuum seals, several undesirable consequences are possible. Saturation of the reactor cell tritium removal system could cause a large, sudden release of tritium to the atmosphere. The escape of tritium would necessarily be increased over steady-state release rates for any removal system. However, a tritium-removal system of sufficiently high capacity and pumping speed could reduce the total tritium resease rate to state-of-the-art levels (< 1 ppm). Therefore, the fundamental limit on detritiation requirements is economic, rather than environmental. For a certain, mandated acceptable level of tritium release, the higher cost of a high entropy tritium removal system, associated with the reactor cell volume, is balanced against the higher down-time associated with thorough detritiation. The same requirements for a good cell-volume tritium

removal system would apply for the hot-cell in which used modules are stored.

A second requirement on detritiation is the requirement for net tritium breeding. Net tritium breeding in a blanket without a large amount of neutron multiplication will be a nontrivial task. The neutron multiplication factor of most lithium-bearing blankets is only 1.1 - 1.2. Remembering that one neutron is produced for each tritium atom consumed, the potential ten to twenty per cent increase in tritium per fusion event is balanced by the percentage of neutrons absorbed in non-blanket structures and the five per cent annual loss of tritium inventory through radioactive decay. Since many of the most desirable first-wall materials from thermostructural considerations are capable of absorbing several months worth of plasma fuel, any unnecessary losses of tritium may adversely affect the ability of the reactor to breed tritium. Although atmospheric release of tritium can be held to low levels by the reactor cell tritium removal system, it is fundamentally limited in its ability to capture all outgassed tritium because of the high surface area of a reactor cell and the extremely high hydrogen absorbence of most plastics and uncoated concrete.

The characteristic time for detritiation of a vacuum vessel first wall is shown in Table (II.H.2), for a thin slab of 305-S stainless steel outgassing on two sides [GA75]. To achieve the 1975 reference outgassing rate of TFTR [GA75] ($G_p = 10^{-16}$ torr - ℓ/sec-cm^2), the following bake-out times would be required for thin-bellows (.105 cm) and thicker (.675 cm) torus body stock:

Table (II.H.2)

FRACTION OF ORIGINALLY CONTAINED HYDROGEN RETAINED AFTER BAKEOUT

Upper Entry ~ L = 0.102 cm, Lower Entry ~ L = 0.675 cm

Bakeout Time Hours	Bakeout Temperature, °C 200	250	300	350	400	450	500
1	8.2×10^{-1}	6.7×10^{-1}	4.5×10^{-1}	2.0×10^{-1}	4.2×10^{-2}	2.7×10^{-3}	3.3×10^{-5}
	9.8×10^{-1}	9.5×10^{-1}	9.2×10^{-1}	8.7×10^{-1}	8.1×10^{-1}	7.4×10^{-1}	6.5×10^{-1}
2	7.4×10^{-1}	5.3×10^{-1}	2.5×10^{-1}	4.9×10^{-2}	2.1×10^{-3}	9.0×10^{-6}	1.3×10^{-9}
	9.7×10^{-1}	9.3×10^{-1}	8.8×10^{-1}	8.2×10^{-1}	7.4×10^{-1}	6.3×10^{-1}	5.1×10^{-1}
3	6.8×10^{-1}	4.3×10^{-1}	1.4×10^{-1}	1.2×10^{-2}	1.1×10^{-4}	3.0×10^{-8}	
	9.6×10^{-1}	9.1×10^{-1}	8.6×10^{-1}	7.8×10^{-1}	6.8×10^{-1}	5.5×10^{-1}	4.1×10^{-1}
4	6.3×10^{-1}	3.4×10^{-1}	7.6×10^{-2}	3.0×10^{-3}	5.7×10^{-6}		
	9.5×10^{-1}	9.0×10^{-1}	8.3×10^{-1}	7.4×10^{-1}	6.3×10^{-1}	4.8×10^{-1}	3.2×10^{-1}
8	4.8×10^{-1}	1.5×10^{-1}	1.6×10^{-2}	1.1×10^{-5}	4.0×10^{-11}		
	9.2×10^{-1}	8.6×10^{-1}	7.6×10^{-1}	6.4×10^{-1}	4.7×10^{-1}	2.9×10^{-1}	1.3×10^{-1}
12	3.7×10^{-1}	6.2×10^{-2}	6.8×10^{-4}	3.9×10^{-8}			
	9.0×10^{-1}	8.3×10^{-1}	7.1×10^{-1}	5.6×10^{-1}	3.6×10^{-1}	1.7×10^{-1}	5.1×10^{-2}
16	2.9×10^{-1}	2.6×10^{-2}	6.4×10^{-5}				
	9.0×10^{-1}	8.0×10^{-1}	6.7×10^{-1}	4.9×10^{-1}	2.7×10^{-1}	1.0×10^{-1}	2.0×10^{-2}
20	2.2×10^{-1}	1.1×10^{-2}	6.1×10^{-6}				
	8.8×10^{-1}	7.8×10^{-1}	6.3×10^{-1}	4.3×10^{-1}	2.1×10^{-1}	6.0×10^{-2}	8.0×10^{-3}
24	1.7×10^{-1}	4.7×10^{-3}	5.7×10^{-7}				
	8.7×10^{-1}	7.5×10^{-1}	5.9×10^{-1}	3.8×10^{-1}	1.6×10^{-1}	3.6×10^{-2}	3.2×10^{-3}
28	1.3×10^{-1}	2.0×10^{-3}					
	8.5×10^{-1}	7.3×10^{-1}	5.6×10^{-1}	3.3×10^{-1}	1.2×10^{-2}	2.1×10^{-2}	1.3×10^{-3}
32	1.0×10^{-1}	8.5×10^{-4}					
	8.4×10^{-1}	7.2×10^{-1}	5.3×10^{-1}	2.9×10^{-1}	9.3×10^{-2}	1.3×10^{-2}	5.0×10^{-4}
36	7.9×10^{-2}	3.6×10^{-4}					
	8.3×10^{-1}	7.0×10^{-1}	5.0×10^{-1}	2.6×10^{-1}	7.1×10^{-2}	7.5×10^{-3}	2.0×10^{-4}
40	6.1×10^{-2}	1.5×10^{-4}					
	8.3×10^{-1}	6.8×10^{-1}	4.7×10^{-1}	2.3×10^{-1}	5.4×10^{-2}	4.4×10^{-3}	7.9×10^{-5}
44	4.7×10^{-2}	6.5×10^{-5}					
	8.2×10^{-1}	6.7×10^{-1}	4.5×10^{-1}	2.0×10^{-1}	4.1×10^{-2}	2.6×10^{-3}	3.1×10^{-5}
48	3.6×10^{-2}	2.8×10^{-5}					
	8.1×10^{-1}	6.5×10^{-1}	4.3×10^{-1}	1.7×10^{-1}	3.1×10^{-2}	1.6×10^{-3}	1.2×10^{-5}
60	1.7×10^{-2}	2.1×10^{-6}					
	7.9×10^{-1}	6.1×10^{-1}	3.6×10^{-1}	1.2×10^{-1}	1.4×10^{-2}	3.3×10^{-4}	7.8×10^{-7}
72	7.7×10^{-3}	1.6×10^{-7}					
	7.7×10^{-1}	5.7×10^{-1}	3.1×10^{-1}	8.1×10^{-2}	6.2×10^{-3}	6.9×10^{-4}	
96	1.6×10^{-3}						
	7.3×10^{-1}	5.1×10^{-1}	2.2×10^{-1}	3.7×10^{-2}	1.2×10^{-3}	3.0×10^{-6}	

Bakeout Temperature °C	Bakeout time required, hr	
	L = 0.102 cm	L = 0.675 cm
300	26	--
350	11	415
400	5	197
450	3	102
500	2	57

It does not appear impossible that a reactor system which was specially designed to have a low detritiation time might be able to achieve very low ($\sim$ 1 day) times before breaking the first-wall vacuum seals. However, a meaningful design would require a level of design detail (detailed tritium inventory, hydrogen absorbence of all reactor materials, rationale for environmental standards) which is beyond the scope of this study.

II.H.3. Comparison with Previous Maintainability Studies

The recommendation of automated replacement of all reactor modules at the same time differs from the maintenance procedures examined in other studies [FU78], [SN79], [MI76]. In particular, a comparative study by McDonnell Douglas[FU78] examined four different reactor concepts and four levels of modularity and attempted to quantify the maintenance cost of each approach. The principal differences between the HFCTR maintenance philosophy and other approaches can be illustrated by a comparison between the conclusions of the McDonnell Douglas report and the recommended HFCTR assembly/disassembly plan.

Most of the "desirable maintainability features" identified by McDonnell Douglas are incorporated in the HFCTR design. These include:

.Employ large modules with minimum access operations for scheduled maintenance.

.Use a single coolant connection per module.

.Use multiple vacuum chamber zones.

.Minimize plasma chamber welded or sealed joints between modules. (Eliminated in HFCTR)

.Constrain remote maintenance to simple operations.

The major difference between the HFCTR and the McDonnell Douglas conclusions is that McDonnell Douglas recommended maximum contact maintenance, while HFCTR module replacement is fully automatic and remote. The McDonnell Douglas recommendation was based on an observed time disadvantage of a factor of about five in favor of contact maintenance over remote maintenance with manipulators. While recognizing a lack of firmness in such time estimates, Sniderman's parallel studies of remote module replacement by manipulators and by fully automated actuators [SN79, MI76] indicated that automated maintenance could be 20 - 30 times as rapid as maintenance with manipulators. The McDonnell-Douglas study also recognized that the most common maintenance act, replacement of a first wall/blanket sector, could not possibly be performed by contact maintenance, and that the large size of the components being handled would further lessen the theoretical advantage of contact maintenance.

The new HFCTR concept of replacing all modules in one operation is not considered in the McDonnell Douglas report. That report treated four published reactor designs as though they were all sixteen module systems and then analyzed the replacement of different-sized sectors, consisting of one, two, four and eight modules apiece. Replacement of all sixteen modules simultaneously was called "impractical" and was not considered further. However, as shown in Table 5.1-3 of that report, the cost models in TOCOMO [MD78] predicted that the simultaneous replacement of eight modules would lead to the lowest cost of electricity. The report concludes that "Removal of one half of the first wall/blanket yields the lowest cost of electricity for both the contact and remote maintenance scenarios." There is, therefore, no support for the strategy of replacing a single module at a time in either study. A potentially important advantage of simultaneous replacement of all modules is that it is the only scenario which will enjoy a substantial decrease in the residual level of radioactivity in the reactor cell during the reassembly process, since all modules will be unirradiated. This may allow the possibility of hands-on assembly for critical tolerance operations, such as aligning the finger joints of interior poloidal field coils or aligning the shear/compression panels of the last-inserted module.

The previously perceived impracticality of simultaneous replacement of all modules is probably based on undesired clutter and mutual interference of large manipulator systems and a possible lack of storage space to remove horizontal neutral beams from the disassembly route. The 1978 HFCTR solves the problem of clutter by mounting in-

dividual automated systems directly on each module transporter. The problem of neutral beam interference is solved by lowering the vertical-injection beams into the subfloor and bridging. A possible difficulty with this method is that of providing sufficient shielding for radiation-sensitive electronic equipment in the basement with penetrations as large as neutral beam lines. This difficulty does not arise in the 1979 HFCTR design, which incorporates a simple, demountable waveguide which does not interfere with modular motion; nor would it arise with any other form of rf heating. It has also been objected that simultaneous replacement of all modules requires excessive storage of spare modules. While the area of the storage bay may be increased, it should be recognized that simultaneous replacement actually decreases the cost of spares. Recall that simultaneous replacement is applied only to scheduled maintenance and that all repair concepts are identical with respect to unscheduled maintenance, requiring one or two spare modules. If only 1/N of all modules are replaced at a time, then spare modules must be available every 1/N maintenance periods, while spares need only be available at the end of life of a first-wall/blanket module if simultaneous replacement is used. Similarly, if simultaneous replacement is not employed, the first sector must be removed and discarded after only 1/N of its design lifetime. Thus, for a large number of sectors, simultaneous replacement will increase the useful lifetime of the first generation of first wall/blanket modules by a factor of $2N^2/N(N - 1)$.

III. Summary and Conclusions

III.A ADVANTAGES OF ECR HEATING

- ECR radiation is predicted to penetrate to the center of a reactor-size tokamak plasma and to be absorbed there. The theoretical heating efficiency is, therefore, close to 100%.
- The ECR radiation should result in heating of the bulk of the electron distribution.
- Moderate $<\beta>$ of about 4% may be achieved in high density, compact tokamak reactors heated with ordinary wave radiation at electron cyclotron resonance with central temperature $\lesssim$ 15 keV.
- There are a number of advantages of ECR heating over neutral beam heating. Many of these advantages are common to all RF heating techniques, including ECRH, LHH (lower hybrid heating) and ICRH (ion cyclotron resonance heating). For example, gyrotron tubes will be sealed and will not share the tokamak reactor vacuum system. Thus, gyrotrons, unlike neutral beam injectors, are not affected by a reactor vacuum failure and vice versa.
- The use of many (about 1000) gyrotron tubes means that the failure of a single unit will not affect operation or require shutdown. Only a few spare units will be needed at any one time. It should be possible to replace failed gyrotron tubes during reactor operation. For a neutral beam injector system, spares are required for both routine maintenance and in case of failure. This

increases the relative cost of the neutral beam system by 33% for a four arm system.

- Gyrotron tubes, once perfected, should be capable of achieving reliable operation for very long periods of time. They should benefit from the experience of microwave tube manufacturers in developing high power tubes with long lifetimes. Many microwave tubes used in high power radar systems are designed with operating lifetimes of 50,000 hours.
- The microwave transmission system for ECR radiation will be at atmospheric pressure. It will be easily disconnected from the reactor modules even by remote handling techniques. This simplifies the replacement of reactor modules, reduces reactor down time and lowers costs, relative to neutral beam injector systems.
- No regular maintenance of the microwave transmission system will be required. Neutral beam injectors require periodic regeneration of cryopanels.
- The gyrotron system cannot be directly affected by backstreaming of neutral particles from the plasma.
- Gyrotron buildings will be constructed outside the reactor containment wall and at ground level. Neutral beam injectors must be located closer to the reactor, complicating the reactor building design.
- ECR heating eliminates the need for ripple field coils, such

as those used in the HFCTR neutral beam injection system.

- The projected cost of an ECR heating system is lower than that of a comparable neutral beam injector system.
- The projected efficiency of the high frequency gyrotrons needed for heating a tokamak power reactor is about 30%. This value is satisfactory for reactor operation.
- Extremely low loss transmission of high frequency radiation over long distances, over 20 km, has already been demonstrated in trial operation of microwave communications systems.
- ECR heating is highly localized. This should allow control of the temperature profile of the tokamak plasma, improving confinement. A reduced power level for heating to ignition may also be possible if profile control is successful.
- Gyrotrons can be applied to gas breakdown and plasma preheating, possibly reducing the size and cost of the ohmic drive system.
- The penetration of ECR radiation to the plasma center is unaffected by edge density gradients or impurities.
- Gyrotrons may be useful for thermal control of the reactor burn cycle.
- ECR heating uses short wavelength radiation. This radiation has small diffraction losses and may be launched from simple horn antennas or focusing mirror systems located far from the tokamak plasma. If several beams of radiation are formed into an array, the beams may differ randomly in phase and in frequency. In LH heating, a complicated phased antenna array may be needed.

III.B DISADVANTAGES OF ECR HEATING

- The efficient, high power, high frequency gyrotrons (or other sources) required for ECR heating of a reactor-size tokamak plasma have not as yet been developed. Although projections of gyrotron technology indicate that we may be optimistic about developing these sources, the actual development will be difficult and time consuming. Also, there is no guarantee that such a development program will be successful.
- A transmission system capable of carrying high frequency radiation at low loss over a 30 m path has been demonstrated at low power levels, but it has never been demonstrated at high power levels. Such a test has not been possible because the necessary high power, high frequency sources have not been available. Transmission systems for high power radiation have worked, however, at lower frequencies, in the microwave region, and at higher frequencies, in the optical region, (using CO_2 lasers).
- There are several technological disadvantages of ECR heating relative to RF heating at lower frequencies, such as LHH or ICRH. One advantage of RF heating at the lower frequencies is that system components, such as waveguide and isolators, have already been developed for high power transmission systems.
- For LHH and ICRH, fundamental mode waveguide can be used for transmission, eliminating problems of multimode excitation. Fundamental

mode waveguide is too lossy for ECR heating.

- Gyrotrons require cryogenic magnet systems, which are not needed for the microwave tubes used in LHH or ICRH.
- The power supply used for the gyrotrons will most likely have to supply two voltages to the tube. It may require slightly better regulation and higher voltage than for the tubes used for LHH or ICRH. This will add to the cost of ECR heating.
- The environmental problem of RF radiation leakage may be worse at high frequencies than at low frequencies.
- The window needed for the gyrotron and for the reactor port must be capable of transmitting high power at high frequencies. Such a window has not yet been demonstrated.
- The efficiency of the gyrotrons is estimated to be 30%, which is adequate but lower than that available at lower frequencies. In the long term, it is possible that the efficiency of gyrotrons or alternative high frequency sources may improve considerably.
- Since gyrotron technology is still under development, it will almost certainly be more costly than lower frequency systems, at least initially.
- A mode transformer for converting the transmitted mode of the ECR radiation (TE_{01}) into a linearly polarized mode at the reactor has not yet been developed.
- In addition to the technological problems with ECR heating, there are also some physical limitations. ECRH results in direct heating

of electrons, with collisional energy transfer required to heat the ions. Neutral beam injection, LHH and ICRH can all heat ions directly. Heating of electrons can also lead to enhanced losses due to synchrotron emission.

- In ECR heating, $<\beta>$ cannot exceed 4% if the preferred heating mode, ordinary wave at Ω_0, is used. Higher $<\beta>$ can only be achieved if heating is done at harmonics with higher frequency radiation. Other heating methods do not have a direct limit on $<\beta>$.
- In ECR heating of a reactor-size tokamak, tail heating may occur, particularly if waves are launched directly normal to the toroidal field. Although tail heating should be avoidable by proper wave launching, this needs to be verified both theoretically and experimentally.
- It appears that ECR heating, unlike LH heating, cannot be used for an RF-driven, steady-state tokamak.

III.C UNRESOLVED AREAS OF INVESTIGATION

A number of areas of research were beyond the scope of the present study and, in several cases, insufficient information is not even presently available to resolve important issues. Some areas of technology require additional research to resolve questions raised in the present study. For example, there are unresolved problems in the area of high frequency gyrotron design. The present study indicates that the 100 kW, 200 GHz gyrotrons needed for ECR heating will have to operate in a relatively high cavity mode. In such a case, we find that mode competition is very likely to occur. The effect of such mode competition on gyrotron performance is not yet well understood. The design of an output waveguide structure and window for a high power, high frequency gyrotron cannot be done reliably at the present time because there is almost no experimental information about such gyrotrons. There is also some uncertainty about the effects of space charge and emitter surface roughness on the quality of the electron beam. In summary, efficient, high power, high frequency gyrotrons cannot be designed in detail with great confidence without a good deal of additional experimental and theoretical research. Such research on high frequency gyrotrons would be of great value.

There are a number of technological aspects of design of the microwave transmission system which also require further analysis.

Although we have selected a transmission system using the TE_{01} mode in oversize circular waveguide, there are other possible transmission systems, including optical systems, which can provide low loss transmission. The relative merits of these systems could be discussed in greater detail, although experimental information would be even more valuable. The mode transformer from the working gyrotron mode to a TE_{01} mode was not considered in great detail because of the great difficulty in designing such a quasi-optical component and because of the lack of information on this topic in high frequency applications. The transformer for converting the TE_{01} mode into linearly polarized waves at the reactor was not considered in great detail for the same reasons. The material for the window at the reactor port could not be designed because of lack of information.

The wave absorption in the plasma should also be studied more thoroughly in order to determine the location of energy deposition and the portion of the electron distribution heated. The required equations describing absorption in a weakly relativistic plasma have been recently developed. An analysis including the effects of the poloidal field might also be of interest. The absorption of ECR radiation should be correlated with the growth of the electron velocity distribution, including the effects of scattering and collisions. This analysis for a reactor-size plasma can be carried out in principle, but the algebraic problems could be rather

severe. Such an analysis would help to identify the optimum angle at which to launch the ECR radiation, the location of the energy absorbing region as a function of temperature, the portion of the ECR radiation which causes tail heating and the maximum value of $\alpha = \omega_{po}^2/\Omega_o^2$ and, thus, $\langle\beta\rangle$ at which heating can be successfully carried out. Heating in plasmas with noncircular cross section or at $2\Omega_o$ could also be studied.

III.D CONCLUSIONS

- In this study, we have analyzed and designed an electron cyclotron resonance heating system for a tokamak power reactor, namely the High Field Compact Tokamak Reactor (HFCTR). It is our principal conclusion that an ECR heating system for the HFCTR should be both feasible and attractive. However the actual realization of such a heating system will require a significant development effort in several areas, including the development of efficient, high power, high frequency gyrotrons and the development of components for the transmission of high power, high frequency (~ 200 GH_z) radiation.
- For a reactor which utilizes ECR heating, there are important constraints on the reactor operating parameters imposed by the cutoff condition for ECR wave penetration. For ordinary wave heating at the electron cyclotron resonance, the cutoff condition is that the heating frequency, ω (= Ω_o, central ECR frequency) exceed ω_{po}, the central plasma frequency. This implies that, for heating of a high density ($n_o > 4 \times 10^{20} m^{-3}$), moderate size tokamak reactor, ECR heating frequencies in the range of 200 GHz will be required (central magnetic field of about 7T). The cutoff condition also imposes a limit on the average plasma β, which is proportional to n/B^2 or equivalently,

ω_{po}^2/Ω_o^2. For ordinary wave heating at $\omega = \Omega_o$ and a central temperature below 15 keV, $<\beta>$ is limited to less than 3.9%, assuming a circular plasma with parabolic temperature and density profiles. Higher $<\beta>$ can be achieved with second harmonic heating, but higher gyrotron frequencies (by $\sqrt{2}$) will be required.

- Ordinary wave heating at $\omega = \Omega_o$ appears to be the most attractive option for ECR heating. Extraordinary wave heating at $\omega = \Omega_o$ does not appear to be practical for heating of a reactor based on the necessity of launching the wave from the inside (small major radius side) of the torus. Second harmonic heating can increase the $<\beta>$ limit by a factor between 2 and 4 and can reduce the required central magnetic field, but the required gyrotron frequency is increased by a factor of about $\sqrt{2}$.
- A previous tokamak reactor design, the High Field Compact Tokamak Reactor (HFCTR), which was designed with neutral beam heating, is also suitable for bulk heating to ignition by ECRH. The ECR heating system for the reactor would require about 100 MW of 200 GHz gyrotron delivered to the plasma. The time for heating to ignition would be about 4 sec.
- A design study has been carried out for a high power, 200 GHz gyrotron. A projected power level of 100 kW for a single gyrotron oscillator appears feasible. The gyrotron would operate with a 70 kV, 4.4 A beam, with an overall efficiency of 33%. The cavity mode would be TE_{051} with a total Q (ohmic plus diffractive) of 2.3×10^3. A detailed

design of the cavity, which must dissipate 5 kW/cm^2, and its cooling system has also been carried out. The overall design represents, in some respects, a significant extension of present day technology, but the design appears to be practical.

- There are, however, a number of technological problems which have to be solved before reliable, high power, 200 GHz gyrotrons can be constructed. These will include electron gun design for high $v_\perp / v_\parallel$ and low space charge; cavity design to prevent multimoding and enhance efficiency; window, collector and output waveguide design; and cooling systems that avoid hot spots.
- Because of the recent interest in developing high frequency microwave sources, very high power devices, such as relativistic gyrotrons, free electron lasers, etc., may eventually be developed with multimegawatt output at 200 GHz. Such devices may prove attractive, but they will have some disadvanges. In particular, the development of techniques for transmission of a multimegawatt beam through a window, or operation without windows by evacuated pipes to the reactor, is also a major technological problem.
- A potentially low loss system has been designed for transmission of the microwave radiation from the gyrotrons to the plasma. Transmission of the TE_{01} mode in oversize, circular, copper waveguide has been selected. This technique has been field tested in high frequency microwave communications systems, but only low power transmission was studied. A projected overall transmission from the gyrotron output to the plasma of 80% should be feasible. However, some new

components will have to be developed in order to achieve this high level of transmission efficiency. Mode transformers, with low insertion loss and high power capability, will have to be developed for mode transformation both from the gyrotron to the oversize TE_{01} mode and from the TE_{01} mode to a linearly polarized mode at the reactor. Mode filters and isolators may also need to be developed.

- Wave absorption is predicted to occur in the central region of the plasma for ordinary wave heating at $\omega \simeq \Omega_o$. This should lead to bulk plasma heating. For ω_{po}^2/Ω_o^2 approaching unity, refraction effects indicate the angle of launch, θ, of the wave with respect to the magnetic field, should be $\gtrsim 70^o$. For reactor size plasmas, absorption will occur in the tail of the absorption profile, at a location where ω does not equal Ω_o. However, the absorption can be forced to occur in the center of the plasma by tuning ω to be slightly larger than Ω_o. The location of the heating zone is a function of plasma density and temperature and the angle of launch of the radiation. As the plasma heats up, the location of the absorbing zone shifts. The magnitude of this shift is not negligible, but absorption will still occur in the central region of the plasma.
- The RF heating system leads to a considerably simpler technique for removal of individual reactor modules (for either scheduled or unscheduled replacement) relative to a neutral beam injector system. The cost of an ECRH system is also projected as less than that of a neutral beam system.

- The optimum method for scheduled replacement of reactor modules is to replace all modules simultaneously. This technique has the advantage of reducing the total time required in scheduled replacements for detritation of the vacuum vessel and for re-establishment of high vacuum after reassembly. It also increases the projected service life of the first generation modules and reduces the activation of the reactor cell, permitting the possibility of human entry (with shielding) into the reactor cell if needed during reassembly.
- The recirculating power fraction is estimated to be 0.34. The influence of gyrotron efficiency on this fraction is found to be very small. Increased gyrotron efficiency could, however, result in significantly lower cost for the gyrotron power supply system.

IV. TABLE OF FUSION REACTOR DESIGN PARAMETERS

IV.A. Design Parameters and Costing

The design parameters of the ECRH - driven reactor are identical with those of the HFCTR demonstration reactor [CO79] and are restated here for convenience. Costing of the HFCTR reactor is also included by Cohn [CO79], but only costing of the auxiliary heating system is included in this study. Reactor parameters are shown in Table IV.1, and ECRH heating system components are shown in Table IV.2. Table IV.2 also compares the cost of the ECRH heating system with the original neutral beam heating system in the HFCTR reference design [CO79].

Improvements in system reliability, lower cost of remote handling because of the greater simplicity and redundancy of the gyrotron-based heating system are not included in this cost comparison.

The ECRH system is costed at approximately 60% of the cost of the original neutral beam system. The cost of the neutral beam system does not include the cost of the ripple coils, necessary for the feasibility of heating a reactor-size plasma with positive ion neutral beams. These coils and their power supplies add another $6.5 M to the cost of the neutral beam heating system.

The power supply of the ECRH system is less expensive than that of the neutral beam heating system primarily because the gyrotron efficiency is 50% higher than that of the beam neutralizer. Cathode

protection is somewhat simpler and less expensive than for neutral beams because of the absence of grids and the suppression of arc pinches by the transverse magnetic field. The first anode also draws less power than the first, second (optional) and suppressor grids in the neutral beam system.

The microwave transmission system is considerably simpler than that of the neutral beam system, consisting mostly of an unevacuated tube and requiring no large cryopanels, beam dumps or magnets. However, the windows will have to be fabricated with great care and the transmission system is also considerably longer than the beam lines, so the system cost is still over the original estimate of one-half the estimate of the beam line costs. The estimate of the neutral beam arm cost of HFCTR appears to be overly optimistic, when compared with the projected costs of the TFTR system and the prediction of a forthcoming standard cost estimating document [SC79]. These predict a cost of approximately $90 M for the neutral beam arms, or nearly double the cost of the nonelectronic portion of the ECRH heating system.

TABLE IV.1

Table of Reactor Design Parameters

	Unit	Value
1. Characteristic Machine Dimensions		
1.2 Vacuum Vessel		
1.2.1 Major Radius	m	6.0
2. Plasma Parameters		
2.1 Plasma Dimensions		
2.1.1 Major Radius, R	m	6.0
2.1.2 Minor Radius, a	m	1.2
2.1.3 Plasma Elongation		1.85
2.2 n_o, centerline density	m^{-3}	5.2×10^{20}
2.3 $\bar{n}$, average density	m^{-3}	3.1×10^{20}
2.4 τ_E, energy confinement time	sec	3.1
2.7 $n\tau_E$, (averaged through plasma)	sec/m^3	9.6×10^{20}
2.9 $<\beta>$, average toroidal beta		0.04
2.11 $<\beta_p>$, average poloidal beta		4
2.12 I_p, plasma current	MA	6.7
2.13 T_{io}, centerline ion temperature	keV	12.4
2.14 $\bar{T}_i$, average ion temperature	keV	6.2
2.15 T_{eo}, centerline electron temperature	keV	12.4
2.16 $\bar{T}_e$, average electron temperature	keV	6.2
2.17 Z_{eff}, effective plasma ion charge		1.2
2.18 q, plasma safety factor		3.0
2.19 Volt-seconds	Volt-Sec.	148 V-S 82 V-S, inductive 66 V-S, resistive
2.20 Reactor Cycle	Steady State/Pulsed	Pulsed

2. Plasma Parameters (continued)		Unit	Value
2.20.1	Burn Pulse Length	sec.	480
2.20.2	Total Pulse Length	sec.	500
2.21	Fuel Cycle (i.e., D-T, D-D, etc.)		D-T
2.22	Plasma Heating Method		ECRH
2.23	Plasma Heating Power		100 MW
2.24	Plasma Heating Energy or Frequency	keV or Hz	2×10^{11}
2.25	Plasma Energy Gain, Q_p		Ignited
3. Power Output			
3.1	Plasma Power (Peak)	MW(th)	2,542
3.2	Plasma Power (Total Cycle Time Average)	MW(th)	2,440
3.3	Power to Blanket (Peak)	MW(th)	2,153
3.4	Power to Blanket (Total Cycle Time Average)	MW(th)	2,067
3.6	Power to Direct Convertor (Peak)	MW(th)	0
3.7	Power to Direct Convertor (Total Cycle Time Average)	MW(th)	0
3.8	Power to Divertor (Peak)	MW(th)	0
3.9	Power to Divertor (Total Cycle Time Average)	MW(th)	0
3.10	Plasma Chamber Power Density (Total Cycle Time Average)	MW/m^3	7.7
4. Reactor Coolant System			
4.1	Blanket Coolant Type	FLIBE	
5. Intermediate Coolant System		not available	

	Unit	Value
6. Steam Generation System	not available	
7. Shield Coolant System	not available	
8. Reactor Auxiliary Systems		
8.1 Vacuum Pumping System		
8.1.1 Plasma Camber Pressure	torr	10^{-8}
9. Reactor Components		
9.3 Magnets		
9.3.1 Superconducting	yes/no	yes
9.3.2 Conductor Material		Nb_3Sn
9.3.3 Structural Material		304SLN
9.3.4 Operating Temperature	K	4.2
9.3.5 Coolant		He
9.3.6 Maximum Stress in Coil	N/m^2	311×10^6
9.3.7 Maximum Force Transmitted to Building	N/m^2	-
9.3.8 Maximum Field	T	13.1
9.3.9 Field on Axis	T	7.4
9.3.10 Number of Magnets		16
9.3.11 Field Ripple - Edge/Center	%	1, edge
9.3.12 Stored Energy	J	40×10^9
10. Electrical Power Requirements	not available	
11. Buildings	not available	
12. Reactor Maintenance	not available	

TABLE IV.2

Cost of ECRH System Components and Comparison with Neutral Beam Heating System Costs

	ECRH	Neutral Beam	
		HFCTR	TFTR Scaling
High-voltage Regulated Power Supplies	$38.4 M	$69.0 M	$69.0 M
Neutral Beam Arms		30.0 M	90.0 M
Magnets and Supplies	5.0 M		
First Anode Power Supplies	1.6 M		
Gyrotrons	25.0 M		
Gyrotron Cooling	0.7 M		
Windows	9.4 M		
Cryogenic Refrigeration	0.6 M		
Waveguide and Miscellaneous Fittings	7.5 M		
TOTAL	$88.2 M	$99.0 M	$159.0 M

IV.B Recirculating Power

An estimate of the recirculating power in the HFCTR tokamak power reactor with ECR heating is presented in Table IV.3 The ECR heating system must supply 100 MW to the plasma. Assuming an 80% transmission efficiency, a 100% heating efficiency and 33% overall gyrotron efficiency, the gyrotrons will require 380 MW of DC regulated power and about 430 MW of 60 Hz power. However, because the ECR heating system is only used during the bulk heating phase and is not used during the burn, the average recirculating power of the ECR heating system is only 4.3 MW. Active control of the burn by the ECR heating system is not considered here. The major portion of the recirculating power is derived from losses in the cryogenic refrigeration system, parasitic losses in the poloidal field system, general plant water, and miscellaneous other systems, as shown in Table IV.3.

Because of the low duty factor of the heating system, the efficiency of the gyrotrons has only a small impact on the overall recirculating power. Gyrotron efficiency, however, is still important since an increase in efficiency would reduce the cost of the ECR heating system and the cost of the high voltage power supplies for the gyrotrons.

Table IV.3

Recirculating Power

		Power
1.	ECRH Auxiliary Heating System	
	RF Power into Plasma	100 MW
	DC Regulated Power to Gyrotrons	380 MW
	60 Hz Power to DC Regualtor	430 MW
	Duty Factor (5s Heating/500s Burn)	0.01
	Average Recirculating Power	4.3 MW
2.	Cryogenic Refrigeration System	28.5 MW
3.	Parasitic losses in Poloidal Field System (Total, 125 MW)	
	A. Friction and Windage, pulsed generator	40 MW
	B. OH Rectifier - Transformer	36.8 MW
	C. Quadrupole Coil	22.1 MW
	D. Misc. Pol. Field Losses	26.1 MW
4.	Water, General Plant	24.7 MW
5.	Misc. Other	39.8 MW
		222.3 MW

Gross Electrical Power, HFCTR 870 MW

Net Electrical Power 648 MW

$$\frac{\text{Recirculating Electrical Power}}{\text{Net Electrical Power}} = 0.34$$

BIBLIOGRAPHY

[AK74] A.I. Akhiezer, I.A. Akhiezer, R.V. Polovin, A.G. Sitenko, K.N. Stepanov, Plasma Electrodynamics, Pergamon Press (1975), (English).

[AL68] V.V. Alikaev, V.M. Glagolev and S.A. Morozov, Plasma Phys. 10, 753 (1968).

[AL72] V.V. Alikaev, G.A. Bobrovskii, M.M. Ofitserov, V.I. Poznyak and K.A. Razumova, J.E.T.P. Lett. 15, 27 (1972).

[AL75] V.V. Alikaev, Yu. I. Arsenyev, G.A. Bobrovskii, V.I. Poznyak, K.A. Razumova and Yu.A. Sokolov, Sov. Phys. Tech Phys. 20, 327 (1975).

[AL76a] V.V. Alikaev, Yu. N. Dnestrovskii, V.V. Parail and G.V. Pereverzev, IAE Report 2610, Moscow, (1976).

[AL76b] V.V. Alikaev, G.A. Bobrovskii, V.I. Poznyak, K.A. Razumova, V.V. Sannikov, Yu.A. Sokolov and A.A. Shmarin, Sov. J. Plasma Phys. 2, 212 (1976).

[AL76c] V.V. Alikaev, Yu.I. Arsenyev, Third Intl. Meeting on Theor. and Expt. Aspects of Heating of Toroidal Plasmas, Grenoble, Vol. 2, 375 (1976).

[AL77a] V.V. Alikaev, Yu.N. Dnestrovskii, V.V. Parail, and G.V. Pereverzev, Sov. J. Plasma Phys. 3, 127 (1977).

[AL77b] D.A. Alsberg, J.C. Bankert, and P.T. Hutchison, Bell System Technical Journal 56, No. 10, 1,829 (1977).

[AL78] V.V. Alikaev, IAEA Conf. on Plasma Phys. and Contr. Nuclear Fusion, Innsbruck (1978).

[AN77] Anderson, J.C., Carlin, J.W., Thomson, D.J., and West, T.J., Bell System Technical Journal, 67, No.10 (1977) p.2157.

[AN78] A.A. Andronov, V.A. Flyagin, A.V. Gaponov, A.L. Gol'denberg, M.I. Petelin, V.G. Usov, and V.K. Yulpatov, Infrared Phys. 18, 385 (1978).

[BA77] G. Bateman, Y.K.M. Peng, Phys. Rev. Lett. 38, 829 (1977).

[BE69] F.A. Benson, editor, Millimeter & Submillimeter Waves, Iliffe Books Ltd., London, (1969)

[BE79] H. Becker, Private Communication, (1979).

[BR79] L. Bromberg, J.L. Fisher and D.R. Cohn, M.I.T. Plasma Fusion Center Report RR-79-17, September 1979.

[BY75a] Yu.V. Bykov, A.F. Gol'denberg, L.V. Nikolaev, M.M. Ofitserov, and M.I. Petelin, Radiophysics and Quantum Electronics 18, 1,141-1,143 (1975).

[BY75b] Yu.V. Bykov and A.L. Gol'denberg, Radiophysics and Quantum Electronics 18, 791-792 (1975).

[CA77] Carlin, J.W., and Moorthy, S.C., Bell System Technical Journal, 56, No. 10. (1977) p. 1849

[CL77] J.F. Clarke, D.J. Sigmar, Phys. Rev. Lett. 38, 70 (1977).

[CA79] R. Cano, A. Cavallo and H. Capes, Bull, Am. Phys. Soc. 24, 969 (1979).

[CL77] J.F. Clarke, D.J. Sogmar, Phys. Rev. Lett. 38, 70 (1977).

[CO77] D.R. Cohn, D.L. Jassby, K. Kreischer, Princeton Plasma Physics Laboratory Report MATT-1405, (1977).

[CO79] D.R. Cohn, J.H. Schultz, L. Bromberg, F. Chang, D.L. Cook, M. Culbert, J. Fisher, D. Hackworth, R.D. Hay, D.L. Jassby, D.L. Kaplan, K.E. Kreischer, L.M. Lidsky, F. Malick, T. McManamy, K. Molvig, J. Murphy, M. Okabayashi, D.O. Oberskei, M. Sniderman, W. Stephany, H.H. Towner, J.E.C. Williams, High Field Compact Tokamak Reactor (HFCTR) Conceptual Design, Final Report, M.I.T. Plasma Fusion Center Research Report RR-79-2, January 1979.

[DA64] R.A. Dandl, A.C. England et al, Nucl. Fusion 4, 344 (1964).

[DA76] Dandl, R.A., Report of the Ad Hoc Panel on RF Heating in Tokamaks, ERDA-76/115 (1976), Appendix D-3.

[EL77] O. Eldridge, W. Namkung and A.C. England, ORNL Report TM, 6,052 (1977).

[EN73] F. Engelmann, M. Curatolo, Nucl. Fusion 13, 497 (1973).

[EN76] A.C. England, O.C. Eldridge, F.B. Marcus, J.C. Sprott, W. Namkung, J.B. Wilgren, ORNL Report TM, 5,425 (1976).

[FI78] I. Fidone, G. Granata, R.L. Meyer, G. Ramponi, Phys. Fluids 21, 645 (1978).

[FL77] V.A. Flyagin. A.V. Gaponov, M.I. Petelin and V.K. Yulpatov, IEEE Trans. Microwave Theory and Tech., MTT-25, 514 (1977).

[FU78] G.M. Fuller, H.S. Zahn, H.C. Mantz, G.R. Kaletta, L.M. Waganer, L.A. Carosella and J.L. Conlee, "Developing Maintainability for Tokamak Fusion Power Systems," McDonnell Douglas Astronautics Company Report COO-4,184, 6(1978).

[GA75a] H.J. Garber, "Studies of the Permeation and Diffusion of Tritium and Hydrogen in TFTR," Westinghouse Electric Corporation, WFPS - TME - 012, October 1975.

[GA75b] A.V. Gaponov, A.L. Gol'denberg, D.P. Grigor'ev, T.B. Pankratova, M.I. Petelin and V.A. Flyagin, Radiophysics and Quantum Electronics 18, No. 2, 204-211 (1975), (English).

[GO72a] V.E. Golant, M.G. Kaganskii, L.P. Pakliomov, K.A. Podushnikova and K.G. Shakhovets, Sov. Phys.-Tech. Phys. 17, 488 (1972).

[GO72b] V.E. Golant, A.D. Piliya, Uspekhi 14, 413 (1972).

[GO73] A.L. Gol'denberg and M.I. Petelin, Radiophysics and Quantum Electronics 16, No. 1, 106-111 (1973), (English).

[GR79] V. Granatstein, Private Communication, (1979). See also Bull. Am. Phys. Soc., Vol 24, No. 8, October 1979.

[HI77] J.L. Hirshfield and V. Granatstein, IEEE Trans. Microwave Theory and Tech., MTT-25, 522 (1977).

[IN76] Institute of Electrical Engineers, International Conference on Millimetric Waveguide Systems, London, England, (1976).

[JA76] D.L. Jassby, D.R. Cohn, R.R. Parker, Nucl. Fusion 16, 1,045 (1976).

[JO77] H.R. Jory, F. Friedlander, S.J. Hegji, J.F. Shively, R.S. Symons, Seventh Symposium on Engineering Problems of Fusion Research, Knoxville, TN, October 1977.

[KA65] A.E. Karbowiak, Trunk Waveguide Communication, Chapman and Hall Ltd., (1965).

[KI74] D.V. Kisel', G.S. Kovablev, V.G. Navel'yev, M.I. Petelin and Sh. Ye. Tsimring, Radio Eng. Electron. Phys. 19, No. 4, 95-100 (1974), (English).

[LI77] A.G. Litvak, G.V. Permitin, E.V. Suvorov, A.A. Frajman, Nucl. Fusion 17, 659 (1977).

[MA78] T. Maekawa, S. Tanaka, Y. Hamada and Y. Terumichi, Phys. Rev. Lett. 40, 1,379 (1978).

[MA79a] T. Maekawa, S. Tanaka, Y. Hamada and Y. Terumichi, Phys. Lett. 69A, 414 (1979).

[MA79b] W.M. Manheimer in Infrared and Millimeter Waves, K.J. Button, editor, Academic Press, New York, (1979).

[MD78] "Impact of Confinement Physics on Fusion Power Station Design and Economics and the Utility Interface, Final Report," prepared by McDonnell Douglas Astronautics Company - St. Louis, EPRI RP 547 - 1, University of Michigan, Subcontract 1, July 1978.

[ME79] J. Meyer, Private Communication, (1979).

[MI54] S.E. Miller, Bell System Technical Journal 33, 661 (1954).

[MI76a] J.T.D. Mitchell, Proc. 9th Symp. on Fusion Technology, (1976).

[MI76b] J.T.D. Mitchell and A. Hollis, Proc. 9th Symp. on Fusion Technology, Garmisch - Partenkirchen, (1976).

[NU72] G.S. Nusinovich and R.E. Erm, Elektronnaya Tekhnika, Ser. 1, Elektronika SVCh, No. 8, 55 (1972).

[OK68] E.C. Okress, editor, Microwave Power Engineering, Academic Press, New York, (1968).

[OT79] E. Ott, B. Hui, and K.R. Chu, NRL Memorandum Report 4,028, (1979).

[PE78] Y.K.M. Peng, S.K. Borowski and T. Kammash, Nuclear Fusion 18, 1,489 (1978).

[PO59] Polytechnic Institute of Brooklyn, Proceedings of the Symposium on Millimeter Waves, New York, N.Y., (1959).

[RO62] Rowe, H.E., and Warters, H.D., Bell System Technical Journal, 41, No.5 (1962) p. 1031.

[RO77] R. Rose, Fusion-Driven Actinide Burner Design Study, EPRI ER-451, Final Report, May 1977.

[RO79] R. Rosenfeld, ORNL Report TM-6,728, April 1979.

[SC79] S.K. Schulte, "Fusion Reactor Design Studies: Standard Cost Estimating Rules," Battelle Memorial Institute Report PNL-2,987, (unpublished).

[SE78a] J.L. Seftor, K.R. Chu and A.T. Drobat, NRL Memorandum Report 3,697, July 1978.

[SE78b] J.L. Seftor, K.R. Chu, A.T. Drobot, IEEE Trans. Electron Devices, (unpublished).

[SN79] M. Sniderman, "Fusion Reactor Remote Maintenance Study," EPRI Report No. WFPS - TME - 087, May 1978, EPRI Contract RP - 1,044 - 1, and EPRI Report, (1979).

[SP76] Sporleder, F., IEE, International Conference on Millimetric Waveguide Systems (London, England, 1976) p.68.

[ST78] D. Steiner, J.F. Clarke, Science 199, 1,395 (1978).

[TA74] V.P. Taranenko, V.N. Glushenko, S.V. Koshevaya, K. Ya. Lizhdvoy, V.A. Prus and V.A. Trapezon, Elektronaya Tekhnika, Ser. 1, Elektron. SVCh, No. 12, 47 (1974).

[TA78] S. Tamor, Nucl. Fusion 18, 229 (1978).

[TE78] R.J. Temkin and S.M. Wolfe, M.I.T. Plasma Fusion Center Research Report No. RR-78-9, (unpublished), (1978).

[TE79] R.J. Temkin, K. Kreischer, S.M. Wolfe, D.R. Cohn and B. Lax, Journal of Magnetism and Magnetic Materials 11, 368 (1979).

[TI79] Tischer, F.J., IEEE-MTT-27, No. 1 (1979) p.31.

[TO77] A.M.M. Todd, M.S. Change, J.M. Greene, R.C. Grimm, J.L. Johnson, J. Manicham, Phys. Rev. Lett. 38, 826 (1977).

[TS72] Sh. E. Tsimring, Radiophysics and Quantum Electronics 15, 952-961, (1972).

[VL69] S.N. Vlasov, G.M. Zhislin, I.M. Orlova, M.I. Petelin and G.G. Rogacheva, Radiophysics and Quantum Electron. 12, No. 8, 972-978 (1969), (English).

[VL74] S.N. Vlasov and I.M. Orlova, Radiophysics and Quantum Electronics 17, No. 1, 115 (1974).

[VL75] S.N. Vlasov, L.I. Zagrijadskaya and M.I. Petelin, Radio Eng. and Electron. Phys. 20, 14 (1975).

[WE78] Wengenroth, R.D., IEEE Trans. Microwave Theory and Tech. MTT-26 (1978) p.332.

[WO79] S.M. Wolfe, D.R. Cohn, R.J. Temkin and K. Kreischer, Nuclear Fusion 19, 389 (1979).

[YO68] Leo Young, editor, Advances in Microwaves, Vol. 3, Academic Press, New York, (1968).

[YO69] Leo Young, editor, Advances in Microwaves, Vol. 4, Academic Press, New York, (1969).

[ZA74] N.I. Zaytsev, T.B. Pankratova, M.I. Petelin and V.A. Flyagin, Radio Eng. Electron. Phys. 19, No. 5, 103-107 (1974), (English).

Acknowledgments

The authors would like to thank L. Bromberg, S. Wolfe, R. Weggel, J.E.C. Williams, H. Becker and L. Lidsky, all of M.I.T., for comments and suggestions that have been helpful in the preparation of this report.